TIDE-INDUCED MASS TRANSPORT IN SHALLOW LAGOONS

By

JACOBUS VAN DE KREEKE

A Dissertation Presented to the Graduate Council of the University of Florida in Partial Fulfillment of the Requirements of the Degree of Doctor of Philosophy

UNIVERSITY OF FLORIDA

1971

ACKNOWLEDGEMENT

First, I would like to thank my wife, Hetty, for her understanding and patience during the time of deprived family life accompanying the preparation of this dissertation.

A dissertation to a large extent is the result of the interplay between the candidate and his academic environment; in this case, the faculty, staff and student body of the Department of Coastal and Oceanographic Engineering. Among those, a special word of thanks is due to Dr. R. G. Dean, Chairman and Professor of the Department, who supervised the dissertation; the many hours of discussion with Dr. Dean have greatly contributed to a better understanding of the subject. The helpful criticism and suggestions by Dr. B. A. Christensen, Professor of Civil Engineering, concerning the experiments is greatly appreciated.

The study was in part supported by the Office of the Water Resources Center and in part by the Florida Department of Natural Resources. All computations were carried out using the University of Florida IBM 360 computer.

TABLE OF CONTENTS

	Page
ACKNOWLEDGEMENT	ii
LIST OF FIGURES	iv
LIST OF TABLES	vi
LIST OF SYMBOLS	vii
ABSTRACT	ix
CHAPTERS:	
1. INTRODUCTION	1
2. THE TIDAL EQUATIONS FOR THE LAGOON AND THE INLETS	4
3. NUMERICAL SOLUTION OF THE TIDAL EQUATIONS	13
4. DETERMINATION OF THE FRICTION FACTOR F	24
5. MASS TRANSPORT IN LAGOONS DUE TO TIDAL ACTION	30
a. Analytic Solution; Physical Concepts	30
b. Influence of Inlets on the Mass Transport	47
6. LABORATORY EXPERIMENTS	52
a. Equipment and Procedure	52
b. Results	59
c. Computation of Mass Transport; Comparison with Measured Data	76
d. Summary	86
7. APPLICATION	90
8. SUMMARY AND CONCLUSIONS	96
APPENDIX	98
A. THE MATHEMATICAL DESCRIPTION OF LONG PERIOD GRAVITY WAVES; EULERIAN DESCRIPTION	99
REFERENCES	109
BIOGRAPHICAL SKETCH	112

LIST OF FIGURES

Figure No.		Page
1	Reference Frame.....	5
2	Inlet Schematization.....	8
3	Location of Variables in the Numerical Grid....	14
4	Grid Scheme for Different Inlet Configurations.	18
5	Curves Represented by Equations (3.3) and (3.4).....	21
6	Tide in a Sea Level Canal.....	27
7	Mean Water Level in a Lagoon in the Presence of a Damped Progressive Wave.....	38
8	Effect of Higher Order Terms on q_*.....	41
9	Effect of "Linearization" of the Friction Term on q_*.....	42
10	Effect of Convective Acceleration and Non-linear Part of the Surface Gradient on the Net Discharge q_*.....	44
11	Lagoon Connected to the Ocean by Inlets.....	47
12	Net Discharge in Lagoon Versus Width of Inlet II.....	50
13	Experimental-Set Up.....	53
14	Measured Tide Curves for Experiment 5.....	55
15	Measured Float Positions for Experiment 4.....	61
16	Measured Float Positions for Experiment 5a.....	62
17	Measured Float Positions for Experiment 13.....	63
18	Measured Float Positions for Experiment 13a....	64
19	Determination of Net Discharge from Measured Float Path.....	68
20	Measured Float Positions for Experiment 22.....	69

LIST OF FIGURES (Continued)

Figure No.		Page
21	Measured Float Positions for Experiment 24.....	70
22	Weir; Flow from Lagoon to Tidal Basin.....	77
23	Grid Scheme for Numerical Computations of Laboratory Experiments.....	80
24	Computed and Measured Net Discharges.....	82
25	Measured and Computed Float Positions for Experiment 22.....	84
26	Measured and Computed Float Positions for Experiment 25.....	85
27	Variation of Net Discharge with Depth.....	87
28	Lake Worth, Florida; Location of Tide Recorders..	91
29	Schematization of Lake Worth.....	93
30	Measured and Computed Water Levels in Lake Worth.....	95

LIST OF TABLES

Table No.		Page
I	Summary of Experiments; Test Series 1.....	58
II	Summary of Experiments; Test Series 2.....	59
III	Reproducibility of Experiments; Particle Excursion Between Successive Slack Tides for Experiments 13 and 13a.....	65
IV	Measured Drift Velocities and Net Discharges....	72
V	Computed Net Discharges; Evaluation of Empirical Method of Determining Net Discharges.....	83
VI	Variation of Net Discharge in Experiment 20 for Different Combinations of Weir Coefficients.....	86

LIST OF SYMBOLS

a	tidal amplitude
c_o	wave celerity in case of no friction
d	total depth
f	Darcy-Weisbach resistance coefficient
g	gravitational acceleration
h	mean depth
k	wave number
k_o	wave number in case of no friction
m	coefficient which accounts for entrance losses and nonuniform velocity distribution
q	discharge per unit width
q_*	net discharge per unit width
s	particle trajectory; in Appendix A used as strength of a source per unit volume
t	time
u	velocity in x direction
u_*	net drift velocity
v	velocity in y direction
w	velocity in z direction
x_o	particle position at $t = t_o$
x	horizontal Cartesian coordinate
y	horizontal Cartesian coordinate
z	vertical Cartesian coordinate, positive upward
A	cross-sectional area
A_b	lagoon area

B	width of the water body
C_c	contraction coefficient
D	total depth
F	resistance coefficient used when considering quadratic friction
F_ℓ	resistance coefficient used when considering linear friction
L	length of the water body
M	lateral flow, rainfall
P	wetted perimeter
Q	total discharge
R	hydraulic radius
S	slope of the water surface
X	free surface stress/(mass density of water) in the x direction
Y	free surface stress/(mass density of water) in the y direction
α	phase angle
ε	relative error
η	water surface elevation
$\bar{\eta}_*$	mean water surface elevation
μ	factor related to the resistance; also used as weir coefficient in Chapter 6
μ_ℓ	"linear" weir coefficient
ρ	density of water
σ	angular frequency of the tide
τ	shear stress
ω	angular frequency of the earth rotation
ϕ	latitude, positive for Northern Hemisphere
Ω	Coriolis factor

Abstract of Dissertation Presented to the Graduate Council
of the University of Florida in Partial Fulfillment of the
Requirements for the Degree of Doctor of Philosophy

TIDE-INDUCED MASS TRANSPORT IN SHALLOW LAGOONS

By

Jacobus van de Kreeke

December, 1971

Chairman: Bent A. Christensen
Co-Chairman: Robert G. Dean
Major Department: Civil Engineering

Analytical, numerical and experimental approaches are employed to describe the hydromechanics of lagoons connected to the ocean by two or more inlets. Because special attention is given to the tide-induced mass transport, all second order terms in the hydrodynamic equations are retained. The study is restricted to lagoons with a one-dimensional flow pattern and water of uniform density. In designing a numerical solution to the equations, the inlet equations are regarded as implicit boundary conditions to the equations describing the flow in the lagoon proper. The advantages of this approach are (1) the size of the computational grid in the lagoon can be chosen independently of the relative small dimensions of the inlets, (2) the flow at branching inlets (an inlet connecting a lagoon to the ocean such that branching of the inlet flow can occur) still can be described by a one-dimensional tidal model.

To gain physical insight into the phenomenon of tide-induced

mass transport, an analytic solution to a simplified set of hydrodynamic equations is presented. This solution demonstrates that the magnitude and direction of the mass transport depend on the difference in mean levels at the two inlets imposed by the ocean and the hydraulic characteristics of the inlets and the lagoon. In particular the mass transport (1) increases with the ratio $\frac{a^2}{h}$ (a = amplitude, h = depth), (2) is sensitive to changes in the friction factor F which must be established by calibration. It may be inferred from (1) and (2), respectively, that a significant tide-induced mass transport should only be expected in shallow lagoons and that accurate calibration procedures are necessary to arrive at a reliable magnitude of the mass transport. In presenting the analytic solution, special attention is given to the role of the inlets; it is demonstrated that by properly choosing the dimensions of the inlet, a considerable increase in net transport of water can be obtained.

The predictive capability of the numerical model with regard to mass transport is confirmed by favorable comparison between measured and computed mass transport for a series of experiments carried out in the laboratory. In the experiments, the tide-induced mass transport was determined in a lagoon of uniform width and depth; at one end the lagoon was connected to a tidal basin and at the other end was connected to the same basin via a submerged weir.

The numerical model is used to compute the mass transport in one of Florida's shallow lagoons, Lake Worth. The order of magnitude of the computed mass transport is such that it is of considerable importance when regarding renewal of lagoon waters and transport of pollutants.

1. INTRODUCTION

Estuaries traditionally have been centers of population concentration. Unfortunately for reasons of economy and convenience, the domestic and commercial wastes accompanying many of these urban areas are discharged into coastal waters thereby degrading the water quality. An improved understanding of the mechanisms responsible for the transport of constituents in estuaries is necessary in order to assess the capability of these systems to assimilate waste loads, to renew their waters by flushing due to fresh water inflow or by exchange with oceanic waters and the possible improvement due to engineering structures, such as inlets. In general, two modes of transport exist, convection and mixing. In tidal waters, often the convective transport is solely attributed to fresh water inflow or wind-driven circulation, while it is generally regarded that the only effect of the tidal motion is to generate the turbulence associated with the mixing process. It will be shown, based on theoretical considerations, that for shallow lagoons (a lagoon is defined here as a body of water connected to the ocean by two or more narrow constricted inlets), the convective transport or mass transport due to the tidal motion only can be an important factor in the renewal of water in the lagoon. Because the magnitude of the mass transport is mainly governed by the location and the dimensions of the different inlets, a considerable increase in mass transport can be obtained by properly designing the inlets. This concept of using tidal inlets for environmental controls has been discussed in a wider context by Lockwood and Carothers [11].

In general, a tidal wave, when entering a lagoon, will be modified by the inlets and the main water body. The special case for which the tidal propagation in the main water body may be neglected will not be discussed here. The reader is referred to Keulegan [9], Van de Kreeke [25], Shemdin [20], and Mota Oliveira [15]. In describing the flow field, different sets of equations are used for the flow in the lagoon proper and the flow in the inlets. The reason for this is that certain assumptions made in deriving the equations for the lagoon do not hold for the flow in the inlets. In the equations for both the lagoon and the inlets the nonlinear terms must be retained because in a mathematical sense the convective transport results from these nonlinear terms. The inlet equations used here are algebraic equations while the flow in the lagoon is described by the well-known long wave equations. In the solution, the inlet equations are regarded as implicit boundary conditions for the long wave equations. This implies that it is not necessary to extend the numerical grid used for the main water body to the inlets which, because of their relatively small horizontal dimensions, would lead to small grid sizes and consequently a considerable increase in computational effort. The study is restricted to lagoons having a definite one-dimensional flow pattern. The one-dimensional numerical model used is based on a space and time staggered explicit finite difference scheme similar to the one described by Reid and Bodine [18].

As stated before, the nonlinear terms in the equations, which include the friction term, are important when regarding convective transport. An accurate value of the friction factor, therefore, is one

of the first requirements to prediction of reliable values for the convective transport. In view of this a special discussion is devoted to the determination of the friction factor.

To evaluate the predictive capability of the computational model, measured and computed mass transport in a lagoon are compared for a series of laboratory experiments. The experiments were carried out in the Coastal Engineering Laboratory of the University of Florida.

Finally, the results of the study are applied to an actual lagoon, Lake Worth, located in southeast Florida.

2. THE TIDAL EQUATIONS FOR THE LAGOON AND THE INLETS

In the Eulerian frame, the velocities and water surface elevations are related to time and the various locations in geometric space by two types of equations, one expressing the conservation of mass, the other expressing the conservation of momentum. The equations are derived in Appendix A. The discharge per unit width and the water levels rather than the velocity and the water levels are chosen as the dependent variables because this leads to a simpler form of the conservation of mass equation. Because the considerations on mass transport will be restricted to those lagoons having a definite one-dimensional flow pattern, only the one-dimensional form of the equations and the assumptions made in deriving these equations will be summarized here.

It may be seen from Appendix A that the equation of conservation of mass takes the form

$$\frac{\partial \eta}{\partial t} + \frac{\partial q}{\partial x} = M \qquad (2.1)$$

in which x is the horizontal Cartesian coordinate, see Figure 1.

η = water surface elevation

q = discharge per unit width

M = net inflow per unit surface area due to rainfall, lateral inflow, etc.

The variables q and η are mean values over a time interval, which is large compared to the turbulence time scale and small compared to the period of the tide.

In deriving the above equation, the fluid was assumed to be incompressible.

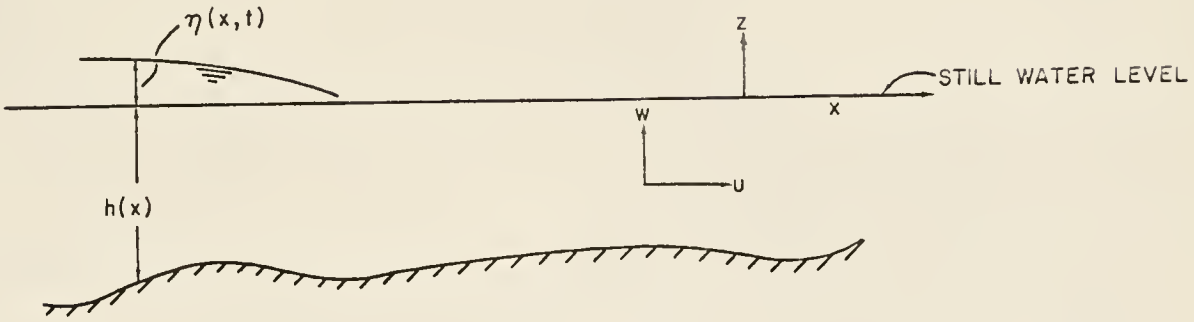

Figure 1. REFERENCE FRAME

The equation of conservation of momentum may be written as

$$\frac{\partial q}{\partial t} + \frac{1}{h}\frac{\partial q^2}{\partial x} + g(h + \eta)\frac{\partial \eta}{\partial x} = -\frac{Fq|q|}{(h + \eta)^2} \qquad (2.2)$$

in which

h = mean depth

F = resistance coefficient.

The main assumptions made in deriving Equation (2.2) are

- incompressible fluid
- uniform density
- vertical accelerations are negligible
- tide-generating forces in the lagoon are negligible
- no free surface stresses.

The assumptions made in deriving the long wave equations, in general, hold very well for large bodies of water but are less justified when dealing with transitions and regions in which the flow is restricted, e.g. inlets. Unfortunately, the complete equations describing the flow in inlets are still very complex and difficult to solve and therefore, recourse is taken to a semi-empirical representation.

The equation commonly used to describe flow in inlets is

$$g\,\bar{R}(\eta_i - \eta_o) = \pm \left(\frac{F\,Q^2\,L}{\bar{P}^2\,\bar{R}^2} + \frac{m\,\bar{R}\,Q^2}{2\bar{P}^2\,\bar{R}^2} \right) \tag{2.3}$$

+ sign for $Q \geq 0$

- sign for $Q \leq 0$.

See for example Keulegan [9]. In Equation (2.3)

$\bar{P}$ = wetted perimeter of inlet cross-section measured at mean ocean level

$\bar{R}$ = hydraulic radius for the inlet cross-section measured at mean ocean level

Q = total discharge

L = length of inlet

η_o = ocean tide

η_i = lagoon tide

m = coefficient which accounts for entrance losses and the non-uniform velocity distribution.

In Equation (2.3) second order effects have been neglected. A revised version of the inlet equation, including all second order terms, will be derived in the next paragraphs.

It is assumed that the flow in the inlet region is one dimensional and storage is neglected. The equation of conservation of mass then becomes

$$\frac{\partial Q}{\partial x} = 0 \qquad (2.4)$$

in which Q = total discharge.

To describe the dynamics of the flow, the inlet is divided into three regions as indicated in Figure 2. During flood, the flow in Region I is governed by the convective acceleration and the pressure forces; bottom friction and local acceleration are considered small. This leads, when neglecting the velocity head in the ocean, to the Bernoulli equation (the Bernoulli equation is the same as the energy equation when neglecting energy losses)

$$\eta_o = \frac{m_1 Q^2}{2gA_1^2} + \eta_1$$

in which

$A_1 = P_1 R_1$ = cross-sectional area at location 1 (see Figure 2).

For most inlets the bank slopes are steep and thus

$$R_1 \simeq \overline{R} + \frac{\overline{B}}{\overline{P}_1}\eta_1$$

$$P_1 \simeq \overline{P}_1$$

in which

$\overline{A}_1$ = cross-sectional area at location 1 measured at Mean Ocean Level

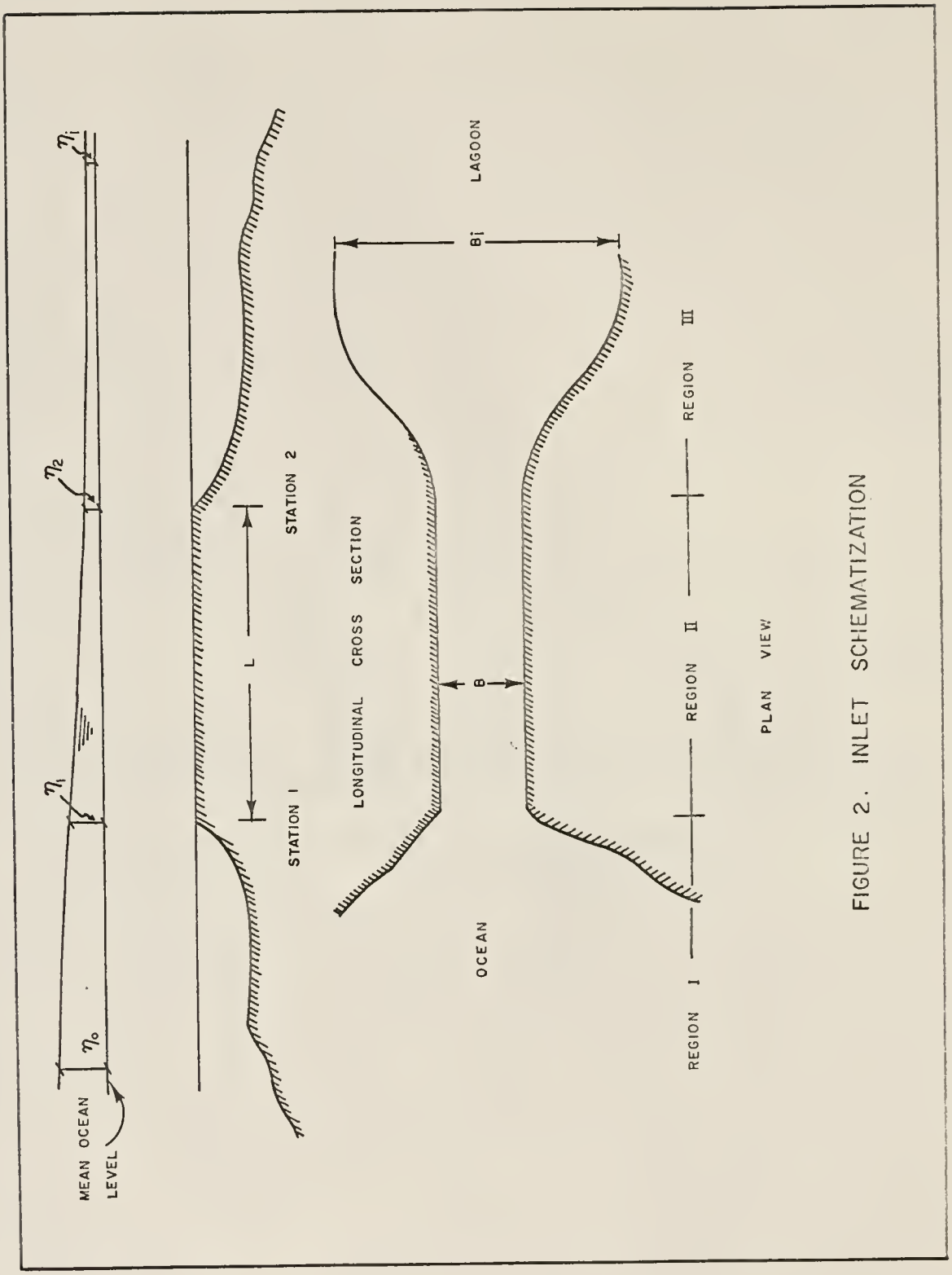

FIGURE 2. INLET SCHEMATIZATION

$\overline{B}$ = width of inlet measured at Mean Ocean Level.

Substituting the expressions for A_1, P_1 and R_1 in the Bernoulli equation yields

$$\eta_o = \frac{m_1 Q^2}{2g\overline{P}^2(\overline{R} + \frac{\overline{B}}{\overline{P}}\eta_1)^2} + \eta_1 \tag{2.5}$$

It is assumed that during ebb all the kinetic energy present at location 1 is lost. Neglecting bottom friction it then follows that for ebb

$$\eta_o = \eta_1 \tag{2.6}$$

The flow conditions in Region III are the reverse of those in Region I. Bernoulli's equation holds during ebb while energy dissipation takes place during flood. The only difference with Region III is that, in general, the velocity head at location i can no longer be neglected as was the case for the corresponding location 0 in Region I. For ebb flows, the equation for Region III now reads

$$\eta_2 + \frac{m_2 Q^2}{2g\,\overline{P}^2(\overline{R} + \frac{\overline{B}}{\overline{P}}\eta_2)^2} = \eta_i + \frac{m_i Q^2}{2g\,\overline{P}_i^2(\overline{R}_i + \frac{\overline{B}_i}{\overline{P}_i}\eta_i)^2} \tag{2.7}$$

Again neglecting bottom friction in Region III, the equation describing the flow during flood becomes

$$\eta_2 = \eta_i \tag{2.8}$$

In Region II, the actual restricted part of the inlet, only pressure forces and bottom friction are taken into account and thus

$$A \frac{\partial \eta}{\partial x} = - P \frac{\tau_o}{\rho g} \tag{2.9}$$

in which $A = \overline{A} + B\eta$ = cross-sectional area

$P \simeq \overline{P}$ = wetted perimeter

τ_o = bottom shear stress

ρ = density of water.

The bottom shear stress is related to the discharge and cross-sectional area by the empirical relation

$$\tau_o = \rho \frac{FQ|Q|}{A^2} \tag{2.10}$$

Furthermore $\overline{A} = \overline{R}\,\overline{P}$.

Substituting these expressions for P, τ_o and A in Equation (2.9) and rearranging slightly yields

$$g(\overline{R} + \frac{\overline{B}}{\overline{P}} \eta) \frac{\partial \eta}{\partial x} = - \frac{FQ|Q|}{\overline{P}^2 (\overline{R} + \frac{\overline{B}}{\overline{P}} \eta)^2} \tag{2.11}$$

This equation holds for both ebb and flood. Integrating Equation (2.11) with respect to x between Stations 1 and 2, the resulting expression can be written, to $O(\eta^2)$ as

$$g(\overline{R} + \frac{\overline{B}}{\overline{P}} \frac{\eta_1 + \eta_2}{2})^3 (\eta_2 - \eta_1) = + \frac{FQ|Q|L}{\overline{P}^2} \tag{2.12}$$

This particular form of Equation (2.12) was chosen to be comparable with Equation (2.3). Equations (2.5), (2.8) and (2.12) are then combined. It is assumed that the velocity head in Equation (2.5) is of $0(\eta)$. When neglecting terms of $0(\eta^3)$ and higher, the following equation describing the dynamics of the flow in the inlet during flood, $Q < 0$, is obtained.

$$g(\bar{R} + \frac{\bar{B}}{\bar{P}} \frac{\eta_o + \eta_i}{2})(\eta_i - \eta_o) = - \frac{FQ^2L}{\bar{P}^2(\bar{R} + \frac{\bar{B}}{\bar{P}} \frac{\eta_o + \eta_i}{2})^2}$$

$$- \frac{m_1 Q^2 \bar{R}}{2\bar{P}^2[\bar{R} + \frac{\bar{B}}{\bar{P}}(\eta_o - \frac{m_1 Q^2}{2g\bar{P}^2\bar{R}^2})]^2}$$

$$+ \frac{m_1 Q^2}{2\bar{P}^2\bar{R}^2}(-2\frac{\bar{B}}{\bar{P}}\eta_o + \frac{\bar{B}}{\bar{P}}\eta_i + \frac{3}{2}\frac{\bar{B}}{\bar{P}}\frac{m_1 Q^2}{2g\bar{P}^2\bar{R}^2}) \qquad (2.13)$$

Similarly for ebb, $Q > 0$, it follows by combining Equations (2.6), (2.7) and (2.12)

$$g(\bar{R} + \frac{\bar{B}}{\bar{P}} \frac{\eta_o + \eta_i}{2})(\eta_i - \eta_o) = \frac{FQ^2L}{\bar{P}^2(\bar{R} + \frac{\bar{B}}{\bar{P}} \frac{\eta_o + \eta_i}{2})^2}$$

$$+ \frac{m_2 Q^2 \bar{R}}{2\bar{P}^2[\bar{R} + \frac{\bar{B}}{\bar{P}}(\eta_i + \frac{m_i Q^2}{2g\bar{P}_i^2\bar{R}_i^2} - \frac{m_2 Q^2}{2g\bar{P}^2\bar{R}^2}]^2} - \frac{m_i Q^2 \bar{R}}{2\bar{P}_i^2(\bar{R}_i + \frac{\bar{B}_i}{\bar{P}_i}\eta_i)^2}$$

$$+ \left(\frac{m_2 Q^2}{2\bar{P}^2\bar{R}^2} - \frac{m_i Q^2}{2\bar{P}_i^2\bar{R}_i^2} \right)\left(- \frac{\bar{B}}{\bar{P}} \eta_o + 2 \frac{\bar{B}}{\bar{P}} \eta_i - \frac{3}{2} \frac{\bar{B}}{\bar{P}} \frac{m_2 Q^2}{2g\bar{P}^2\bar{R}^2} \right.$$

$$\left. - \frac{m_i Q^2}{2g\bar{P}_i^2\bar{R}_i^2} \right) \qquad (2.14)$$

Equations (2.13) and (2.14) are the same as Equation (2.3) when neglecting the second order terms and also the velocity head in the lagoon and assuming $m_1 = m_2 = m$. Finally, it is noted that in deriving Equations (2.13) and (2.14) the actual restricted part of the inlet, Region II, is assumed to be a prismatic channel. Many inlet channels do not fulfill this condition, because the width and depth vary from point to point. In that case, the irregular channel may be replaced by a prismatic one having the same discharge for a given head difference. For a detailed outline of this procedure, see Keulegan [9], page 19.

3. NUMERICAL SOLUTION OF THE TIDAL EQUATIONS

The numerical procedure presented here is based upon an explicit finite difference scheme; the unknowns depend only on values previously computed at a lower time level. This, in general, leads to a more stringent stability requirement (see for instance Vreugdenhil [30]) as compared to implicit methods but has the advantage that the different steps in the computation are easier to trace.

The numerical scheme is space and time staggered. Water levels are computed at $n.\Delta t$ and discharges at $(n + 1/2)\Delta t$. The water levels apply at the center of the grid blocks and the discharges are computed at the gridlines; see Figure 3. The mean depth h and the lateral inflow or rainfall are given at the time level and location of η. The basic recurrence equations for the one-dimensional tidal equations are

$$q'(i) = \frac{1}{G(i-1)} \left[q(i) + \frac{g\Delta t}{2\Delta x} (D(i) + D(i-1))(\eta(i-1) - \eta(i)) \right] \qquad (3.1)$$

$$\eta'(i) = \eta(i) + \frac{\Delta t}{\Delta x} (q'(i) - q'(i+1)) + M(i)\Delta t \qquad (3.2)$$

in which

$$D(i) = \eta(i) + h(i)$$

$$G(i-1) = 1 + \frac{4F\,\Delta t\,|q(i)|}{(D(i) + D(i-1))^2} + 2\,\frac{\Delta t}{\Delta x}\,\frac{(q(i+1) - q(i-1))}{(h(i) + h(i-1))}$$

Primed symbols denote values of the variables at time step Δt later. Equations (3.1) and (3.2) are based respectively upon the differential Equations (2.2) and (2.1). The differential quotients in these

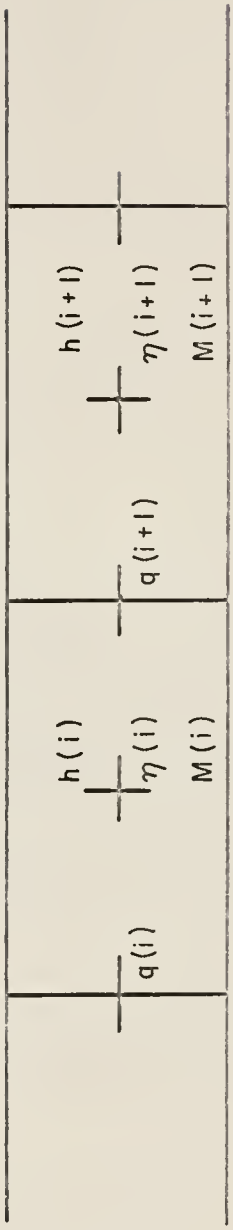

FIGURE 3. LOCATION OF VARIABLES IN THE NUMERICAL GRID

equations are replaced by different quotients using central differences. The difference quotients for Equation (2.1) are centered about $(n + 1/2)\Delta t$ and the location of η. The difference quotients for Equation (2.2) are centered about time level $n\Delta t$ and are centered in space about the location of q. Starting from the initial conditions, all the q's are computed for the next time level by means of Equation (3.1), then the η's are computed using Equation (3.2). It is noted that because of the convective acceleration, the recurrence formula (3.1) includes values as far apart as 2 space steps; see expression for G(i-1). This leads to difficulties when the boundary conditions at open boundaries are given as water levels. In that case, the convective acceleration is taken off center for the grids adjacent to those boundaries. For a more detailed outline of the numerical scheme, the reader is referred to Reid and Bodine [18] and Verma and Dean [28].

Because of the nonlinearities in the differential equations, the existing mathematical theory is inadequate to determine the exact criteria for stability and convergence of the numerical scheme. However, some insight might be obtained by regarding a simplified set of equations. The equations describing the tidal flow, Equations (2.1) and (2.2), may be replaced by two wave equations in respectively η and q, when neglecting the nonlinear terms and the source term, and assuming a horizontal bottom. It then can be shown, starting from the recurrence formulae for the simplified set of equations that, for this case, the difference scheme is equivalent to solving the wave equation on the mesh Δx, Δt. The stability and convergence criterion then is (see Platzman [16])

$$\frac{\Delta x}{\Delta t} > \sqrt{gh}$$

(For the two-dimensional equations the condition is $\frac{\Delta x}{\Delta t} > \sqrt{2gh}$.)

When regarding the solution of the tidal equations as a sum of Fourier components, stability as used here implies that there should be a limit to the extent to which any component of the solution is amplified in the numerical procedure. Platzman [16] showed that even before the stability criterion is reached, the amplitude of especially the highest modes might be greatly magnified and might obscure the true solution. To study the eventual magnification of higher harmonies, a few computations were carried out for a 17-mile-long and 7-ft.-deep channel, open at one end and closed at the other. In addition, these computations provided some insight as to whether the terms neglected when discussing the stability criteria in the previous paragraph give rise to instabilities. The tide at the open end of the channel was sinusoidal with an amplitude of 1.5 ft. and a period of 12.5 hours. The computations were carried out for values of the friction factor $F = 0.002$ and $F = 0.004$ and for the time steps $\Delta t = 100$ sec., $\Delta t = 200$ sec. and $\Delta t = 300$ sec. The space step $\Delta x = 5000$ ft. was the same for all computations. The stability criterion for the case discussed here is $\Delta t = \frac{\Delta x}{\sqrt{gh}} = 333$ sec. Each computation extended over 4 tidal cycles. The results were judged visually; no overflow occurred, and amplification of higher modes was not apparent. The source term and the free surface forces were not included in the computations.

In the computational procedure, the inlet equations, Equations (2.13) and (2.14) may be regarded as an implicit boundary condition for the flow in the lagoon. The way in which this boundary condition is incorporated in the numerical scheme depends on the inlet configuration. The following two cases are considered:

- An inlet connecting a lagoon to the ocean such that no branching of the inlet flow occurs; see Figure 4a.
- An inlet connecting a lagoon to the ocean such that branching of the inlet flow can occur; see Figure 4b.

Consider the "nonbranching inlet;" see Figure 4a. The total discharge Q rather than the discharge per unit width, q, is used as a dependent variable. An auxiliary water level η_i is introduced which is computed at the same time level as the water levels in the lagoon. Starting from the initial conditions, all the discharges in the lagoon except Q(i + 1) can be computed using the procedure described before. The value of Q(i + 1) is then computed as follows. Q(i + 1) is related to the known ocean level η_o and the auxiliary level η_i by means of the inlet equations. The difference form of the inlet equations used here is based on the following simplified form of Equations (2.13) and (2.14).

$$g(\bar{R} + \frac{\bar{B}}{\bar{P}} \frac{\eta_o + \eta_i}{2})(\eta_i - \eta_o) = \pm \frac{FQ^2 L}{\bar{P}^2 (\bar{R} + \frac{\bar{B}}{\bar{P}} \frac{\eta_o + \eta_i}{2})^2} \pm \frac{mQ^2 \bar{R}}{2\bar{P}^2 (\bar{R} + \frac{\bar{B}}{\bar{P}} \frac{\eta_o + \eta_i}{2})^2}$$

- sign for $\eta_i \leq \eta_o$

+ sign for $\eta_i \geq \eta_o$.

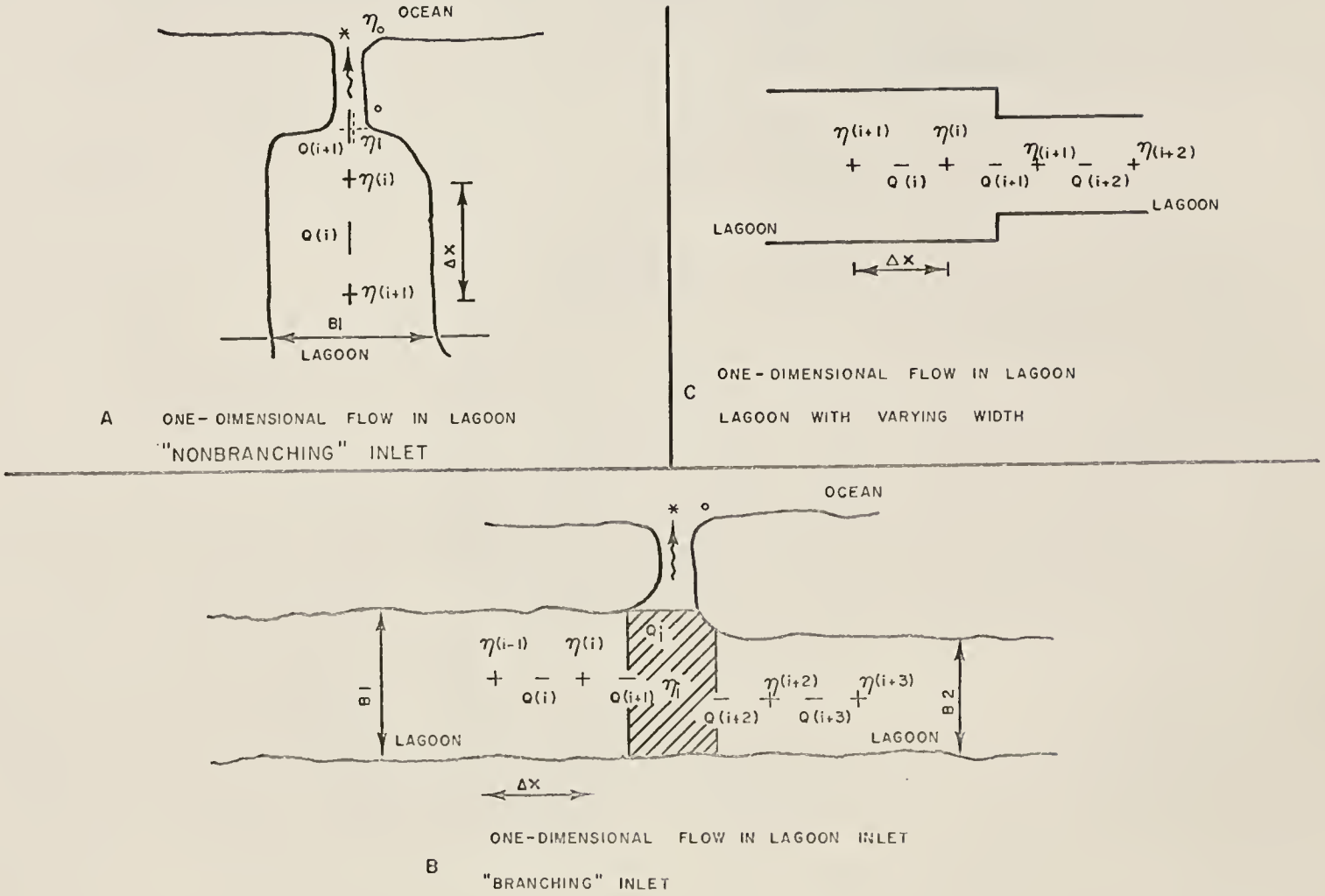

FIGURE 4. GRID SCHEME FOR DIFFERENT INLET CONFIGURATIONS

It is assumed that $m_1 = m_2 = m$. After some algebraic manipulation, the following result is obtained.

$$Q = \pm DD \sqrt{|\eta_i - \eta_o|}$$

+ sign for $\eta_i \geq \eta_o$

- sign for $\eta_i \leq \eta_o$

in which

$$Q = \frac{Q'(i+1) + Q(i+1)}{2} \tag{3.3}$$

$$DD = \sqrt{\frac{2g\bar{P}^2}{2FL + m\bar{R}}} \left(\bar{R} + \frac{\bar{B}}{\bar{P}} \frac{\eta_o + \eta_i}{2}\right)^{3/2}$$

It is noted that for many practical cases the modifications made in Equations (2.13) and (2.14) are justified. They were introduced here to simplify the algebra; however, the computational procedure applies equally well when using the complete Equations (2.13) and (2.14).

A second equation relating $Q(i + 1)$ and η_i is found by applying the dynamic equation, Equation (2.2), between the discharge stations $Q(i + 1)$ and $Q(i)$. Note that when computing the flow in the lagoon, the dynamic equations are applied between two water level stations. The difference form of the dynamic equation applied between $Q(i + 1)$ and $Q(i)$ yields

$$Q = AA(\eta_i - \eta_o) + BB + AA\,\eta_o \tag{3.4}$$

in which

$$Q = \frac{Q'(i+1) + Q(i+1)}{2}$$

$$AA = \frac{-g\ D(i)\ B1\ \Delta t}{G\Delta x}$$

$$BB = \{Q(i+1) + Q(i) - Q'(i) \cdot G + \frac{g\ B1\ D(i)\ \Delta t}{\Delta x}$$

$$[\eta(i) + \eta(i-1)]\} \Big/ 2G + \frac{Q(i+1)}{2}$$

$$G = 1 + \frac{F\Delta t|Q(i+1) + Q(i)|}{2D(i)^2 B1} + \frac{2\Delta t[Q(i+1) - Q(i)]}{\Delta x h(i) B1}$$

In determining the difference form, the terms in both the inlet and dynamic equation are centered about n · Δt.

The general shapes of the curves $Q = f(\eta_i - \eta_o)$ represented by the Equations (3.3) and (3.4) are indicated in Figure 5. Equation (3.4) represents a straight line. The slope of this line, AA, is for most practical cases negative. Therefore, the sign of $(BB + AA\eta_o)$, which is a known quantity, determines the sign of $(\eta_i - \eta_o)$ which in turn determines the sign to be used in Equation (3.3). Eliminating $(\eta_i - \eta_o)$ between Equations (3.3) and (3.4) yields

$$Q = \frac{1 - \sqrt{1 - 4\frac{AA}{DD^2}(AA\eta_o + BB)}}{2\frac{AA}{DD^2}} \qquad (3.5)$$

for $(BB + AA\eta_o) \geq 0$

and

$$Q = \frac{1 - \sqrt{1 + 4\frac{AA}{DD^2}(AA\eta_o + BB)}}{-2\frac{AA}{DD^2}} \qquad (3.6)$$

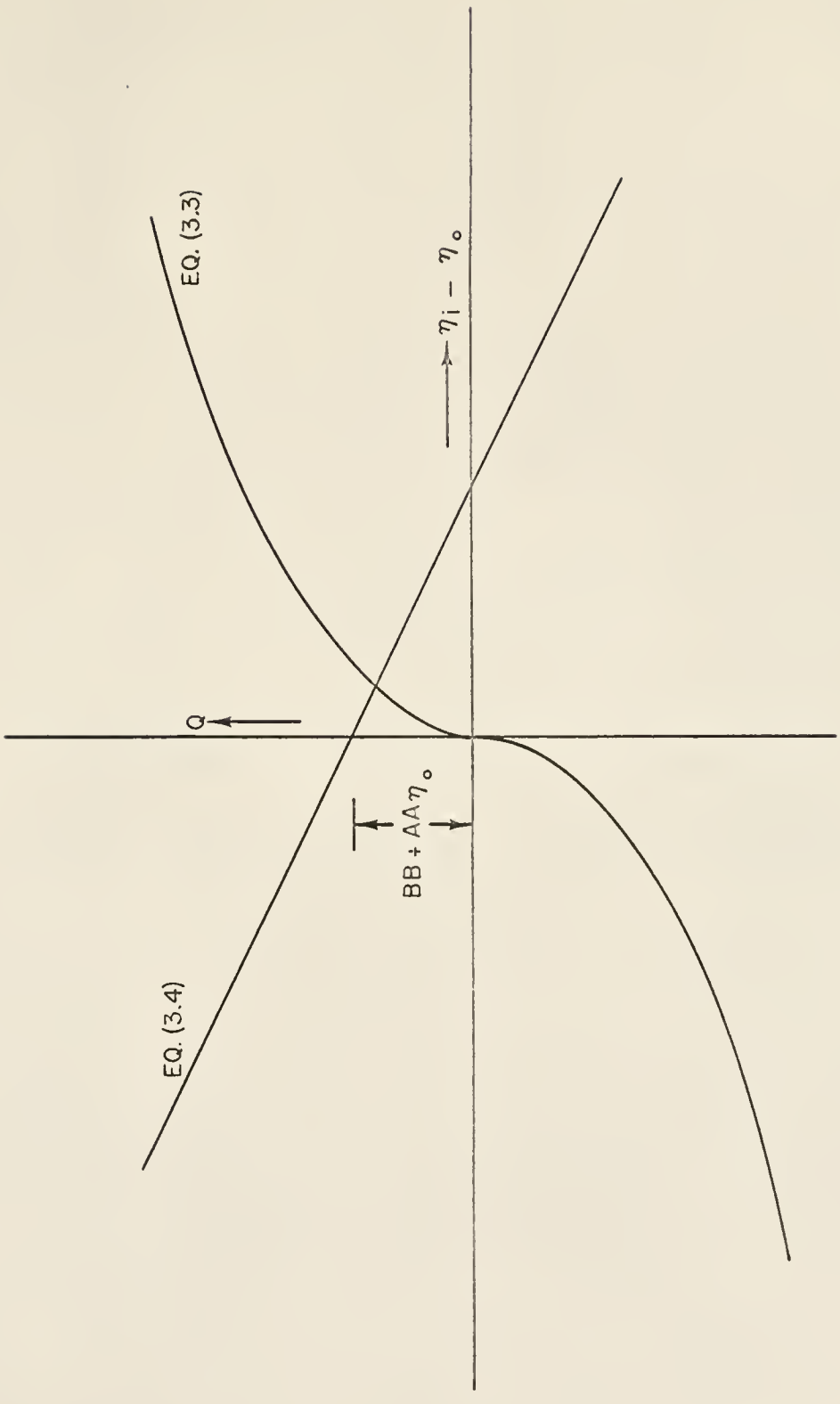

FIGURE 5. CURVES REPRESENTED BY EQUATIONS (3.3) AND (3.4)

for $(BB + AA\eta_o) \leq 0$.

Note that only the first order terms in $(\eta_i - \eta_o)$ are eliminated because second order terms are still present in the factor DD. Equations (3.5) and (3.6) therefore may be regarded as being quasi-linear, which suggests finding a solution by means of a perturbation method. First the value of $(\eta_i - \eta_o)$ in DD is taken equal to the value at the previous time step. The value of Q can then be found from Equation (3.5) or (3.6) depending on the sign of $(BB + AA\eta_o)$. Knowing Q, the value of $(\eta_i - \eta_o)$ is determined from either Equation (3.3) or (3.4). This value of $(\eta_i - \eta_o)$ is substituted in DD. The procedure then is repeated until the difference between the computed and previously computed value of Q is within certain limits.

The numerical scheme for the "branching inlet" (see Figure 4b) involves four unknowns Q'(i+1), Q'(i+2), Q_i' and η_i as compared to only two, Q(i+1) and η_i, for the "nonbranching inlet." The four unknowns are related by the following four equations

- the inlet equation which takes the form of Equation (3.3) with $Q = \dfrac{Q_i' + Q_i}{2}$
- the dynamic equation applied between the locations of Q(i) and Q(i+1); this equation takes the form of Equation (3.4).
- the dynamic equation applied between the locations of Q(i+2) and Q(i+3); this equation takes the form of Equation (3.4) with Q(i) replaced by Q(i+3), Q(i+1) replaced by Q(i+2), η(i) replaced by η(i+2), η(i-1) replaced by η(i+3), h(i) replaced by h(i+2), Δx replaced by $-\Delta x$, and B1 replaced by B2.

- the continuity condition which, when assuming that the water level in the hatched area is the same everywhere, takes the form

$$Q(i+1) = Q_i + Q(i+2)$$

Elimination of Q(i+1) and Q(i+2) between the two dynamic equations and the continuity equation yields a relation between Q_i and η_i similar to Equation (3.4). This equation together with the inlet equation then can be solved following the procedure described before.

Finally, it is noted that in one-dimensional flow computations, it is often necessary to divide the lagoon into parts with different widths; see Figure 4c. The flow at the boundary of two such parts may be computed following a procedure similar to the one applied to the "nonbranching inlet," replacing the inlet equation by a second dynamic equation between the location of Q(i+1) and Q(i+2).

The foregoing procedure of incorporating the inlet equations in the numerical scheme, including the case with two-dimensional flow in the lagoon, can also be found in Chiu, Van de Kreeke and Dean [2].

4. DETERMINATION OF THE FRICTION FACTOR F

The factor F in the friction term of the conservation of momentum equation is difficult to estimate in advance; therefore, an appropriate value is usually based on measurements. Two methods for determining F are compared. One method is based on matching computed and measured water levels, the other is based on matching computed and measured discharges. Special attention is given to the influence of errors in the measured water levels and discharges on the value of F.

To calibrate a tidal model, i.e., to determine the value of F, the area covered by the model is divided into sections each with approximately uniform geometry for which the values of F may be assumed constant. It is assumed that at both ends of each section the water levels are known from measurements. Given these water levels and assuming a value of F, the water levels and discharges within each section can be computed. The computations are carried out for different values of F until a good match exists between computed and measured water levels or discharges. The F value obtained in this manner reflects, in addition to friction, the effects of schematization, neglected terms in the equations and measurement errors. These effects may cause large variations in the value of F during a tidal cycle especially during periods of slack tide when the inertia forces are predominant. Therefore, in determining F these periods should be disregarded. Furthermore, a realistic value of F, that is a value mainly determined by friction and more or less constant during a tidal cycle can only be obtained in cases for which the flow is friction-dominated during the larger part of the tidal cycle (see Dronkers [5], page 425). It should be noted that in

many actual cases not all of the field data necessary for this ideal procedure are available. In that case recourse should be taken to trial and error methods.

As stated before, measurement errors result in errors in F. In this paragraph, some general considerations concerning these errors are put forward. In the next paragraph an example will be presented showing the order of magnitude of the errors in F resulting from errors in the "calibration curves" (a calibration curve is defined as measured water levels or discharges within a section and used to determine F by matching with computed water levels or discharges). The water surface in each section may, as a first approximation, be regarded as a straight line because in practice the length of the sections are small compared to the length of the tidal wave. The end points of the straight line are determined by the water levels at the boundaries. Therefore a change in F will hardly affect the computed water level in the section. From this it may be inferred that, when determining F by matching computed and measured water levels, an error in the latter or in the boundary conditions will lead to a large error in F. When calibrating on discharges the effect of measuring errors can be expressed as follows. During periods of friction-dominated flow a first approximation of the equation of conservation of momentum is

$$gh \frac{\partial \eta}{\partial x} = - \frac{Fq|q|}{h^2}$$

and thus

$$\varepsilon(F) = \varepsilon\left(\frac{\partial \eta}{\partial x}\right) + \varepsilon(q|q|)$$

in which ε = relative error.

The error in F thus is of the same order as the error in the boundary conditions $\left(\frac{\partial \eta}{\partial x}\right)$ and the calibration curve (q).

The following example serves to illustrate the order of magnitude of errors in F due to errors in the calibration curve. Consider a section with a constant depth h = 7 ft. and a length L = 50,000 ft. The boundary condition at x = 0 is $\eta_1 = 1.3 \sin (2\pi t/45000)$ and at x = L is $\eta_2 = 1.3 \sin (2\pi(t-2700)/45000)$; see Figure 6a. The water levels and discharges in the middle of the section are computed for F = 0.002, F = 0.0025 and F = 0.003. The results are plotted in Figures 6b and 6c. The differences between the water levels for the different values of F were too small to be reproduced in the figure. In addition, for the same location and for F = 0.002, the values of the different terms in the equation of conservation of momentum are plotted; see Figure 6d. The latter results provide some insight in the relative magnitude of the forces and accelerations represented by these terms and their phase relationship with water levels and discharges. It may be seen from Figure 6d that the flow is friction-dominated during the larger part of the tidal cycle, which as stated before is a condition to arrive at a realistic value of F. When using a measured water level in the section as calibration curve, the effect of an error in this curve on the F value can be demonstrated as follows. Let the curve corresponding to F = 0.002 in Figure 6b represent the correct water level (calibration curve) in the section. Let the curve

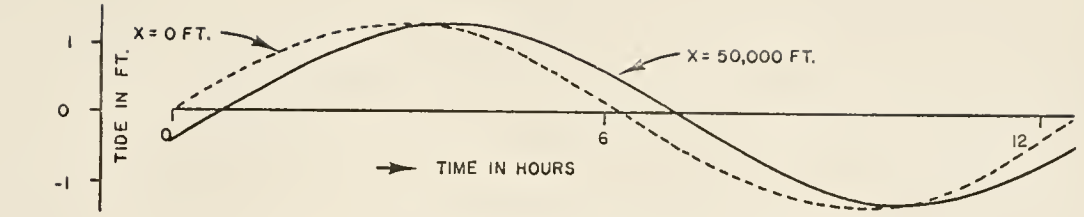

(a) TIDE AT X = 0 FT. AND X = 50,000 FT.

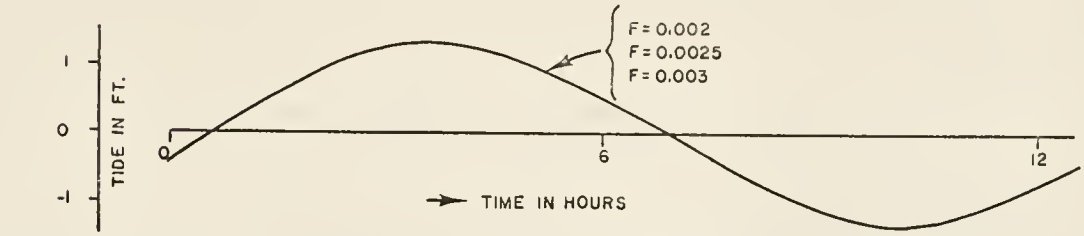

(b) TIDE AT X = 25,000 FT.

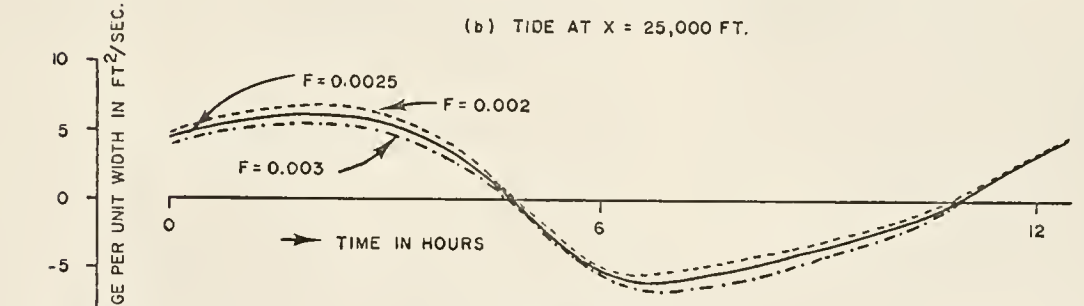

(c) DISCHARGE AT X = 25,000 FT.

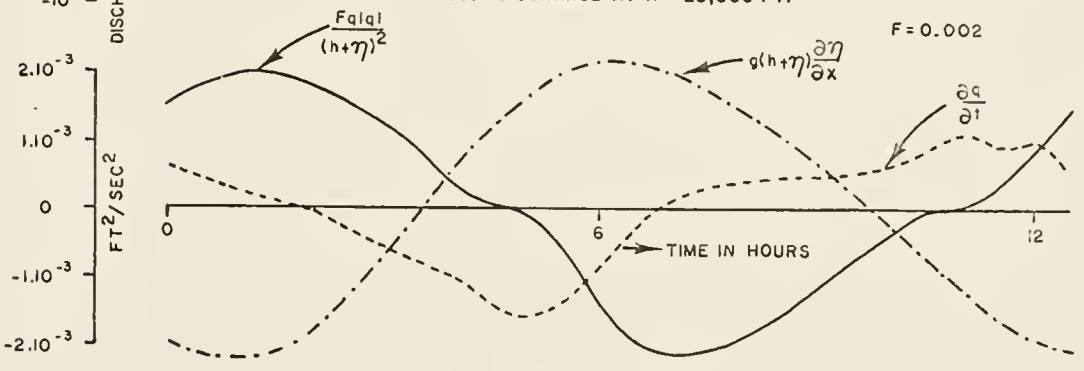

(d) MAGNITUDE OF TERMS IN CONSERVATION OF MOMENTUM EQUATION AT X = 25,000 FT.

FIGURE 6. TIDE IN A SEA LEVEL CANAL

corresponding to F = 0.003 in the same figure be the measured calibration curve. This curve deviates from the correct curve at the most by 0.03 ft.;* the relative error (maximum deviation divided by tidal amplitude times hundred) is 2%. An error of 2% in the water level (calibration curve) would thus lead to a ($\frac{0.003 - 0.002}{0.002} \cdot 100\% =$) 50% error in F and as may be seen from Figure 6c an error of 20% in q. The influence of errors in the calibration curve on the F value when using discharges can be demonstrated in a similar way. Let the curve in Figure 6c corresponding with F = 0.002 be the correct discharge curve. Consider the curve corresponding with F = 0.0025 in the same figure to be the measured discharge curve. The relative error in the measured discharge is approximately 10%. The resulting error in F is 25% and the error in the water level appears to be 1.2%.

To summarize for the example presented here, when calibrating on the water level a maximum error of 2% in the water level leads to an error of 50% in F and a maximum error in q of 20%. When calibrating on a discharge curve an error of 10% in the calibration curve leads to an error of 25% in F and a maximum error in the water level of 1.2%.

The relative errors in the measured water levels and discharges of respectively 2% and 10% used in the previous example are realistic values for conventional types of equipment and measuring procedures. Also the example is a typical case for flow in lagoons of the type considered here. Therefore it may be safely concluded that, when

---

*This value cannot be read from Figure 6b; it was taken directly from the computer output.

calibrating on water levels and assuming that the boundary conditions for a section are given as water levels, small inaccuracies in the measured calibration curve lead to large errors in F and q. When calibrating on discharges, the errors resulting from inaccuracies in the calibration curves are far less.

5. MASS TRANSPORT IN LAGOONS DUE TO TIDAL ACTION

In this chapter an analytic solution is presented for the mass transport due to tidal waves in lagoons. The analytic approach is restricted to lagoons and inlets of relatively simple geometry, which prohibits its application to the often irregular shaped tidal waters in nature. In such cases, recourse has to be taken to numerical techniques. Therefore the analytic model cannot replace the numerical procedure; it merely serves to build faith in the numerical results and to obtain a better understanding of the physics underlying the phenomenon of mass transport. In the final part of the chapter the effect of inlets on the net transport is discussed.

a. Analytic Solution; Physical Concepts

Consider a straight lagoon of finite length ℓ in which the ocean tide can freely enter at both ends. The depth and width of the lagoon are uniform. The conservation of mass equation neglecting the source term is

$$\frac{\partial \eta}{\partial t} + \frac{\partial q}{\partial x} = 0 \tag{5.1}$$

The conservation of momentum equation, when neglecting the nonlinear terms except the friction term, reduces to

$$\frac{\partial q}{\partial t} + gh \frac{\partial \eta}{\partial x} = - \frac{Fq|q|}{(h + \eta)^2} \tag{5.2}$$

The term on the right-hand side of Equation (5.2) was derived (see Appendix A) by relating the bottom shear stress and the mean velocity by means of a Darcy-Weisbach type friction law.

$$S = f \frac{1}{4R} \frac{u|u|}{2g} \tag{5.3}$$

in which S = slope of the water level

f = Darcy-Weisbach friction factor

u = mean velocity over depth

R = hydraulic radius.

Furthermore

$$\frac{\tau_o}{\rho} = - gRS \tag{5.4}$$

in which τ_o = bottom shear stress. From Equations (5.3) and (5.4), it then follows

$$\frac{\tau_o}{\rho} = - \frac{f}{8} u|u| \tag{5.5}$$

The friction term in Equation (5.2) will now be re-derived by replacing Equation (5.5) by its linearized version. Assume that as a first approximation the velocity u in the lagoon is simple harmonic in t

$$u = \hat{u} \cos(\sigma t + \alpha) \tag{5.6}$$

in which α = a phase angle. Substituting this expression for u in Equation (5.5) and expanding in a Fourier series yields

$$\frac{\tau_o}{\rho} = - \frac{f}{8} \frac{8}{3\pi} \hat{u}u + \text{third order term} + \ldots$$

The second, fourth, etc. harmonics are zero. Thus neglecting third order terms and higher yields

$$\frac{\tau_o}{\rho} = - \frac{f}{8} \frac{(\frac{8}{3\pi} \hat{u})q}{h + \eta} \tag{5.7}$$

When approximating

$$\frac{1}{h + \eta} = \frac{1}{h} - \frac{\eta}{h^2}$$

and introducing

$$F_\ell = \frac{f}{8} \frac{8}{3\pi} \hat{u} = F \frac{8}{3\pi} \hat{u} \tag{5.8}$$

Equation (5.7) may be written as

$$\frac{\tau_o}{\rho} = - \frac{F_\ell q}{h} + \frac{F_\ell q\eta}{h^2} \tag{5.9}$$

With this expression for the bottom friction, the conservation of momentum equation becomes

$$\frac{\partial q}{\partial t} + gh \frac{\partial \eta}{\partial x} = - \frac{F_\ell q}{h} + \frac{F_\ell q\eta}{h^2} \tag{5.10}$$

Equations (5.1) and (5.10) are used to describe the flow in the lagoon. Equation (5.1) is a linear equation while Equation (5.10) may be regarded as quasi-linear because the nonlinear term is small compared to the first term on the right-hand side. The ocean tides at both ends of the lagoon serve as the boundary conditions. To avoid lengthy computations, the amplitude and phase of the ocean tides are taken such that when neglecting the nonlinear term in Equation (5.10) the resulting solution represents a damped progressive wave. The water levels and discharges for such a wave as a function of x and t are

$$\eta = a\, e^{-\mu x} \cos(\sigma t - kx) \tag{5.11}$$

$$q = a\, c_o \frac{k_o}{\sqrt{\mu^2 + k^2}}\, e^{-\mu x} \cos(\sigma t - kx + \alpha) \tag{5.12}$$

in which μ, k and α are defined by

$$k_o^2 = k^2 - \mu^2$$

$$\frac{F_\ell}{h} = \frac{2\mu\sigma k}{k^2 - \mu^2}$$

$$\alpha = \tan^{-1}\left(\frac{\mu}{k}\right)$$

with $k_o = \sigma/c_o$ and $c_o = \sqrt{gh}$.

Thus when

$$\eta_o = a \cos \sigma t \tag{5.13}$$

is the boundary condition for $x = 0$, it then follows from Equation (5.11) that the boundary condition at $x = L$ should be

$$\eta_L = a\, e^{-\mu L} \cos(\sigma t - kL) \tag{5.14}$$

It is furthermore assumed that the mean level at both ends of the lagoon is the same and equal to the mean ocean level. A trial solution for Equations (5.1) and (5.10) when including the nonlinear term in the last equation and considering the boundary conditions (5.13) and (5.14) is

$$\eta = \eta_*(x) + a\, e^{-\mu x} \cos(\sigma t - kx) + \ldots \tag{5.15}$$

$$q = q_*(x) + a\, c_o \frac{k_o}{\sqrt{\mu^2 + k^2}} e^{-\mu x} \cos(\sigma t - kx + \alpha) + \ldots \qquad (5.16)$$

Substituting this trial solution in Equation (5.1) and averaging over the tidal period yields

$$\frac{\partial q_*}{\partial x} = 0 \qquad (5.17)$$

(Note: This must be true for any periodic forcing function.) Substituting in Equation (5.10) and neglecting higher order terms yields after time averaging

$$gh \frac{\partial \eta_*}{\partial x} = - \frac{F_\ell}{h} q_* + \frac{F_\ell}{h} \frac{a^2 c_o}{2h} \frac{k_o k}{\mu^2 + k^2} e^{-2\mu x} \qquad (5.18)$$

For $x = 0$ and $x = L$, $\eta_* = 0$ because of the assumption that at both ends of the lagoon the mean level equals the mean ocean level. With these boundary values of η_* the solutions for η_* and q_* from Equations (5.17) and (5.18) are

$$q_* = \frac{a^2 c_o}{2h} \frac{1}{2\mu} \frac{k_o k}{\mu^2 + k^2} \frac{1}{L} (1 - e^{-2\mu L}) \qquad (5.19)$$

$$\eta_* = \frac{F_\ell}{gh^2} \frac{a^2 c_o}{2h} \frac{k_o k}{\mu^2 + k^2} \frac{1}{2\mu} \left[\frac{x}{L} (e^{-2\mu L} - 1) - (e^{-2\mu x} - 1) \right] \qquad (5.20)$$

Equation (5.19) is the expression for the net discharge in a straight lagoon when imposing the boundary conditions (5.13) and (5.14) and assuming the same mean level at both ends of the lagoon. Equation (5.20) represents the mean water level in the lagoon.

The following serves as an explanation of the physics underlying the expression for the net transport and mean water level in a lagoon derived in the preceding paragraph. Considered is a damped progressive wave in an infinitely long channel. The velocity u, rather than the discharge per unit width q, is introduced as a dependent variable. Assuming a horizontal bottom Equations (5.1) and (5.10), which represent the conservation of mass and conservation of momentum, can be written as respectively

$$\frac{\partial \eta}{\partial t} + h \frac{\partial u}{\partial x} = - \frac{\partial u \eta}{\partial x} \tag{5.21}$$

and

$$h \frac{\partial u}{\partial t} + gh \frac{\partial \eta}{\partial x} = - \frac{\partial u \eta}{\partial t} - F_{\ell} u \tag{5.22}$$

The expressions for the damped progressive wave and the accompanying velocity field, satisfying the linear part of Equations (5.21) and (5.22), are

$$\eta = a\, e^{-\mu x} \cos(\sigma t - kx)$$

$$u = \frac{a c_o}{h} \frac{k_o}{\sqrt{\mu^2 + k^2}}\, e^{-\mu x} \cos(\sigma t - kx + \alpha)$$

See, for example, Ippen [8], page 507.

The net transport accompanying such a wave, q_{*_w}, may be found from

$$q_{*_w} = \frac{1}{T} \int_0^T \int_{-h}^{\eta} u \, dz \, dt$$

Substituting the expression for u in this equation and integrating yields

$$q_{*_w} = \frac{a^2 c_o}{2h} \frac{k_o k}{\mu^2 + k^2} e^{-2\mu x} \tag{5.23}$$

This expression shows the net transport to decrease with increasing x. Continuity requires the net discharge to be the same for every cross-section and equal to the net discharge at x = 0. Conveniently taking the net discharge at x = 0 equal to zero, the net discharge in the channel, q_*, is written as

$$q_* = q_{*_w} + q_{*_s} = 0 \tag{5.24}$$

in which q_{*_s} results from the slope in the mean water level

$$q_{*_s} = - \frac{gh}{F_\ell / h} \frac{\partial \eta_*}{\partial x} \tag{5.25}$$

Substituting the expression for q_{*_w} and q_{*_s}, respectively Equations (5.23) and (5.25), in Equation (5.24) yields

$$\frac{a^2 c_o}{2h} \frac{k_o k}{\mu^2 + k^2} e^{-2\mu x} - \frac{gh}{F_\ell / h} \frac{\partial \eta_*}{\partial x} = 0 \tag{5.26}$$

Integration of Equation (5.26) and arbitrarily setting $\eta_* = 0$ at x = 0 yields

$$\eta_* = \frac{F_\ell}{h} \frac{1}{gh} \frac{1}{2\mu} \frac{a^2 c_o}{2h} \frac{k_o k}{\mu^2 + k^2} (1 - e^{-2\mu x}) \tag{5.27}$$

Equation (5.27) represents the mean water level in an infinite long channel in the presence of a free damped progressive wave and zero net transport. See also Figure 7a.

When regarding a channel or lagoon of finite length L, at both ends connected to the ocean, the mean level at x = 0 and x = L is the same and equal to the mean level in the ocean. The resulting net flow and mean water level in the channel of finite length can be derived from the mean flow and mean water level for the infinite long channel, as follows. A slope

$$S_m = - \frac{\eta_*(L)}{L}$$

is added to the mean water surface in the infinite channel, which renders the mean level at x = L zero. The expression for the mean water surface becomes

$$\eta_* = - \frac{\eta_*(L)}{L} x + \frac{F_\ell}{h} \frac{1}{gh} \frac{1}{2\mu} \frac{a^2 c_o}{2h} \frac{k_o k}{\mu^2 + k^2} (1 - e^{-2\mu x}) \qquad (5.28)$$

See Figures (7b) and (7c).

Substituting the expression for $\eta_*(L)$ from Equation (5.27) in Equation (5.28) yields Equation (5.20).

The discharge q_{*_m} accompanying the slope S_m is

$$q_{*_m} = - \frac{gh}{F_\ell/h} \frac{\eta_*(L)}{L} \qquad (5.29)$$

and the total net transport q_* is

$$q_* = 0 - \frac{gh}{F_\ell/h} \frac{\eta_*(L)}{L} \qquad (5.30)$$

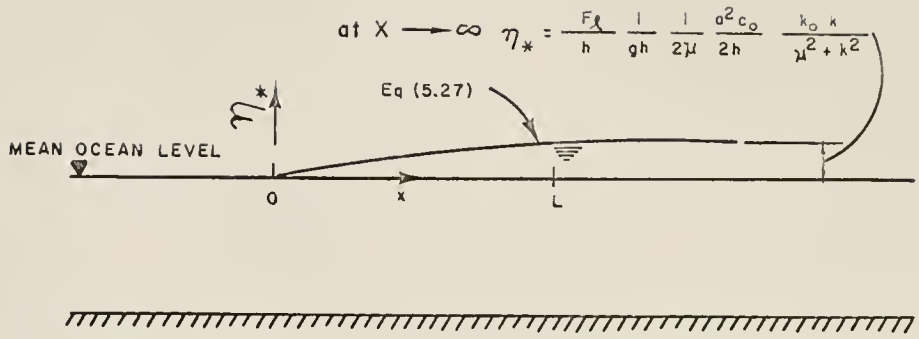

a. MEAN WATER LEVEL IN AN INFINITELY LONG CHANNEL

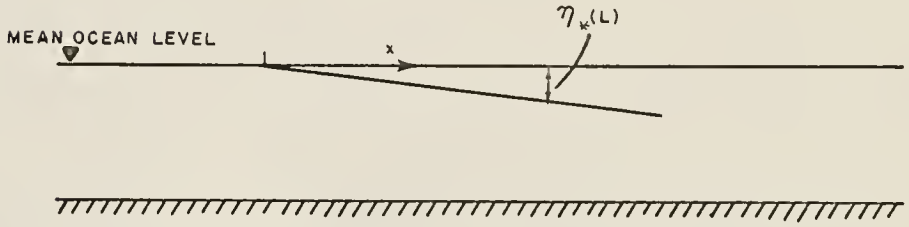

b. SLOPE , S_m

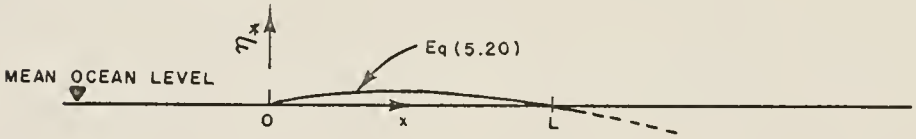

c. MEAN WATER LEVEL IN CHANNEL OF FINITE LENGTH, L

FIGURE 7. MEAN WATER LEVEL IN A LAGOON IN THE PRESENCE OF A DAMPED PROGRESSIVE WAVE

Substituting the expression for $\eta_*(L)$ as given by Equation (5.27) yields Equation (5.19).

It may be inferred from the previous considerations that the net transport in the finite channel may be regarded as the result of forcing the mean level at the boundaries to be different from the mean level at these boundaries in the case of a free wave. Note also that in case the friction approaches zero the expression for the net transport, Equation (5.19), approaches

$$q_* = \frac{a^2 c_o}{2h} \tag{5.31}$$

which is the expression for the net transport accompanying a free undamped wave with amplitude a, traveling in shallow water.

When substituting the trial solutions Equations (5.15) and (5.16) in Equation (5.10), all higher order terms were neglected. To evaluate the effect of these terms on the net transport the q_* as given by Equation (5.19) is compared with the true q_*, by taking into account the third and higher order terms. The true q_* is found by numerically integrating Equations (5.1) and (5.10) with the boundary conditions (5.11) and (5.12) following the procedure described in Chapter 3 and then averaging q over a tidal period. The computations were carried out for a lagoon with a length L = 70,000 ft. and a depth h = 7 ft., a tidal period T = 45,000 sec., a time step Δt = 100 sec., and a space step Δx = 5,000 ft. Two values for the amplitude a and three values for the linear friction factor F_ℓ are considered. The results of both the analytic and numerical (true) solution are presented

in Figure 8. From this figure, it may be seen that neglecting the third and higher order terms introduces only a very slight error.

The question might arise whether the "linearization" of the friction term as outlined on pages 31 and 32 is a valid procedure when discussing effects caused by second order terms in the equations. To shed some light on this, the net discharges when using Equations (5.1) and (5.10) and the net discharges when using Equations (5.1) and (5.2), which include the quadratic friction, are compared. The same lagoon is considered as in the previous paragraph. The boundary conditions again are presented by Equations (5.11) and (5.12). The "linear" friction factor F_ℓ and the "nonlinear" friction factor F are related by Equation (5.8). The value of $\hat{u}$ in this equation is taken equal to the average of the $\hat{u}$ values at both ends and the $\hat{u}$ in the middle of the lagoon. The equations are integrated numerically using a time step Δt = 100 sec. and a space step Δx = 5000 ft. To find q_*, q is averaged over a tidal period. Two different values for the amplitude a and three values for the friction factor F are considered. The results, which are plotted in Figure 9, compare well especially considering the way in which $\hat{u}$ was determined. The agreement is better for larger than for smaller values of F which probably stems from the fact that for larger values of the net flow and thus smaller values of F, the approximation of u as given by Equation (5.6) becomes less justified. It is noted that methods do exist to arrive at a better estimate of the representative average value $\hat{u}$. However, incorporating these methods would lead to a considerable increase in computational effort which is not warranted by the purpose of the computations. The

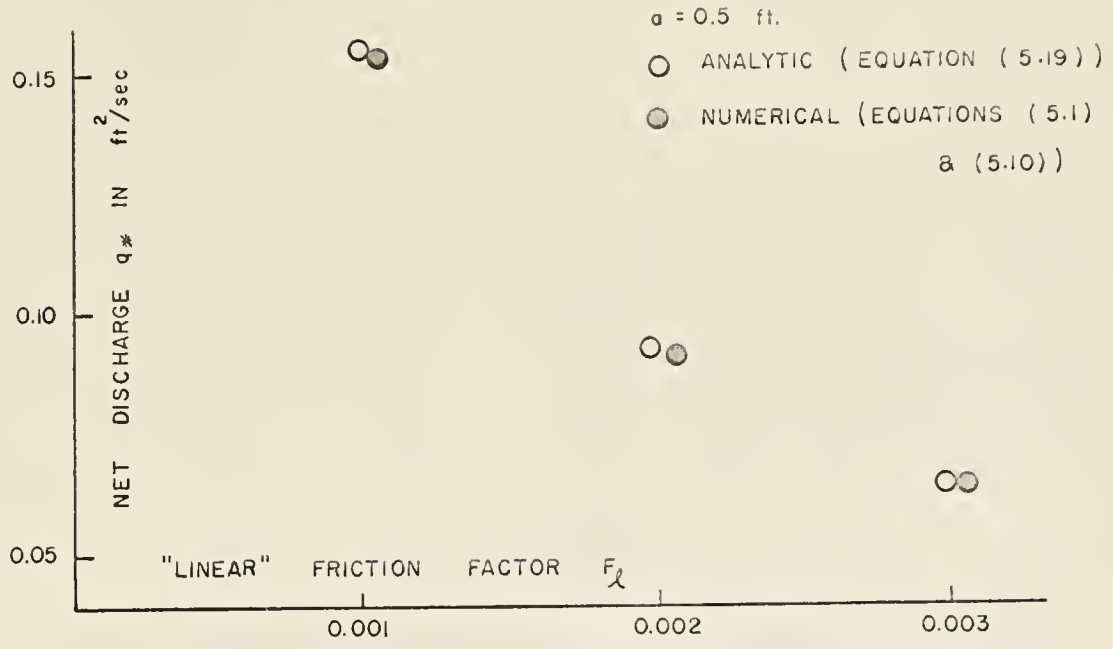

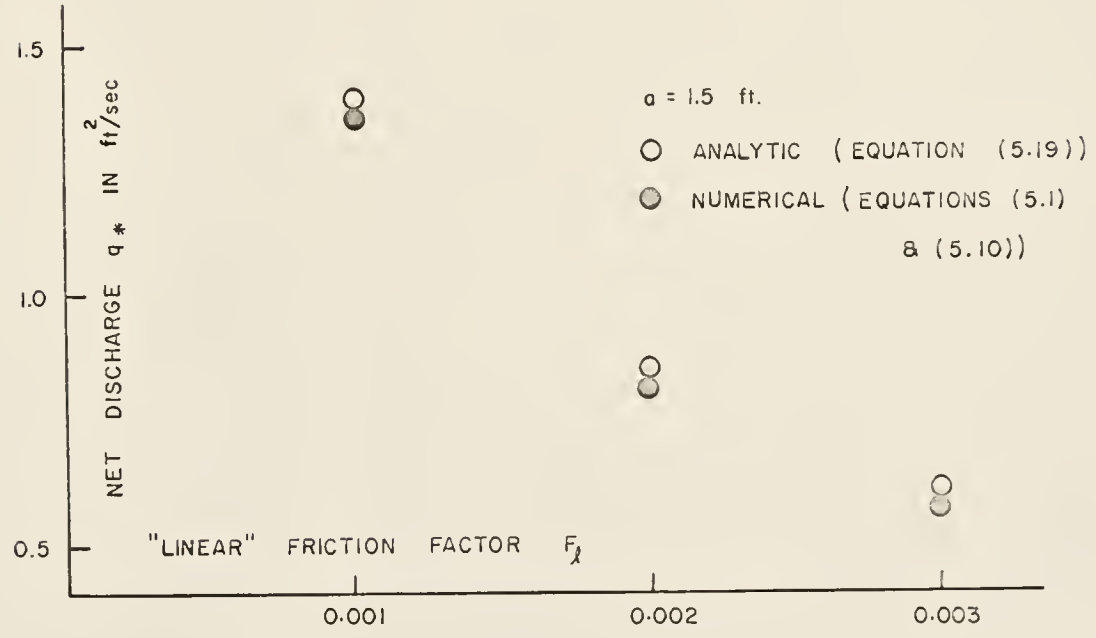

FIGURE 8. EFFECT OF HIGHER ORDER TERMS ON q_*

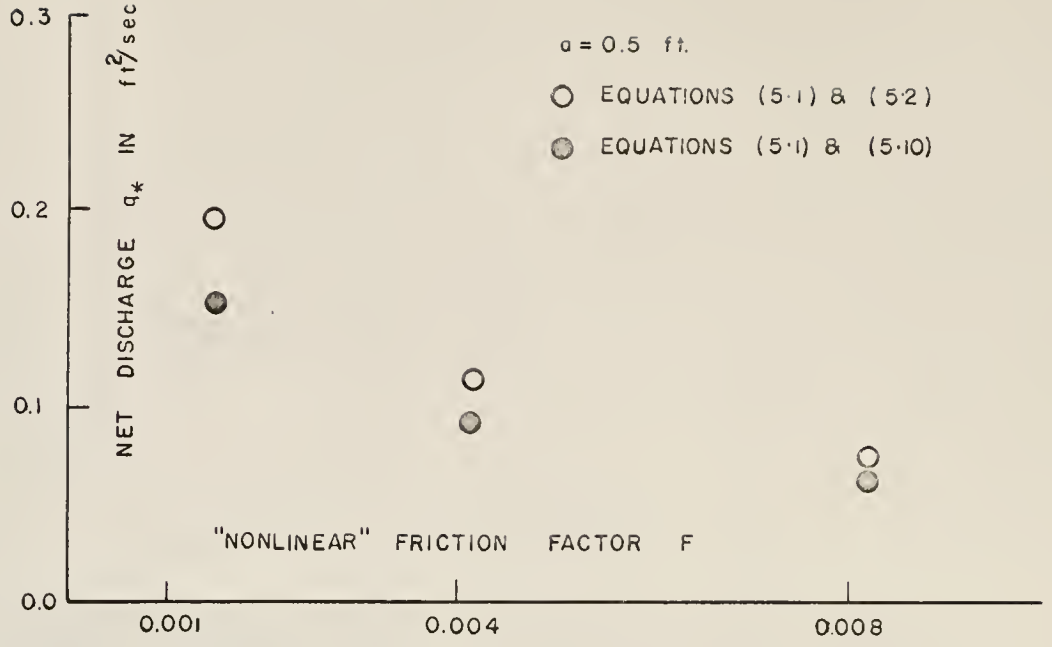

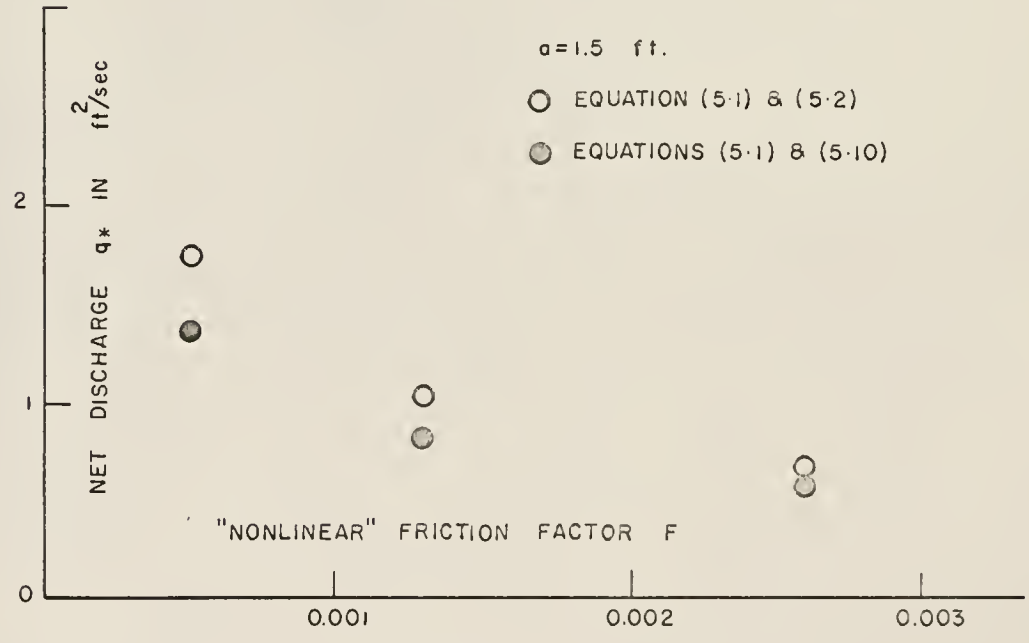

FIGURE 9. EFFECT OF "LINEARIZATION" OF THE FRICTION TERM ON q_*

reader is referred to Dronkers [6], Ippen [8] and Van de Kreeke [26].

In deriving Equation (5.19) the nonlinear terms associated with the convective acceleration and surface gradient have been neglected. These terms can easily be taken into account. In doing so, the only change in the differential Equation (5.18) will be in the expression preceding $e^{-2\mu x}$. In the initial derivation these nonlinear terms were omitted to simplify the algebra as much as possible. They should, however, be taken into account when requiring quantitative accurate results. This may be seen from Figure 10 in which the net transport with and without the convective acceleration and the nonlinear part of the surface gradient is presented for a lagoon at both ends freely connected to the ocean. The results plotted in Figure 10 were obtained numerically.

Also in deriving the expression for q_*, the boundary conditions were chosen such that to a first order of approximation, the water motion in the lagoon was a single damped progressive wave. However, expressions for q_* can be derived in a similar way for arbitrary boundary conditions. For example, consider a lagoon connected to the ocean by inlets at both ends. The implicit boundary conditions, formed by the inlet Equations (2.13) and (2.14), and the field Equation (5.2) first are made quasi-linear. This is done by linearizing the factors Q^2 and $q|q|$ in respectively the inlet and dynamic equation. A first order solution is obtained by omitting the second order terms (the nonlinear terms) from both the field equations and the boundary condition. The trial solution given by Equations (5.15)

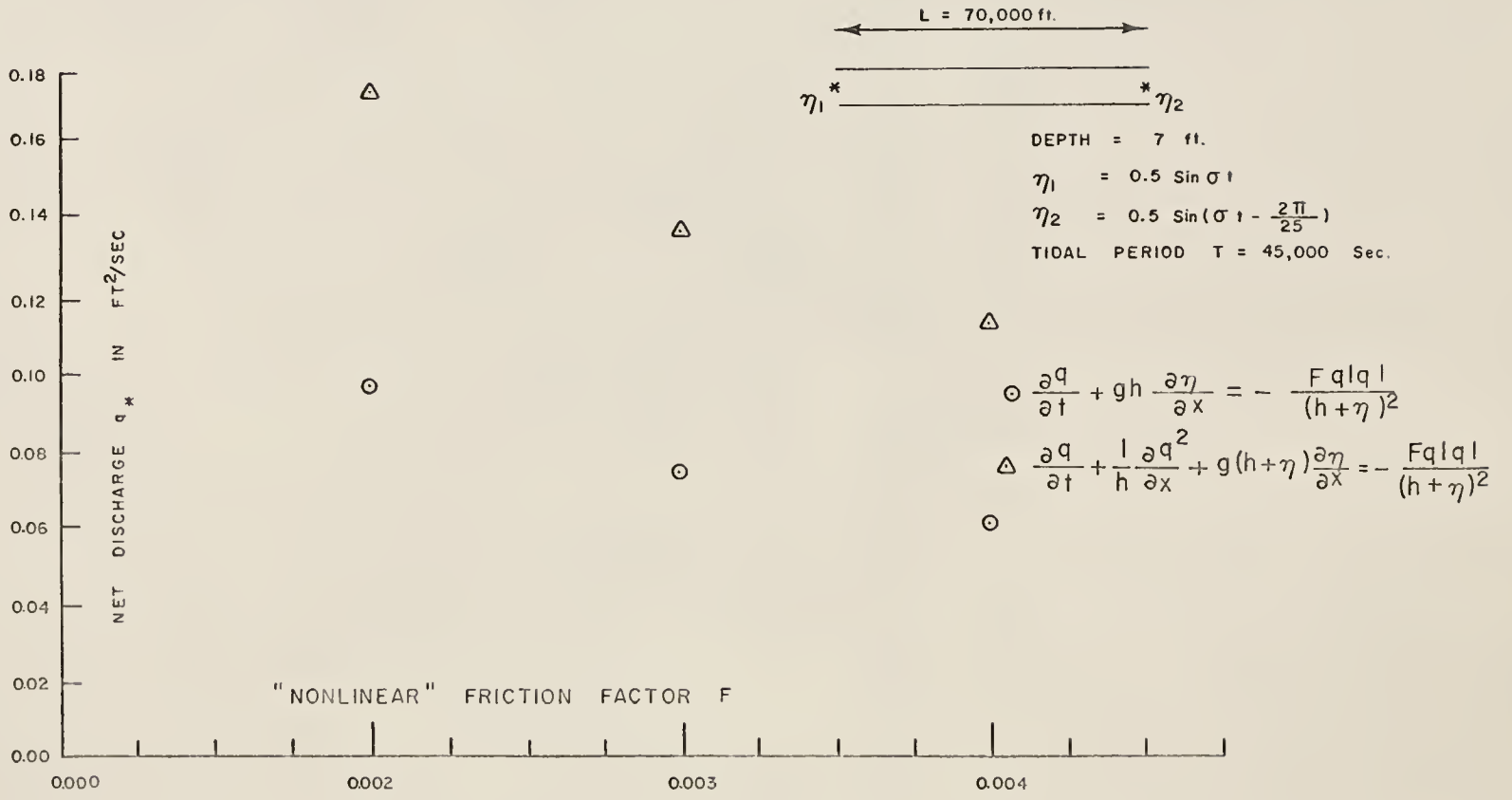

FIGURE 10. EFFECT OF CONVECTIVE ACCELERATION AND NONLINEAR PART OF THE SURFACE GRADIENT ON THE NET DISCHARGE q_*

and (5.16) is then substituted in the complete equations and boundary conditions including the nonlinear terms. The resulting expressions are time averaged which yields two linear differential equations in η_* and q_*, corresponding to Equations (5.17) and (5.18), and two linear boundary conditions. It is thus possible to solve for η_* and q_*. Preliminary computations showed the resulting expressions for η_* and q_* to be of such a nature (long algebraic forms with implicit expressions for amplitude and phase angles) that they defy the purpose of presenting the analytic solution, that is, gaining physical insight.

When considering a straight lagoon of uniform depth and width at both ends freely connected to the ocean, one obvious conclusion can be arrived at without any algebra; when the tides at both ends of the lagoon are the same, the net transport is zero because of the symmetry of the problem. Therefore, in order to have mass transport in a straight lagoon of uniform depth and width, the ocean tide at both ends of the lagoon must be different. This is an important consideration when discussing the effect of inlets on the mass transport; see Chapter 5b.

So far the vertical profile of the net drift has not been discussed; an important factor when designing an experimental apparatus for measuring the mass transport. Neglecting viscosity and thus neglecting bed friction, the net drift is the same for all levels. For example, Stokes' [22] second order wave theory gives for shallow water waves in an inviscid fluid a mass transport velocity

$$u_* = \frac{a^2 c_o}{2h^2}$$

However, when accounting for viscosity the net drift is no longer uniformly distributed as shown theoretically by Longuet-Higgins [12] for the case of null net transport.

Experimental results on drift profiles in a progressive shallow water wave and null net transport, U. S. Beach Erosion Board [23], Bagnold [1], Russell and Osorio [19] are in qualitative agreement with Longuet-Higgins so-called conduction solution even though the conditions imposed on the solution (wave amplitude small compared to the thickness of the boundary layer) are not satisfied in the experiments. Generally speaking, the theory and experimental results show a forward drift, that is in the direction of wave propagation, near the bottom and near the surface with a return flow in the middle of the water column. It is noted here than the $k_o h$ value, being one of the characteristic parameters describing the "shallowness" of the waves, was not less than 0.3 for any of the experiments presented in references [23], [1] and [19]. Longuet-Higgins' [12] conduction solution for the net drift in a pure standing wave shows a net drift near the bottom towards the location of the anti node while the net drift at the surface is from the anti node towards the nodes. The total picture is a circulation of mass between the vertical planes through nodes and anti nodes. To the writer's knowledge, no experimental results exist to verify this net drift pattern.

b. Influence of Inlets on the Mass Transport

Consider a lagoon of uniform depth and width connected to the ocean by inlets at each end; see Figure 11.

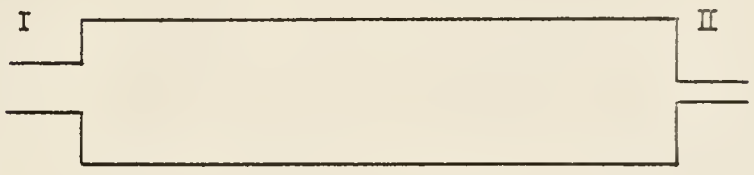

FIGURE 11. LAGOON CONNECTED TO THE OCEAN BY INLETS

It is assumed that the depth of the lagoon is so large that the propagation of the tide in the lagoon itself can be neglected. The continuity equation then may be written as

$$Q_I + Q_{II} = Q = A_b \frac{\partial \eta_i}{\partial t} \tag{5.32}$$

in which

A_b = lagoon area

Q = discharge into lagoon

η_i = lagoon level.

Equation (2.3) is used to describe the dynamics of the flow in the inlet. From this equation, it follows

$$Q = \pm \bar{A} \sqrt{\frac{2g\bar{R}}{2FL + m\bar{R}}} \cdot \sqrt{|\eta_o - \eta_i|}$$

or in Keulegan's [9] notation

$$Q = \pm K \frac{2\pi H}{T} \frac{A_b}{\sqrt{H}} \sqrt{|\eta_o - \eta_i|} \tag{5.33}$$

in which

$$K = \frac{T}{2\pi H} \frac{\bar{A}}{A_b} \sqrt{\frac{2g\bar{R}H}{2FL + m\bar{R}}}$$

K = coefficient of repletion

2H = tidal range in the ocean

$\bar{A}$ = cross-sectional area of the inlet measured at mean ocean level.

The solution to this problem, for a simple harmonic ocean tide, is given by Keulegan [9]. For an ocean tide of the form

$$\eta_o = H \sin \frac{2\pi t}{T}$$

in which H = tidal amplitude in the ocean, the corresponding bay level η_i is

$$\eta_i = A_1 \sin\left(\frac{2\pi t}{T} + \varepsilon_1\right) + A_3 \sin 3\left(\frac{2\pi t}{T} + \varepsilon_3\right) + \ldots \tag{5.34}$$

The amplitudes A_1 and A_3... and the phase angles ε_1, ε_3... are a function of the coefficient of repletion $K = K_1 + K_2$; K_1 and K_2 are the coefficients of repletion, respectively, for the Inlets I and II. It may be seen from Equation (5.34) that both amplitude and phase of the ocean tide are modified while in addition, higher harmonics are generated.

The foregoing solution pertains to relative deep lagoons. No analytic solution is known in case of a shallow lagoon. However, it is likely that each inlet again will modify the ocean tide but not to the

same extent (except when the inlets have the same dimensions), as was the case for the deep lagoon, because the propagation of the tide in the lagoon can no longer be neglected. In general, therefore, the amplitude and phase of the lagoon tide at one inlet will be different from the amplitude and phase of the lagoon tide at the other inlet, even though the ocean tide is the same for both inlets. A difference in tide at both ends of the lagoon is a requirement for net transport because in case of equal tides, the net transport is zero as a result of the symmetry of the problem. See also Chapter 5a.

It may be inferred from the foregoing general considerations that inlets may play an important role in the flushing of the lagoon. By properly choosing the dimensions of the inlets, the net transport of water in the lagoon can be considerably increased. This is illustrated for the bay system presented in Figure 11. The ocean tide is assumed simple harmonic and the same at both inlets; the amplitude is 1.30 ft. and the tidal period is 45,000 sec. For the dimensions of the lagoon and the inlets, see Figure 12. In the same figure, the results of the computations are presented; the net discharge per tidal cycle is plotted versus the width of Inlet II. A definite maximum in the net discharge occurs when the width of Inlet II is in the order of 300 - 400 ft. The computations were carried out for both the complete inlet Equations (2.13) and (2.14), neglecting terms resulting from the velocity head in the bay and the ocean, and for the simplified version of the inlet equation, Equation (2.3), again neglecting the velocity heads. The results for the two inlet equations differ only slightly. Equation (2.2) in which the convective term was neglected, was used to

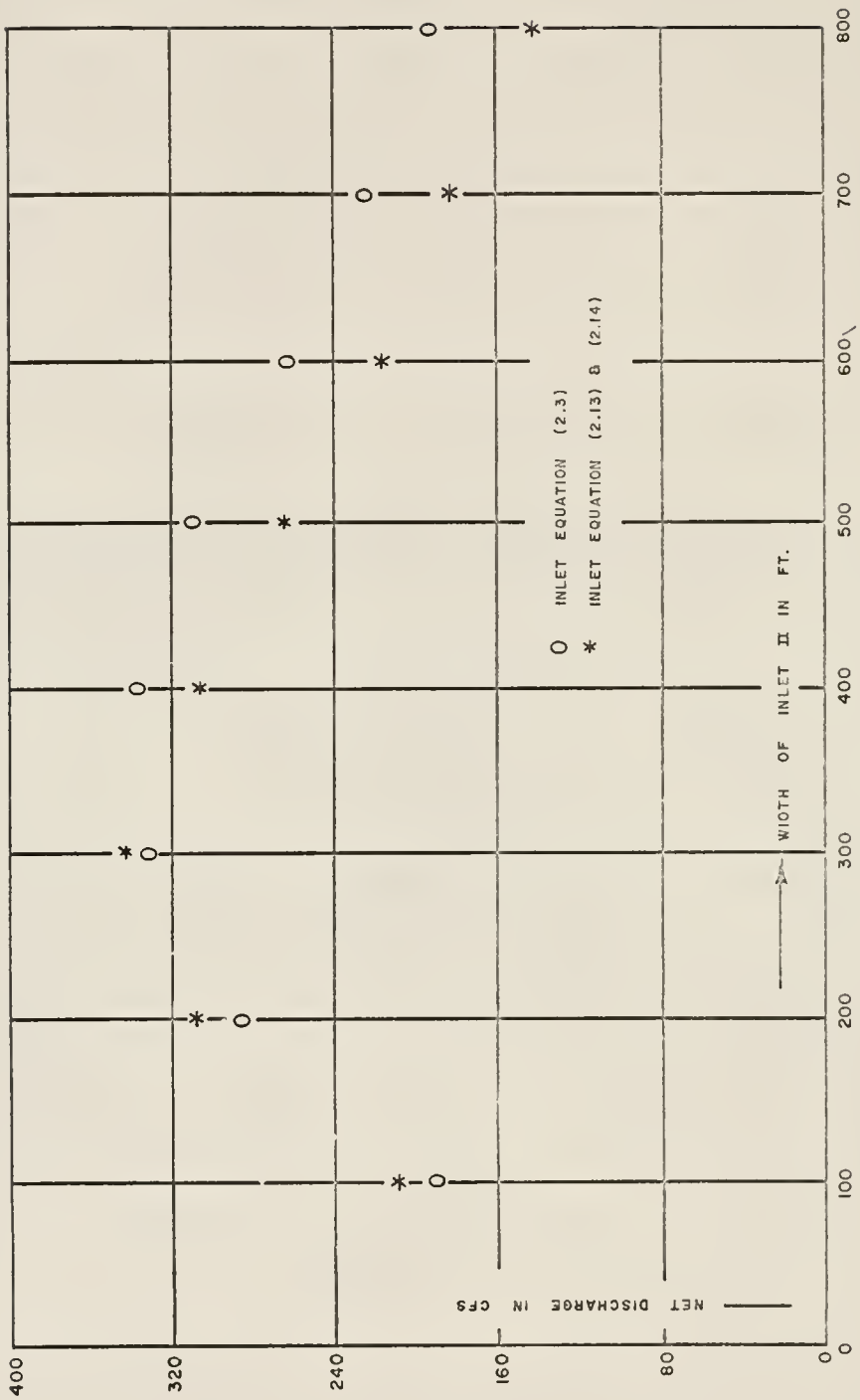

FIGURE 12. NET DISCHARGE IN LAGOON VERSUS WIDTH OF INLET II

describe the dynamics of the flow in the lagoon. The equations were solved by applying the numerical method discussed in Chapter 3. The net discharge was found by integrating the computed discharge over a tidal period. The time step in the computations was $\Delta t = 100$ sec. and the space step was $\Delta x = 5000$ ft.

6. LABORATORY EXPERIMENTS

A series of laboratory experiments was designed to measure the net drift in a lagoon of uniform width and depth connected at both ends to a tidal basin by openings of different dimensions. The purpose of the experiments was to evaluate the capability of the computational model described in the previous chapters to predict mass transport in tidal lagoons. The experiments were carried out in the Coastal Engineering Laboratory of the University of Florida.

a. Equipment and Procedure

Test Set-Up and Measuring Devices - A straight canal of uniform depth and width, simulating a lagoon, was constructed in a tidal basin; see Figure 13. The canal was 488 cm long and 30 cm wide. As outlined in Chapter 5, a necessary condition for mass transport is that the geometry of a lagoon be asymmetric. In nature, the asymmetry in many cases results from the different dimensions of the inlets connecting the lagoon to the ocean. The asymmetry in the experimental lagoon was introduced by providing one end of the lagoon with a submerged sharp crested weir. (A weir was preferred over an inlet because it led to a more regular flow pattern.) The weir was made of 1.5 mm steel plate. The edge of the weir was 3.35 cm above the bottom of the canal. The average water depths used in the tests were 5 cm and 6.5 cm.

The dimensions of the tidal basin were 600 x 600 cm, and the average water depth in the basin was 30.5 cm. Two weir boxes, one at each side of the basin provided a constant discharge of 22 liters/sec. A filter of honeycomb placed across the basin and wave damping material

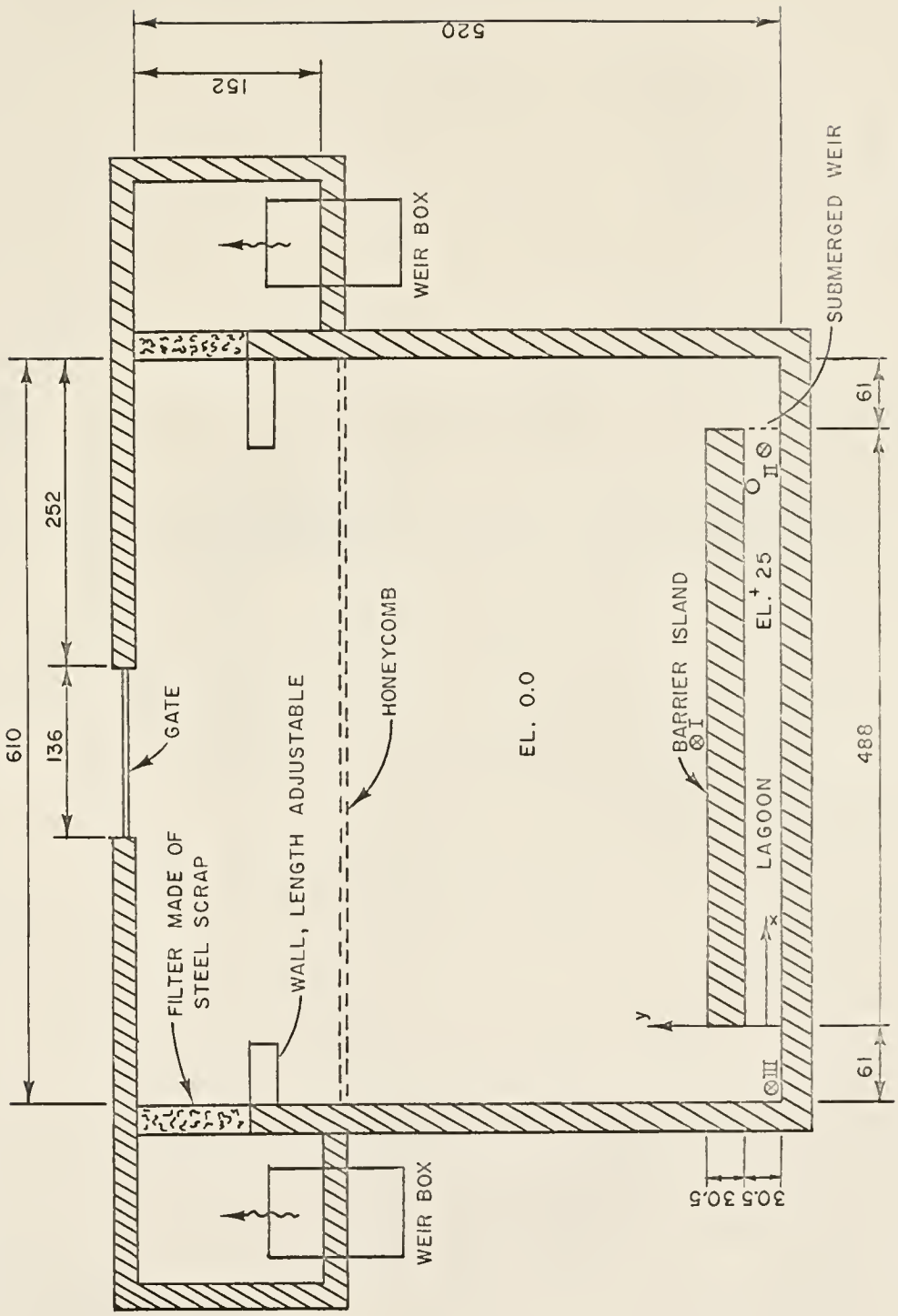

FIGURE 13. EXPERIMENTAL SET-UP

attached to the walls served to absorb small disturbances caused by the inflow from the weir boxes. The tide in the basin (later referred to herein as the ocean tide) was generated by letting the discharge gate move up and down at approximately constant speed (the downward speed of the gate was about 4% larger than the upward speed) between two fixed points. The distance between the two fixed points and the speed of the gate could be varied to generate tides of different amplitude and period.

An example of the ocean tide is presented in Figure 14. As demonstrated in this figure the ocean tide can very well be approximated by two half sines with slightly different periods (a result of the discharge gate moving faster down than up). In all of the tests the periods of the two half sines differed by less than 15%. The corresponding tide at the lagoon side of the weir is also presented in Figure 14. The weir tide lags the ocean tide by 1-2 sec while the tidal ranges are approximately the same.

Water surface elevations were measured by vibrating point level recorders. For the location of these recorders, see Figure 13. A quick indication of the water level was provided by a conventional point gage located in the lagoon. The same gage also served to determine the maximum and minimum water depth in each experiment. The mean depth was taken equal to the average of the maximum and minimum water depth. Net discharges were determined from measured float paths using a method that will be described in Section b of this chapter. Floats of different lengths were used. The floats which were made either of wood or styrofoam were weighted so that the top of the cone just

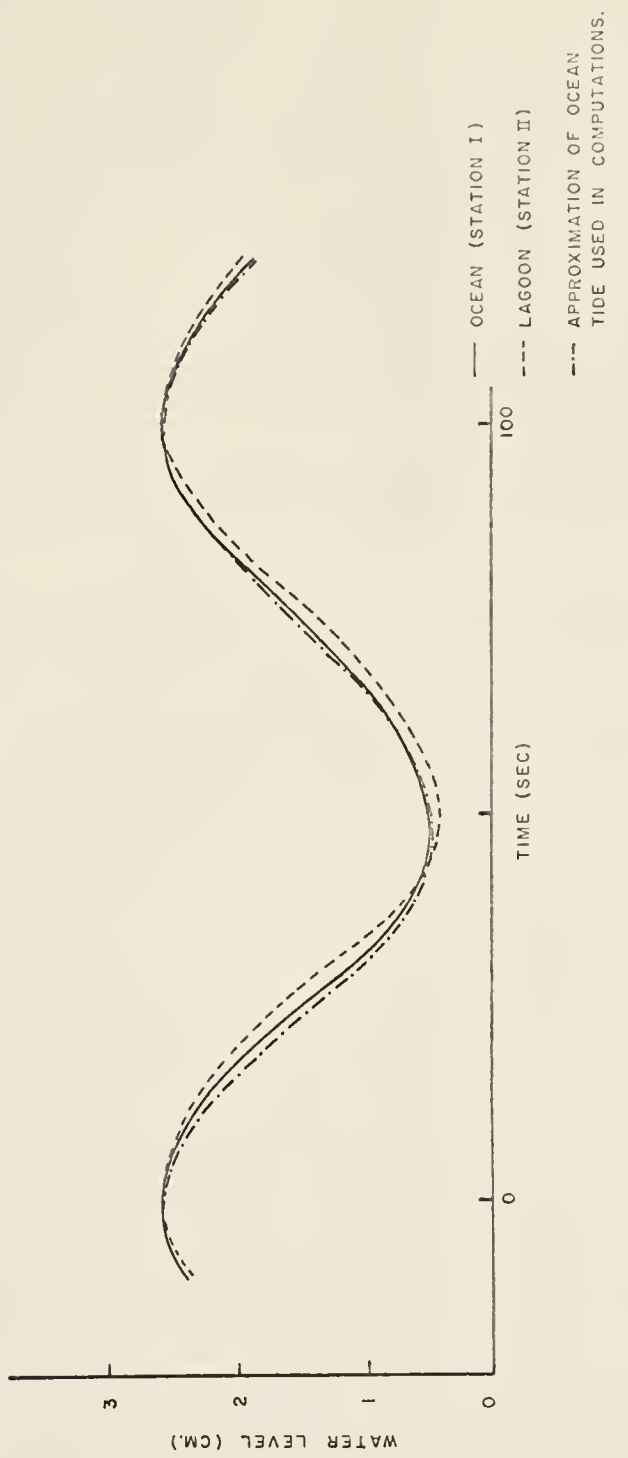

FIGURE 14. MEASURED TIDE CURVES FOR EXPERIMENT 5

contacted the water surface. All floats were cylindrical and had a diameter of approximately 0.5 cm, the top was given a conical shape to minimize effects of surface tension. For positioning of the floats a right-handed coordinate system was introduced, the x axis coinciding with the longitudinal axis of the lagoon and the zero located at the open end of the lagoon.

In addition to floats, dye (Rhodamine B) was used to determine the horizontal motion of the water in the lagoon. It was noticed that solutions with a high dye concentration, visible to the eye, when released in the lagoon water had a tendency to stick together and to settle (like a turbidity current) thus indicating only the motion of the bottom layers. An attempt was made to avoid this problem of settling by using dye solutions of a low concentration. After injection of the dye, water samples were taken from the lagoon by means of a rack provided with seven 1 cm glass tubes, spaced 10 cm apart. The glass tubes were placed vertically in the lagoon and sealed off at the top, by means of corks. The rack was then lifted out and the samples collected in test tubes. The samples thus obtained cover the entire water column. The dye concentrations in the test tubes were determined using a Fluorometer. It was hoped that when plotting concentration versus location of the samples a maximum could be indicated, the location of the maximum being the coordinate of the water mass initially located at the location of dye release. Unfortunately, many of the measured distributions did not have a clearly defined maximum and

it appeared that test results were not reproducible. It is believed that the dye still tended to stick together and settle rather than disperse--the reason being the low turbulence intensity in the lagoon. (The Reynolds number $Re = \frac{q}{\nu}$ in the experiments was on the order of 1000.) It might well be that in experiments with a higher turbulence level, the previously described technique would be successful. In view of the negative results, the test procedures and test results for the low concentration dye techniques will not be discussed further.

Test Procedure - First the discharge gate was left in a position resulting in the required average depth and the lagoon checked for circulation induced by the inflow from the weir boxes. This circulation could be compensated for by varying the length of the adjustable walls; see Figure 13. The discharge gate then was started and run for at least two hours to dampen possible disturbances caused by the sudden start of the gate.

Actual testing began with measuring water surface fluctuations at Stations I and III (see Figure 13). Initially also the surface fluctuations at Station II were measured. They appeared not to differ noticeably from those at Station III, and therefore have not been measured in the later experiments. Floats were released one at a time either in the middle of the lagoon or 5 cm from the side walls. Positions of the floats were marked at each slack tide for a period of at least five tidal cycles. In case the lateral displacement of the floats was more than 5 cm, the tests were disregarded and started again until a good run was obtained. The water motion near the bottom was determined by releasing dye in sufficient concentrations to be visible by eye.

Summary of Tests - Two series of experiments were carried out. A preliminary series, Test Series 1, to study the variation of the drift velocities in a cross section, the possible side and end effects and the reproducibility of the experiments, and Test Series 2 in which an attempt was made to determine the average net discharge. A summary of the experiments in each test series is presented in respectively Table I and Table II. Test Series 1 consists of 14 experiments numbered 1 through 14. The experiments 1, 2, 6, 7, 9, 10, 12 and 14 only served to develop the experimental procedure and therefore are omitted in Table I. Test Series 2 consists of 11 experiments numbered 15 through 25. Water depths in the experiments range from 5 to 6.5 cm, wave periods range from 70 to 100 sec. and amplitudes range between 0.75 to 1.15 cm. No attempt was made to systematically study the effect of different parameters on the net discharge because of the difficulty of varying water depth, amplitude and period independently.

TABLE I

SUMMARY OF EXPERIMENTS; TEST SERIES 1

Experiment	Tidal Amplitude (cm)	Tidal Period (sec)	Ave. Depth (cm)
3	0.77	71	5.10
4	0.92	72	5.00
5	1.05	100	4.90
5a	1.05	104	4.90
8	1.00	69	5.00
11	1.10	70	6.45
13	1.15	71	5.30
13a	1.15	71	5.30

TABLE II

SUMMARY OF EXPERIMENTS; TEST SERIES 2

Experiment	Tidal Amplitude (cm)	Tidal Period (sec)	Ave. Depth (cm)
15	1.13	70	5.00
16	0.87	70	5.05
17	1.13	70	6.60
18	1.03	70	6.60
19	0.91	69	6.55
20	0.81	70	6.45
21	0.95	70	6.70
22	1.09	71	6.60
23	0.96	70	5.00
24	0.94	70	4.80
25	1.05	70	4.95

b. Results

Test Series 1 - Introductory tests with confetti and dye showed the flow in the middle part of the lagoon to be regular but indicated a somewhat irregular flow pattern at both ends, especially during periods of reversal of the tide. Therefore tracking of the floats was restricted to the region between x = 50 cm and x = 450 cm. Maximum velocities in the experiments varied between 3 cm/sec and 5 cm/sec, depending on water depth, amplitude and period. Reynolds numbers ($Re = \frac{q}{\nu}$) were larger than 800 (the limit for fully turbulent flow) 60% - 80% of the time (the exact percentage depending on depth, period and amplitude).

Actual experiments were carried out with three different float lengths, 3 cm, 2 cm and 1 cm. Floats were placed in the middle

of the lagoon, y = 0 cm, and 5 cm from the side wall, y = +10 cm. In addition, in Experiments 13 and 13a floats were also placed at y = -10 cm. Typical examples of measured float positions are presented in Figures 15, 16, 17 and 18. In these figures the positions of the floats, at the time they first reversed their path, are reduced to the same coordinate, which is taken equal to the average of the positions of the floats at the first reversal point (the positions usually did not differ more than 20 cm). The time a float arrives at the first reversal point is set equal to zero. Because of the difficulty of determining the exact time a float reverses its path, the subsequent times of reversal are set equal to the average of the reversal times of all the floats used in an experiment (reversal times for different floats at corresponding slack tides differed at the most by 10 sec). Positions of the floats are plotted at these average reversal times.

Figures 17 and 18 show the results of two identical Experiments 13 and 13a. From these figures it may be seen that the positions of corresponding floats differ somewhat, but the range covering the positions of the floats at corresponding slack tides is approximately the same for both experiments. For a better comparison, the particle excursion between successive slack tides of the two longer floats in the middle of the canal are tabulated for both experiments in Table III.

Most floats when placed in the water moved parallel to the side walls; in unusual cases, a float was traced again because it had displaced laterally more than 5 cm and when this happened it nearly always occurred for those floats initially placed 5 cm from the wall.

FIGURE 15. MEASURED FLOAT POSITIONS FOR EXPERIMENT 4

FIGURE 16. MEASURED FLOAT POSITIONS FOR EXPERIMENT 5a

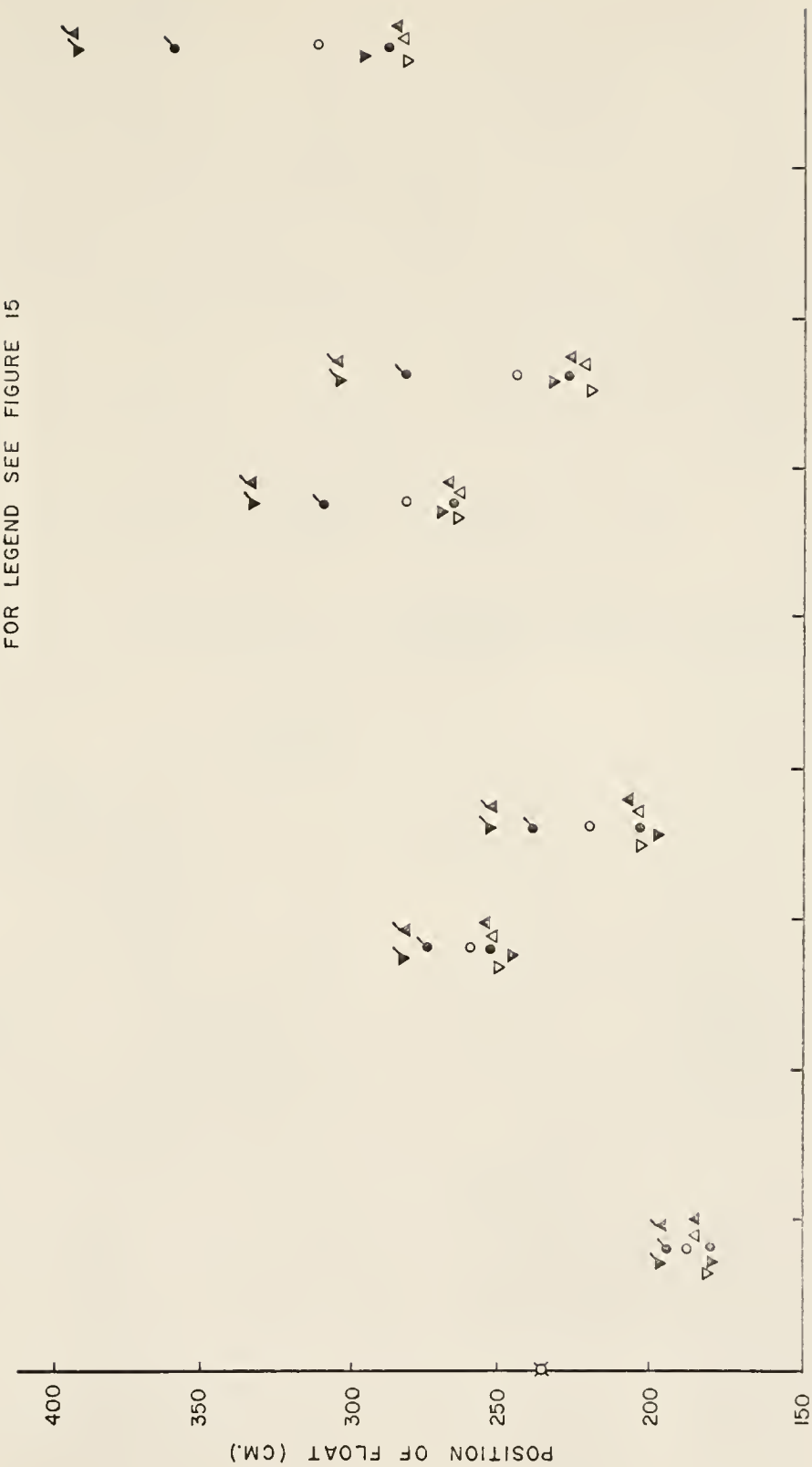

FIGURE 17. MEASURED FLOAT POSITIONS FOR EXPERIMENT 13

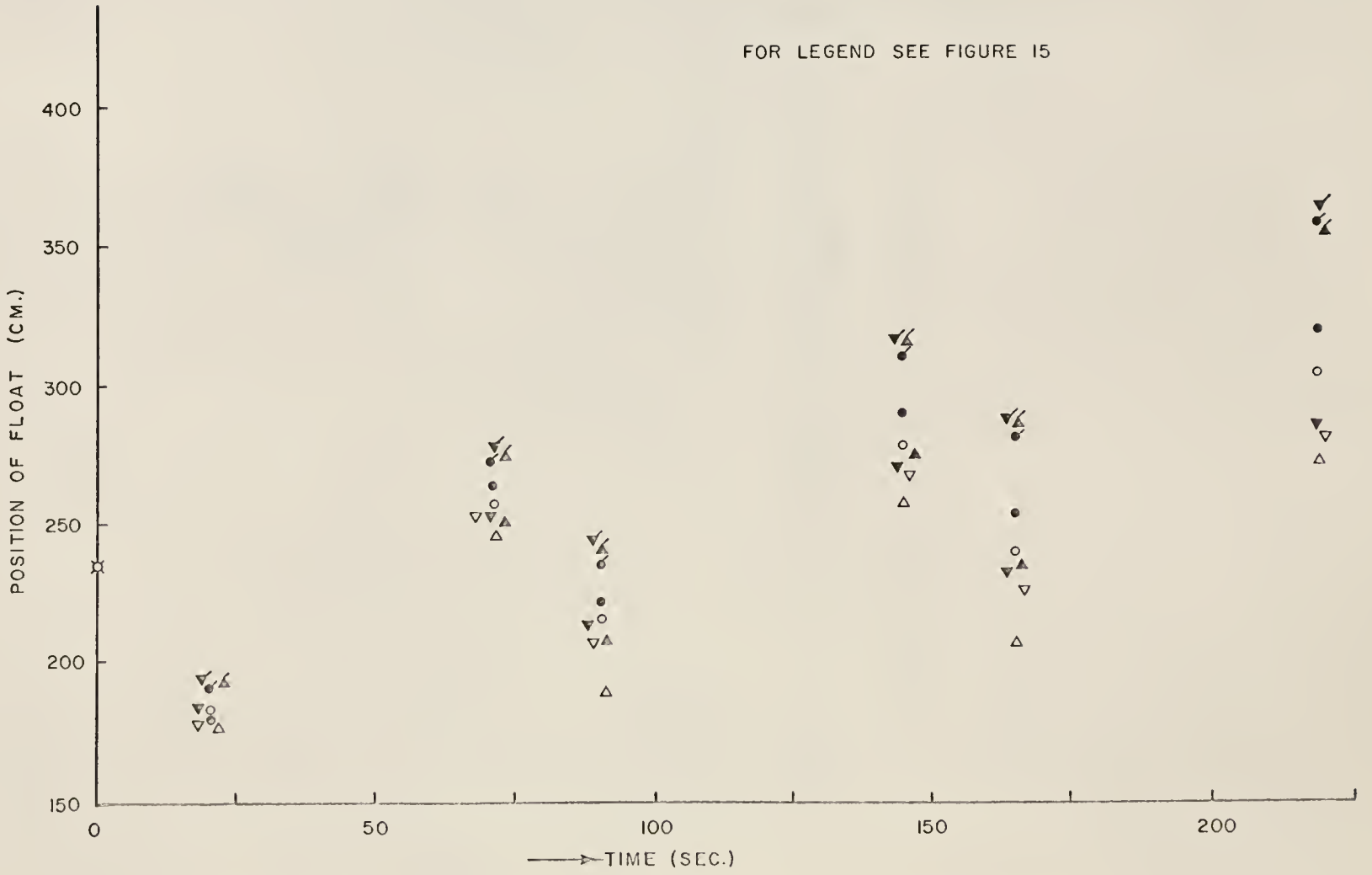

FIGURE 18. MEASURED FLOAT POSITIONS FOR EXPERIMENT 13a

TABLE III

REPRODUCIBILITY OF EXPERIMENTS;
PARTICLE EXCURSION BETWEEN SUCCESSIVE SLACK TIDES
FOR EXPERIMENTS 13 AND 13a

	Experiment 13		Experiment 13a	
Slack Tide	3 cm Float	2 cm Float	3 cm Float	2 cm Float
1 - 2	+72	+69	+74	+69
2 - 3	-41	-48	-41	-58
3 - 4	+62	+60	+62	+69
4 - 5	-35	-43	-38	-50
5 - 6	+66	+61	+63	+67

Floats were placed in the middle of the lagoon.

Tabulated values are excursions in cm.

From this it may be inferred that the flow pattern in the experimental lagoon is one dimensional in a sense that no significant meandering of the flow occurs.

It may be seen from the examples presented in Figures 15, 16, 17 and 18 that the net drift differs for each float length which is not surprising in view of the discussion of the vertical drift profile on page 45. For all experiments the following was noted: the direction of the net drift in each experiment was the same for all floats, however, the magnitude of the net drift varied with the length of the float. This and the fact that injected dye clouds always moved in the same direction as the floats suggests that the direction of the net drift is the same for each point in the vertical. The experiments do not define the shape of the drift profile over depth.

Results of Experiments 13 and 13a in which floats were tracked at both sides of the lagoon show that the net drift is not uniformly distributed over the width of the lagoon; the net drift at the north side is considerably larger than in the middle and at the south side. This probably is a result of the flow in and out the lagoon not being symmetric with respect to the longitudinal axis of the lagoon.

Determination of Net Discharge from Float Paths - Before presenting the results of Test Series 2, the method used to determine the net discharge q_* from a float path s will be discussed. Mainly because of the different nature of the two parameters, q_* is an Eulerian parameter and s is a Lagrangian parameter, the mathematical relation between these two quantities gets rather complicated and unmanageable. Therefore for the determination of q_* from s recourse is taken to the

following empirical method. Assume that the path of a float is representative of the average horizontal particle motion. As an example the (fictitious) measured positions of such a float at successive slack tides are indicated in Figure 19. The successive float positions are connected by straight lines. The midpoints of these straight lines are determined and a straight line is drawn through these points. The slope of this line represents a velocity u_*, which may be interpreted as an average net drift velocity. The net discharge q_* then is found by multiplying this average velocity and the average depth. Numerical experiments to be discussed in Section c show this method to yield good results.

Test Series 2 - The range of hydraulic parameters used in Test Series 2 (see Table II) is approximately the same as those used in Test Series 1 and thus also the velocities and Reynolds numbers are on the same order as earlier mentioned.

In contrast to the Test Series 1 experiments, the Test Series 2 program was carried out with only one float length. The length of the float was chosen as large as possible to arrive at an average over depth drift velocity. This and the requirement that the float not contact the bottom at all times resulted in float lengths of 3.5 and 4.5 cm, respectively, for depths of 5 and 6.5 cm. Because of the irregular flow pattern at both ends of the lagoon (see discussion of result of Test Series 1) the tracking of the floats was limited also to the lagoon section between x = 50 cm and x = 450 cm. Typical results of float tests for Test Series 2 are presented in Figures 20 and 21. In both figures straight lines representing the "average net drift velocity" u_*

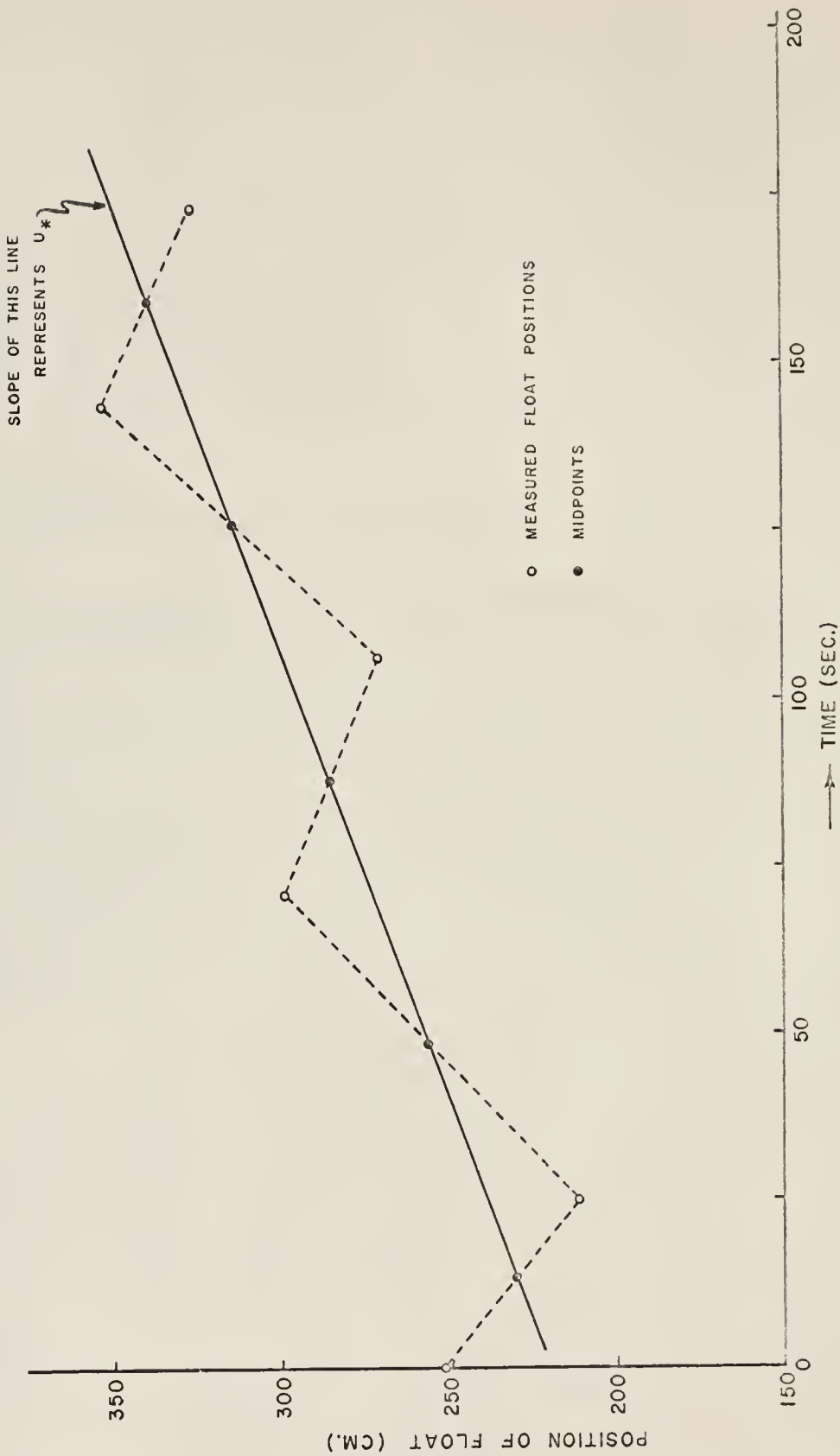

FIGURE 19. DETERMINATION OF NET DISCHARGE FROM MEASURED FLOAT PATH

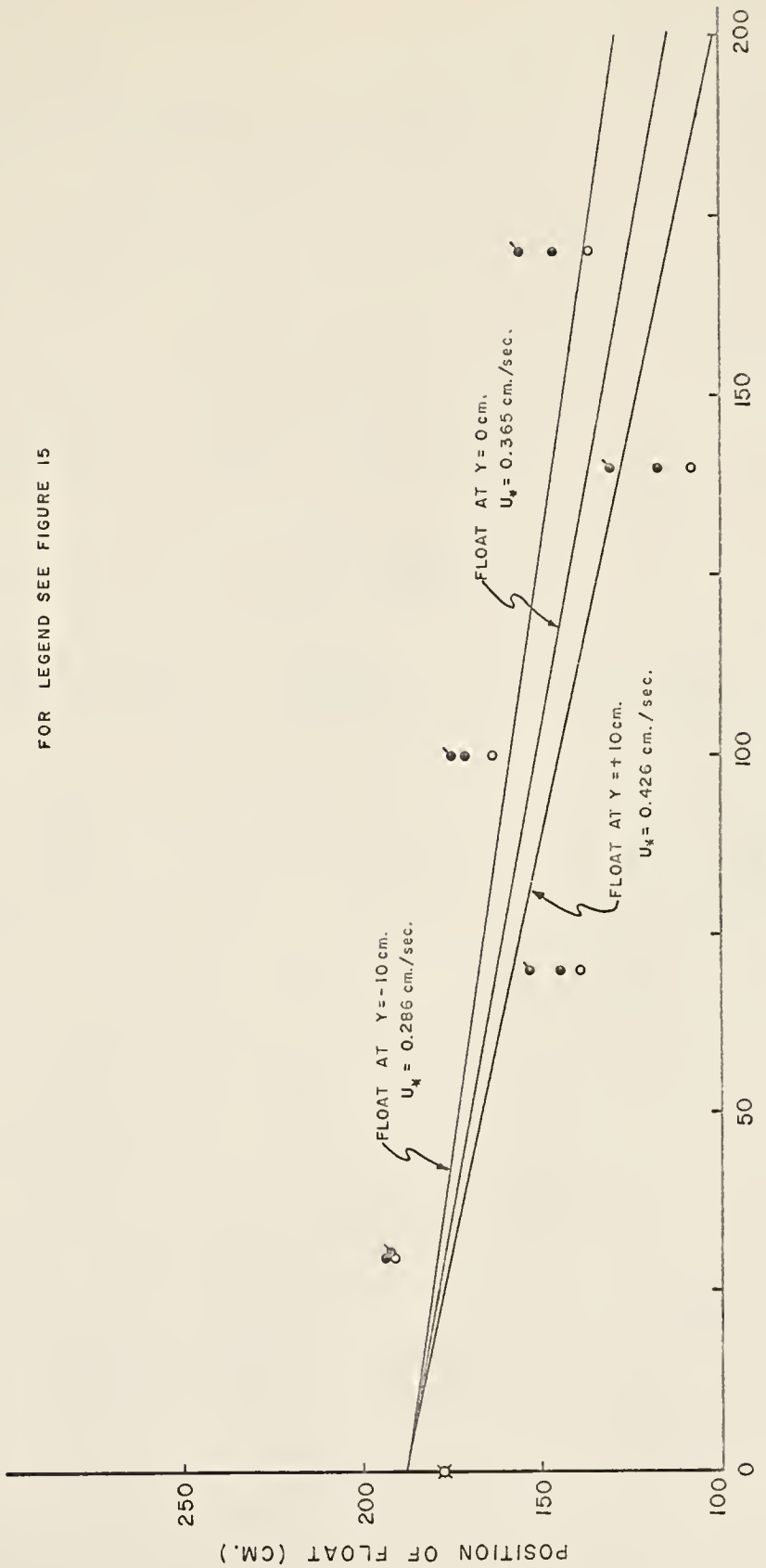

FIGURE 20. MEASURED FLOAT POSITIONS FOR EXPERIMENT 22

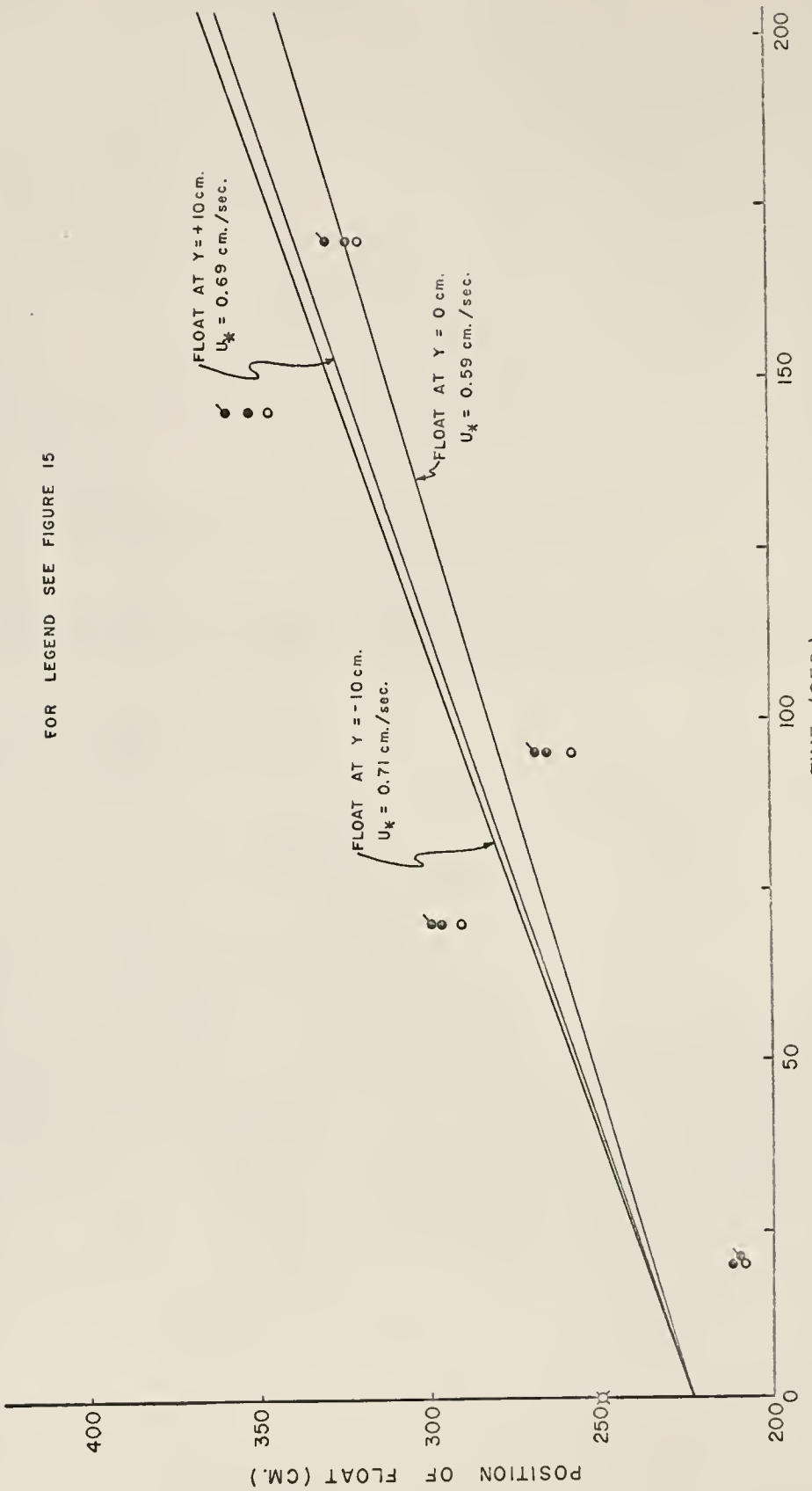

FIGURE 21. MEASURED FLOAT POSITIONS FOR EXPERIMENT 24

are drawn using the previously described method. A complete summary of the "average net drift velocities" and net discharges for the different experiments is presented in Table IV.

The net discharge q_*, presented in the last column of Table IV, is found by multiplying the average of the three net drift velocities by the average depth h. Velocities and discharges are also listed for Experiments 13 and 13a, which were the only experiments in Test Series 1 in which floats were used in the middle and both sides of the lagoon.

The results listed in Table IV show that the net drift velocity strongly depends on the lateral position of the float; in general, for the experiments with 5 cm depth the net drift is largest for the floats placed at y = -10 cm, for the experiments with 6.5 cm depth the net drift is largest for the floats placed at y = +10 cm. As mentioned earlier the lateral variation in net drift should probably be attributed to the asymmetry of the experimental set-up; see page 66.

In each of the Test Series 2 experiments, in addition to the tracking of floats, the water motion was also studied by observing the displacement of a dye cloud released in the middle of the experimental lagoon. The dye cloud, initially about 30 cm long and extending over the full width of the channel, stretched longitudinally and at the same time gradually moved in the same direction as the floats. In all cases, the net displacement of the dye patch was observed to be in the same direction as that of the floats.

One of the more striking results of the experiments is (see Table IV) that the net drift in the experiments with a water depth of

TABLE IV

MEASURED DRIFT VELOCITIES AND NET DISCHARGES

Exper.	Tidal Ampl(cm)	Tidal Period(sec)	Aver. Depth(cm)	u_*(cm/sec) y = +10 cm	u_*(cm/sec) y = 0 cm	u_*(cm/sec) y = -10 cm	q_*(cm^2/sec)
15	1.13	70	5.00	1.04	1.30	1.60	6.40
16	0.87	70	5.05	0.13	0.09	0.37	1.00
17	1.13	70	6.60	-0.47	-0.47	-0.27	-2.68
18	1.03	70	6.60	-0.42	-0.43	-0.42	-2.79
19	0.91	69	6.55	-0.33	-0.39	-0.27	-2.16
20	0.81	70	6.45	-0.25	-0.31	-0.19	-1.61
21	0.95	70	6.70	-0.29	-0.40	-0.27	-2.18
22	1.09	71	6.60	-0.36	-0.42	-0.28	-2.34
23	0.96	70	5.00	0.43	0.27	0.39	1.81
24	0.94	70	4.80	0.69	0.59	0.71	3.18
25	1.05	70	4.95	0.95	1.02	0.95	4.80
13	1.15	71	5.30	0.29	0.37	0.58	2.18
13a	1.15	71	5.30	0.43	0.33	0.55	2.32

about 5 cm (Experiments 15, 16, 23, 24, 25, 13 and 13a) is toward the weir while the direction of the net drift is reversed for the experiments with a water depth of approximately 6.5 cm (Experiments 17, 18, 19, 20, 21 and 22). An explanation for this might be the following. Consider the hydrodynamic Equations (2.1) and (2.2) neglecting friction and storage. (This simplification is justified because in the experiments the storage is zero and friction is of relatively little importance.) Equations (2.1) and (2.2) then read:

$$\frac{\partial \eta}{\partial t} + \frac{\partial q}{\partial x} = 0 \tag{6.1}$$

$$\frac{\partial q}{\partial t} + \frac{1}{h}\frac{\partial q^2}{\partial x} + g(h + \eta)\frac{\partial \eta}{\partial x} = 0 \tag{6.2}$$

The boundary condition at x = 0, the open end of the experimental lagoon is

$$\eta_o = a \cos \sigma t \tag{6.3}$$

in which

$\sigma = \frac{2\pi}{T}$ = angular frequency of the tide

T = tidal period.

A linearized version of the weir equation is used for the boundary condition at the weir side of the lagoon.

$$q = \mu_\ell 2gh_w(\eta_i - \eta_o) + \mu_\ell 2g\eta_o(\eta_i - \eta_o) \tag{6.4}$$

in which

η_i = water level at the lagoon side of the weir

μ_ℓ = "linear" weir coefficient

h_w = average water depth over the weir.

The last term on the right-hand side of Equation (6.4) represents the influence of varying depth over the weir on the discharge.

A trial solution for the system of Equations (6.1) through (6.4) is

$$\eta = \eta_*(x) + \eta_\ell(x,t) + \ldots \tag{6.5}$$

$$q = q_*(x) + q_\ell(x,t) + \ldots \tag{6.6}$$

in which η_ℓ and q_ℓ are the solutions of the system of equations when neglecting the nonlinear terms in the Equations (6.1) and (6.2) and the last term on the right-hand side of Equation (6.4). In view of Equation (6.3), η_ℓ and q_ℓ are periodic functions with period T. Substituting the trial solution, Equation (6.5), in Equations (6.1) and (6.2) and time averaging yields

$$q_* = \text{const.} \tag{6.7}$$

$$gh\frac{\partial \eta_*}{\partial x} + \overline{\frac{2}{h} q_\ell \frac{\partial q_\ell}{\partial x}} + \overline{g\eta_\ell \frac{\partial \eta_\ell}{\partial x}} = 0 \tag{6.8}$$

Equation (6.8) with the boundary condition, $\eta_* = 0$ at $x = 0$, yields a solution $\eta_*(x)$. Substituting Equation (6.5) in Equation (6.4) yields after time averaging

$$q_* = \mu_\ell 2gh_w\eta_* + \mu_\ell 2g\,\overline{\eta_o\eta_\ell} - \mu_\ell 2g\,\overline{\eta_o^2} \tag{6.9}$$

in which η_* and η_ℓ are evaluated at the lagoon side of the weir. The

first term on the right-hand side of Equation (6.9) results from the nonlinear terms in the field Equations (6.1) and (6.2); the last two terms result from the term in the weir equation representing the influence of the time varying depth over the weir. It is known that for a channel closed at one end η_* at the closed end is positive; see Longuet-Higgins [13]. It seems reasonable to assume that η_* is also positive in case of a partially closed channel. Furthermore, because of the phase shift between η_o and η_ℓ at the lagoon side of the weir (see Figure 14) it follows that in Equation (6.9) $\overline{\eta_o \eta_\ell} < \overline{\eta_o^2}$. The first term on the right-hand side of Equation (6.9) thus is positive while the sum of the last two terms is negative. In the experiments, the net drift results from two opposing effects.

- the net drift resulting from the nonlinear terms in the field equations
- the net drift resulting from the variation in depth over the weir during a tidal cycle.

The resultant direction of the net drift thus depends on which of these effects is predominant.

It seems tempting to translate the experimental data to a prototype scale. In this context, however, it should be mentioned that translating to realistic prototype dimensions is not possible because the relative magnitude of the terms in the dynamic equation is entirely different for model and prototype. In the experiments the friction term is very small compared to the total acceleration while in a natural lagoon these terms are of the same order of magnitude; see e.g. Figure 6.

c. Computation of Mass Transport; Comparison with Measured Data

Equations (2.1) and (2.2) are used to describe the conservation of mass and momentum in the experimental lagoon. In Equation (2.1) the term M representing the storage is set equal to zero. The flow over the weir is described by an equation of the form

$$q_w = - \mu_n (h_w + \eta_i) \sqrt{2g(\eta_o - \eta_i)} \qquad (6.10)$$

for flow from the ocean to the lagoon, and

$$q_w = + \mu_p (h_w + \eta_o) \sqrt{2g(\eta_i - \eta_o)} \qquad (6.11)$$

for flow from the lagoon to the ocean. In these equations

q_w = discharge per unit width over the weir

μ_n and μ_p = weir coefficients; the subscript n refers to flow from the ocean to the lagoon; the subscript p refers to flow from lagoon to ocean

h_w = average depth over weir

η_o = water level in ocean

η_i = water level at Station III; see Figure 23.

The weir equations involve empirical constants μ_n and μ_p. A literature search [27], [29], [14], [10] for values of these so-called weir coefficients did not show any data for the combination of parameters (down-stream water level, up-stream energy level and weir height) encountered in the experiments. In addition, all tests described in the literature deal with steady-state conditions while also the turbulence level is much higher than found in the experiments described here. Therefore,

to arrive at an order of magnitude value for the coefficients μ_n and μ_p the following theoretical approach is taken. Bernoulli's equation is applied up-stream of the weir between Stations I and II; see Figure 22. This yields for positive flow (flow from the lagoon to the ocean).

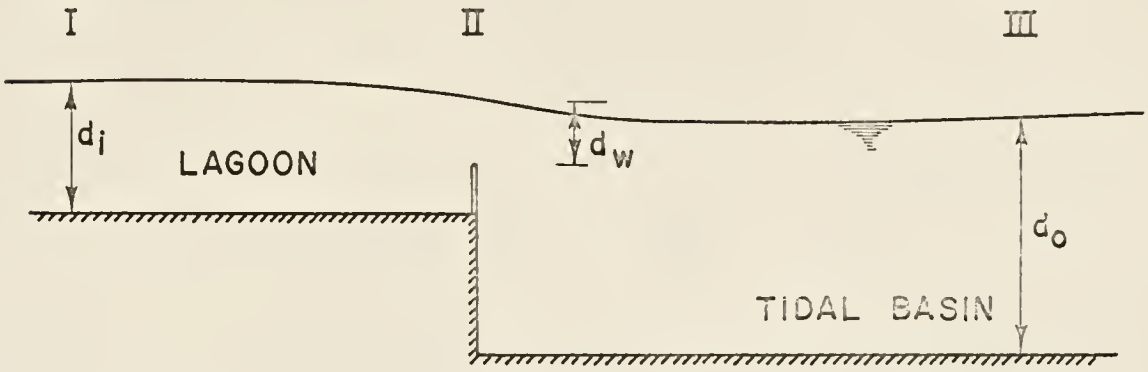

Figure 22. WEIR; FLOW FROM LAGOON TO TIDAL BASIN

$$\eta_i + \frac{q^2}{2gd_i^2} = \eta_w + \frac{q^2}{2gd_w C_c^2} \tag{6.12}$$

in which

d_i and d_w represent the total depths at respectively Stations I and II; see Figure 22.

η_w = the time varying water level at the weir measured with respect to mean level of the weir

C_c = coefficient to account for the stream lines over the weir not being horizontal.

At the down stream side of the weir, the momentum equation is applied between Stations II and III which yields

$$\eta_w - \eta_o = \frac{q^2}{g} \frac{1}{C_c d_w d_o} \left[\frac{C_c d_w}{d_o} - 1 \right] \tag{6.13}$$

in which

d_o = total depth at Station III; see Figure 22.

Eliminating η_w between (6.12) and (6.13) and writing the result in the form of Equation (6.11) yields

$$q = \frac{1}{\sqrt{\left[\frac{1}{C_c^2} - \frac{d_w^2}{d_i^2} + \frac{2d_w}{C_c d_o} \left(\frac{C_c d_w}{h_o} - 1 \right) \right]}} d_w \sqrt{2g(\eta_i - \eta_o)} \tag{6.14}$$

and thus

$$\mu_p = \frac{1}{\sqrt{\left[\frac{1}{C_c^2} - \frac{d_w^2}{d_i^2} + \frac{2d_w}{C_c d_o} \left(\frac{C_c d_w}{d_o} - 1 \right) \right]}} \tag{6.15}$$

Similarly, for flow from the ocean to the lagoons it is found

$$\mu_n = \frac{1}{\sqrt{\left[\frac{1}{C_c^2} - \frac{d_w^2}{d_o^2} + \frac{2d_w}{C_c d_i} \left(\frac{C_c d_w}{d_i} - 1 \right) \right]}} \tag{6.16}$$

Values of μ_p and μ_n are computed from, respectively, Equations (6.15) and (6.16) for two typical sets of values for d_i, d_o and d_w. The results are listed below.

d_i = 5 cm	d_w = 1.65 cm	d_o = 30 cm
C_c = 0.7	μ_p = 0.75	
	μ_n = 0.87	
C_c = 0.8	μ_p = 0.87	
	μ_n = 1.02	
C_c = 0.9	μ_p = 1.00	
	μ_n = 1.18	

d_i = 6.5 cm	d_w = 3.15 cm	d_o = 31.5 cm
C_c = 0.7	μ_p = 0.81	
	μ_n = 0.95	
C_c = 0.8	μ_p = 0.95	
	μ_n = 1.12	
C_c = 0.9	μ_p = 1.13	
	μ_n = 1.34	

The foregoing "theoretical" values of the weir coefficients indicate that

- the order of magnitude of the weir coefficients is one
- the coefficient μ_n is always larger than μ_p.

Within this framework the final combination of values for μ_p and μ_n will be chosen such that measured and computed net discharges for the experiments are in good agreement.

The equations describing the flow in the lagoon and the flow over the weir are solved using the numerical technique described in Chapter 3. The grid scheme used in the computations is indicated in Figure 23. The value of the friction factor F = 0.005 (this value

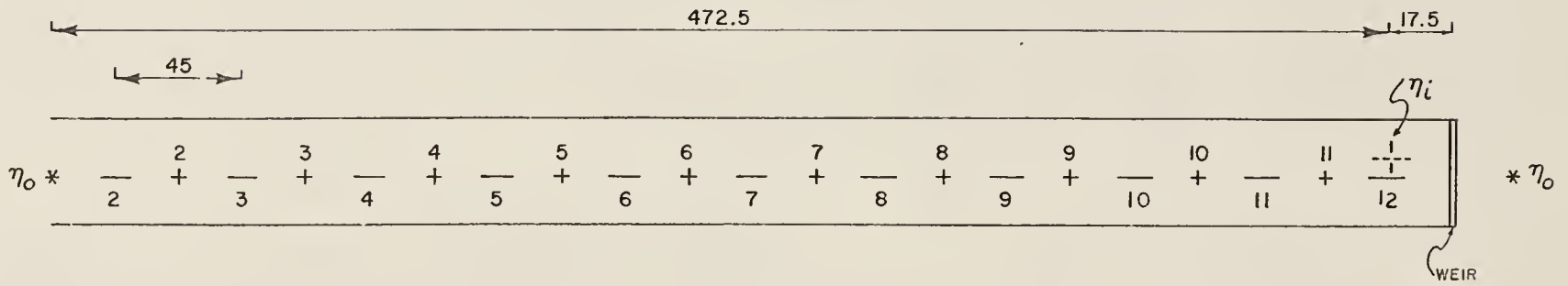

FIGURE 23. GRID SCHEME FOR NUMERICAL COMPUTATIONS OF LABORATORY EXPERIMENTS

was obtained from experiments carried out in a hydraulic flume with a bottom of the same roughness as the experimental lagoon). The space and time steps are: $\Delta x = 45$ cm and $\Delta t = 0.1$ sec. Recorded tides in the basin (Station I; see Figure 13) are approximated by two half sines. In the computational procedure, first the discharges q and the water levels η in the lagoon are determined, starting from the given tide in the basin. The net discharge q_* then follows from

$$q_* = \frac{1}{T} \int_0^T q \, dt \tag{6.17}$$

The integral is evaluated numerically.

Trial and error procedures indicate that for the combination of weir coefficients, $\mu_p = 0.8$ and $\mu_n = 1.2$, computed and measured net discharges are in good agreement as shown in Figure 24. In Figure 24, the net discharges computed with this combination of weir coefficients and measured net discharges (see Table IV) are presented for all experiments of Test Series 2 and for Experiments 13 and 13a of Test Series 1. For each of these experiments, also the particle path $s(x_o,t)$ is computed from

$$s(x_o,t) = \int_0^t \frac{q(s(x_o),t)}{h + \eta(s(x_o,t)} \, dt \tag{6.18}$$

The integral is evaluated numerically. The computed particle paths are used to verify the empirical method of determining net discharges from particle trajectories; see page 66. Net discharges are determined from the computed particle paths using the empirical method and are

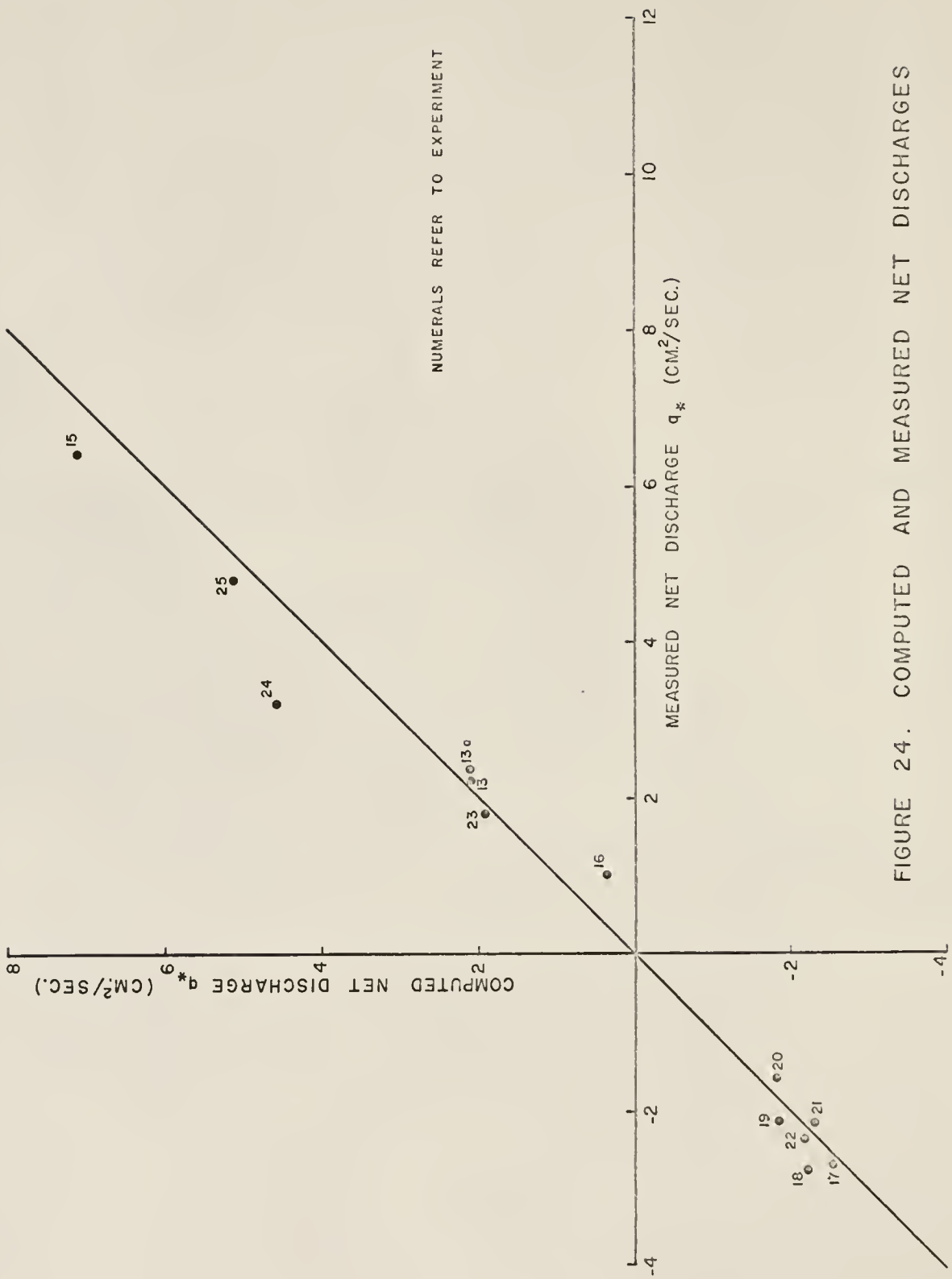

FIGURE 24. COMPUTED AND MEASURED NET DISCHARGES

compared with the net discharges obtained by integration of Equation (6.17). For results, see Table V. The good agreement proves the empirical method to be a reliable tool in deriving net discharges from particle trajectories.

TABLE V

COMPUTED NET DISCHARGES; EVALUATION OF EMPIRICAL METHOD OF DETERMINING NET DISCHARGES

Exper.	Tidal Ampl(cm)	Tidal Period(sec)	Aver. Depth(cm)	$q_*(cm^2/sec)$ Eq. (6.18)	$q_*(cm^2/sec)$ Empirical
15	1.13	70	5.00	7.10	7.40
16	0.87	70	5.05	0.27	0.30
17	1.13	70	6.60	-2.60	-2.70
18	1.03	70	6.60	-2.16	-2.26
19	0.91	69	6.55	-1.87	-1.90
20	0.81	70	6.45	-1.83	-1.87
21	0.95	70	6.70	-2.26	-2.28
22	1.09	71	6.60	-2.14	-2.24
23	0.96	70	5.00	1.92	2.00
24	0.94	70	4.80	4.54	4.70
25	1.05	70	4.95	5.10	5.35
13	1.15	71	5.30	1.60	1.65
13a	1.15	71	5.30	1.60	1.65

Examples of computed particle paths for Experiments 22 and 25 are presented in Figures 25 and 26. In the same figures, the measured float positions at slack tide are plotted also.

Finally, it is noted that a comparison between computed and recorded data can only be as good as the quality of the individual data.

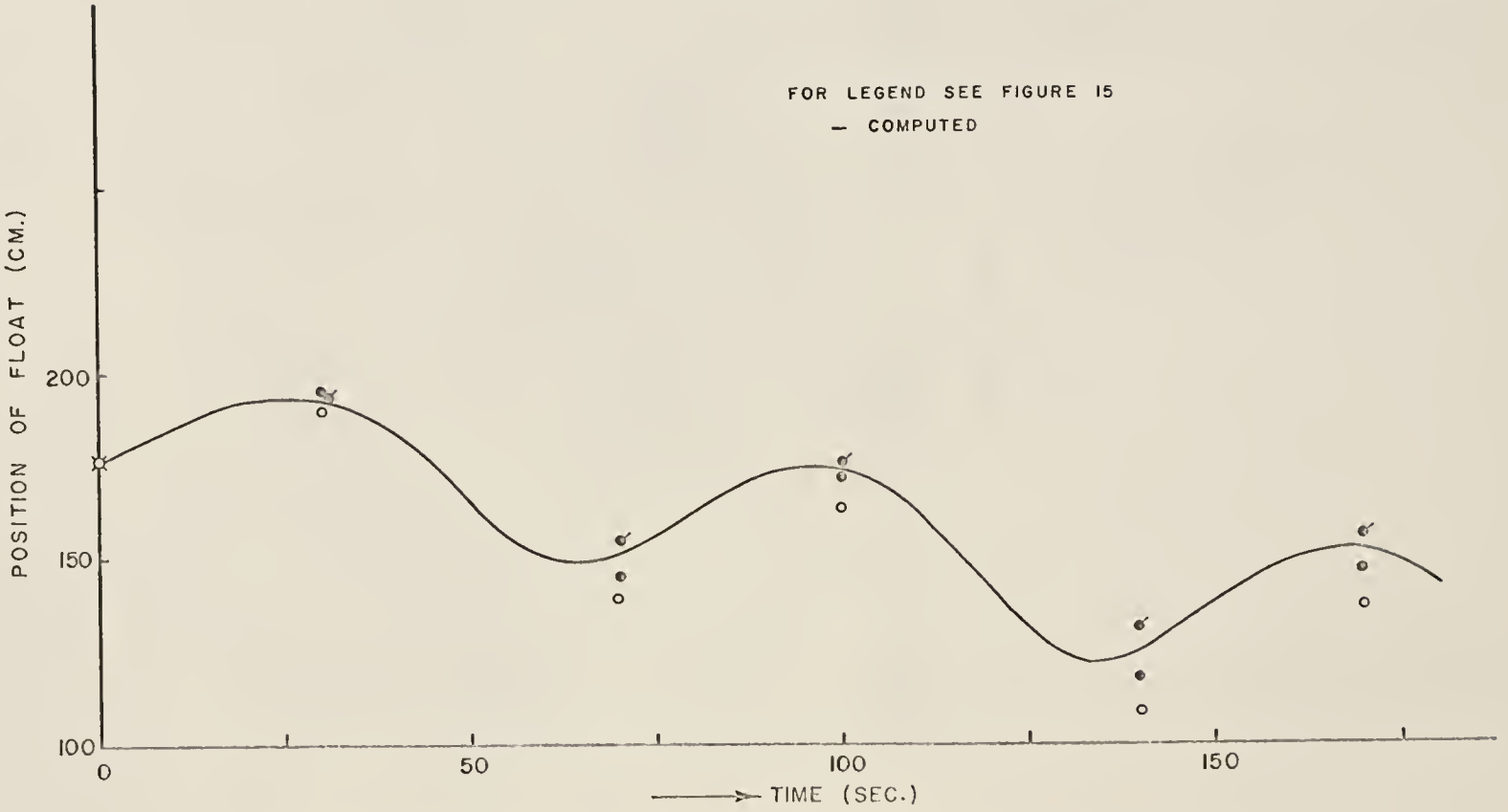

FIGURE 25. MEASURED AND COMPUTED FLOAT POSITIONS FOR EXPERIMENT 22

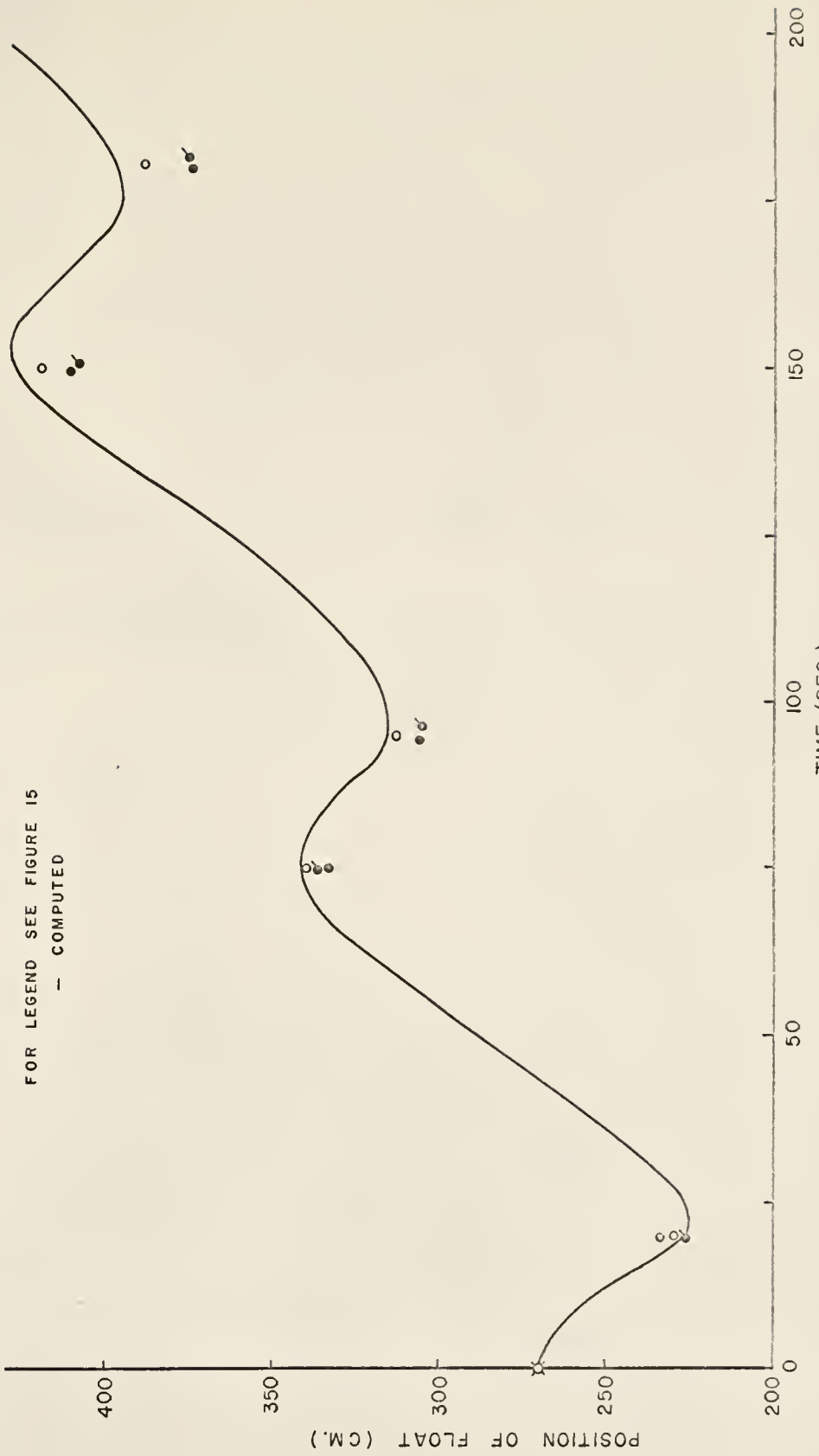

FIGURE 26. MEASURED AND COMPUTED FLOAT POSITIONS FOR EXPERIMENT 25

In this respect, it should be kept in mind that the measured net discharges are empirically derived from float trajectories which are assumed to represent the average horizontal particle motion. The validity of the latter assumption cannot be judged with any certainty until more detailed experiments on the distribution of the net drift over the vertical have been carried out. With regard to the computational model, it should be mentioned that inaccuracies in measured depth, especially for the smaller depths, lead to relatively large errors in the net discharge as demonstrated in Figure 27. Also, the trial and error procedure necessary to determine the weir coefficients is a poor substitute for a well-defined description of the flow over the weir, especially when variations in those weir coefficients lead to rather large changes in the net discharge as shown for Experiment 20 in Table VI. It is admitted that this to a certain extent reduces the value of a comparison between computed and recorded data.

TABLE VI

VARIATION OF NET DISCHARGE IN EXPERIMENT 20
FOR DIFFERENT COMBINATIONS OF WEIR COEFFICIENTS

$\mu_p - \mu_n$	0.75-0.95	0.75-1.05	0.8-1.1	0.8-1.2	0.9-1.15	0.9-1.2	1-1.3
$q_*(cm^2/sec)$	-0.65	-1.37	-1.23	-.83	-0.67	-0.96	-0.68

d. Summary

The displacement of water masses in an idealized lagoon constructed in the laboratory has been studied (1) by tracking floats

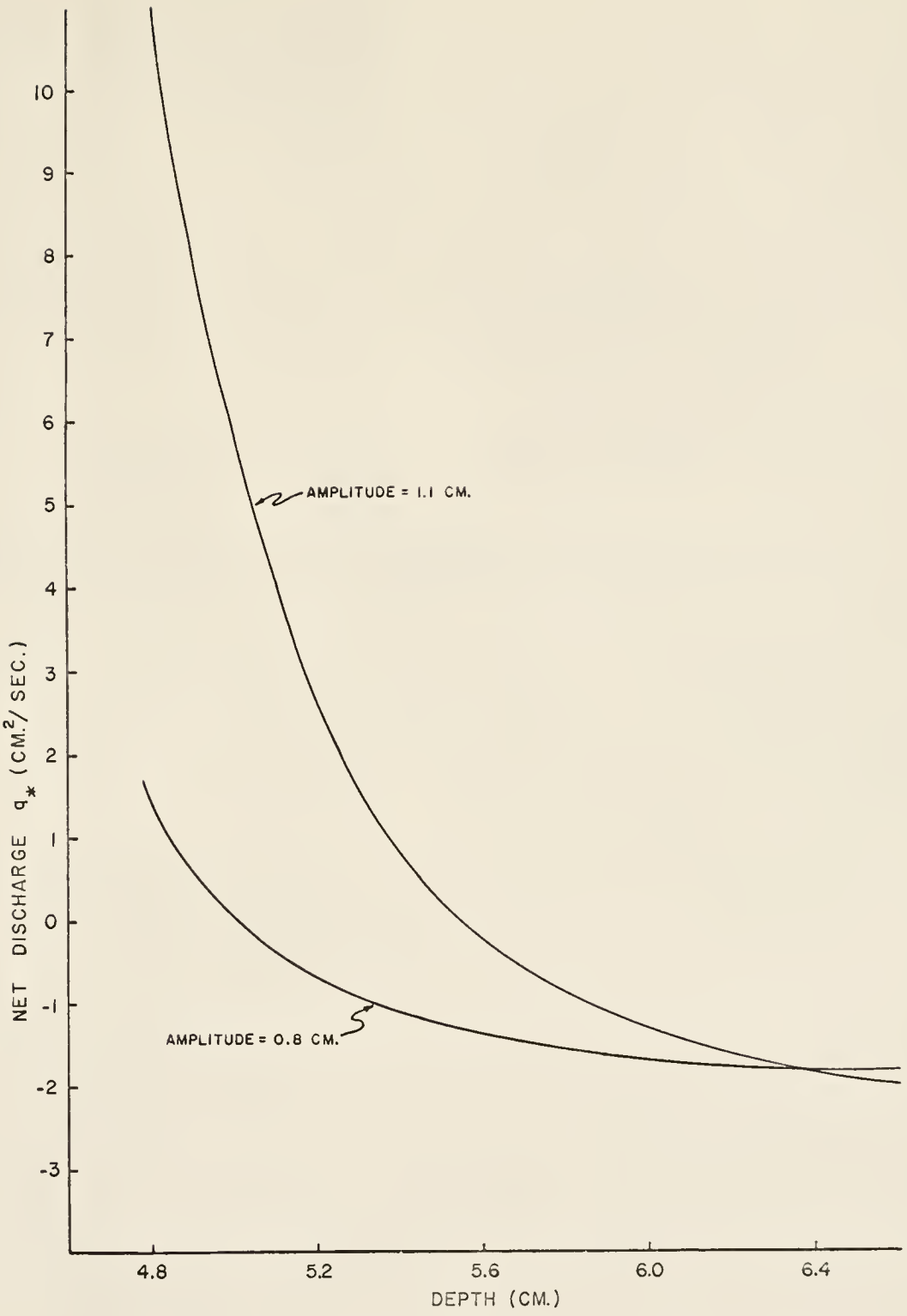

FIGURE 27. VARIATION OF NET DISCHARGE WITH DEPTH

of different lengths and tracing of injected dye clouds and (2) by conducting calculations to represent this phenomenon. The lagoon which had a uniform width and depth was at one end freely connected to a tidal basin and on the other end was connected to the same basin via a submerged sharp crested weir. The experimental results showed that for a given set of hydraulic conditions (1) the magnitude of the net drift of a float depends on its length, (2) the direction of the net drift is the same for each float length and (3) the dye clouds move in the same direction as the floats. These observations suggest that the direction of the net drift is the same for each point over the entire depth.

The direction of the net drift is not the same for all experiments. An explanation for this is that the net drift is the result of two opposing effects: (1) the net drift due to the nonlinear terms in the field equations and (2) the net drift resulting from the nonlinear terms in the weir equation.

Net discharges are derived from measured float paths using an empirical method described on page 66. To account for lateral variation in the drift, net discharges are based on the average path of three floats placed in the middle and at the two sides of the lagoon.

The computational model describing the flow in the lagoon involves two weir coefficients. The value of these weir coefficients is determined by matching computed and measured net discharges. This admittedly reduces the value of the computation model; however, the good agreement between measured and computed net discharges and thus

between measured and computed mass transport for all experiments for the same combination of weir coefficients indicates the validity of the theory on which the computations are based.

7. APPLICATION

To demonstrate that the convective transport in lagoons resulting from tides only is not merely a matter of academic interest but of practical significance as well, the net discharge is calculated for Lake Worth, Florida, which is one of a number of typical lagoons of the U. S. east coast and Gulf of Mexico. The computations were carried out using the model described in Chapters 2, 3 and 4. Because the purpose of the computations is to demonstrate the effect of the tide only, wind stresses and fresh water inflow are not included in this treatment.

Lake Worth, located on the lower east coast of Florida, is a narrow tidal lagoon; see Figure 28. The lake is generally parallel to the coastline and is about 20 miles long and 5 to 8 ft. deep. The actual flow-conveying portion is approximately 2000 ft. wide; the shallow areas at the east side of the lake serve primarily as storage. Near the north end, Lake Worth is connected to the ocean by North Lake Worth Inlet, which has a width of 800 ft. between the two entrance jetties and is about 35 ft. deep. At the south end, Lake Worth is connected to the ocean by a much smaller inlet, South Lake Worth Inlet, with dimensions of 130 ft. wide and 10 ft. deep. Lake Worth is part of the Intracoastal Waterway for its entire length.

The tides in the Lake Worth area have a predominantly semi-diurnal character. According to the tide tables [24], the mean tidal range in the Atlantic Ocean at Palm Beach is 2.8 ft. and the spring tidal range is 3.3 ft. Going inland the corresponding tidal ranges at the

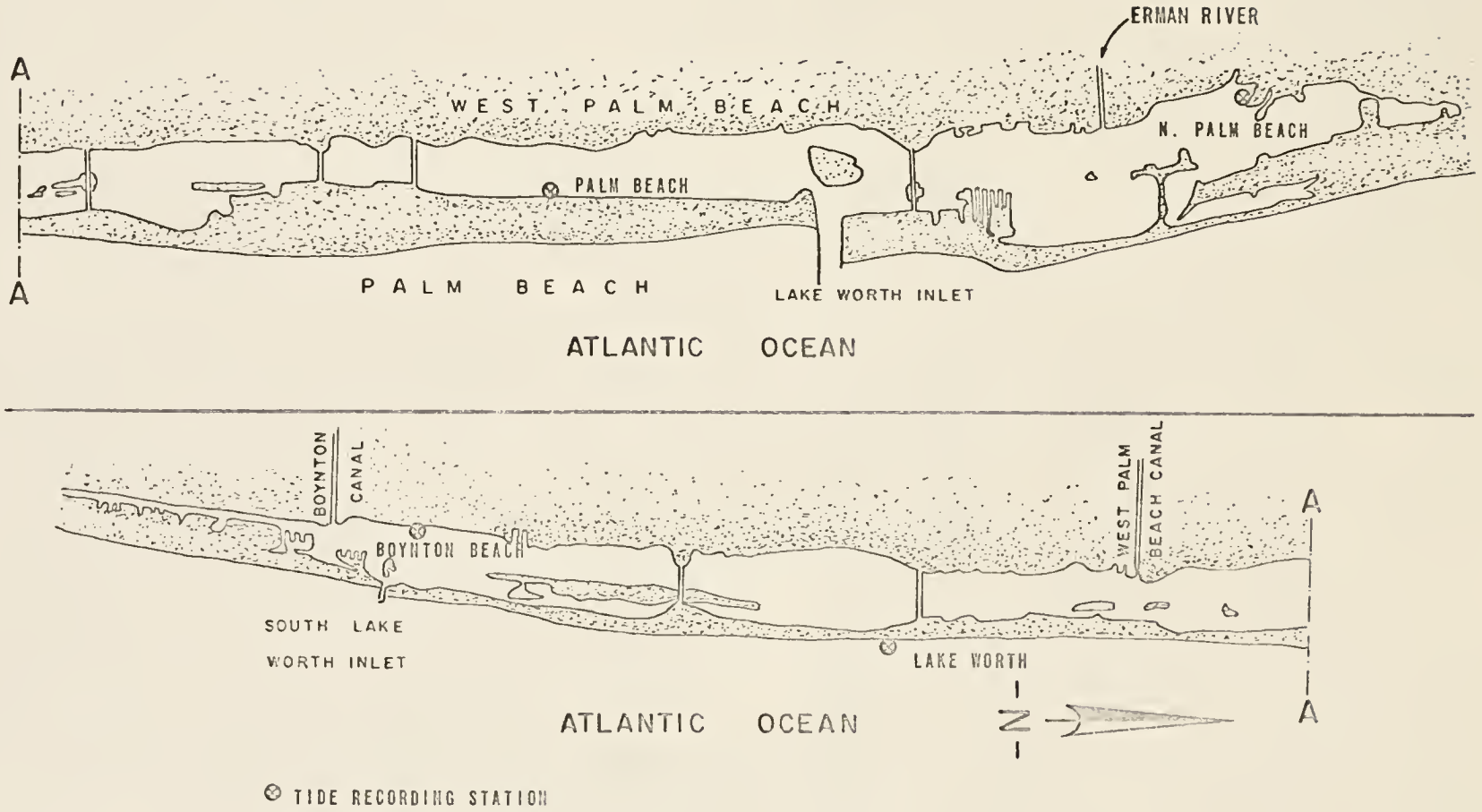

FIGURE 28. LAKE WORTH, FLORIDA; LOCATION OF TIDE RECORDERS

Port of Palm Beach decrease to respectively, 2.6 ft. and 3.1 ft. Velocities in Lake Worth are on the order of 1-2 ft./sec. Velocities can be as high as 2-4 ft./sec. in North Lake Worth Inlet and 7-8 ft./sec. in South Lake Worth Inlet.

For the purpose of computation, the actual geometry of Lake Worth is schematizied as presented in Figure 29. The lagoon is divided into three different sections for which the friction factor F is assumed constant. Each of the sections has a conveying channel and a storage area. Lake Worth is assumed to be closed at both the northern end (North Palm Beach) and the southern end (Boynton Beach).

In formulating the mathematical description, the flow is assumed to be one dimensional, that is the current direction is always along the longitudinal axis of the lagoon. Equations (2.1) and (2.2) are employed to describe the time varying flow in the main water body of the lagoon system. The flow in the inlets is described by the simplified version of the inlet equations presented on page 17. The equations are solved using the numerical scheme described in Chapter 3. The space step used in the computations is $\Delta x = 5000$ ft., the time step is $\Delta t = 180$ sec.

Simultaneous tide recordings at the tide stations, LAKE WORTH, NORTH PALM BEACH, PALM BEACH and BOYNTON BEACH (for locations; see Figure 28), serve to calibrate the numerical model. (The tide stations are operated by National Ocean Survey. The recorders are Fisher and Porter punched tape level recorders, Model 1550. Water levels are measured in a stilling well by means of a cable-float assembly and recorded on punched paper tape every 6 min.) No discharge measurements

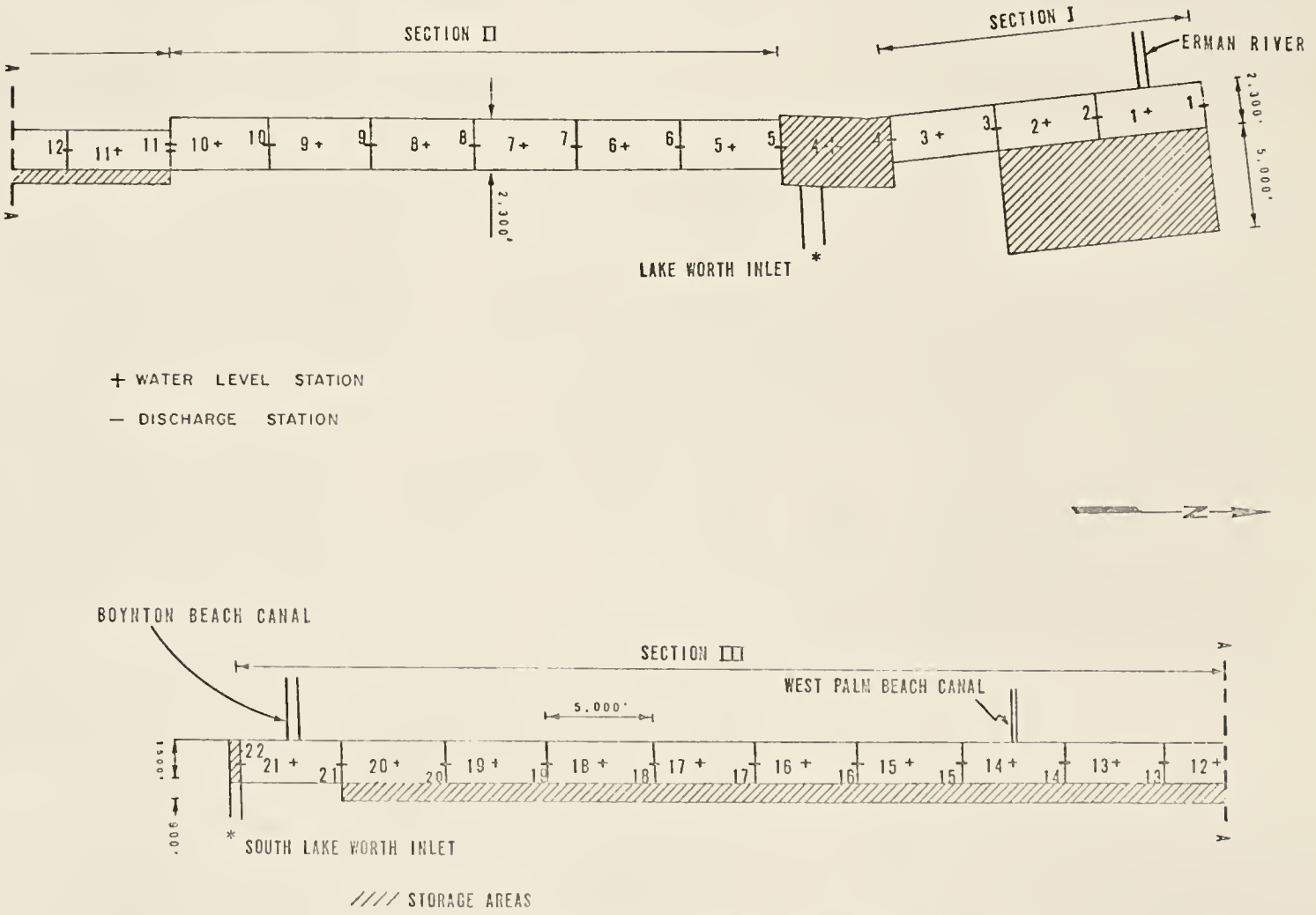

FIGURE 29. SCHEMATIZATION OF LAKE WORTH

are available. It will be clear that these data are not sufficient for the ideal calibration procedure described in Chapter 4 and a trial and error procedure must be employed. Based on experience and sound judgment, friction factors for the different sections and inlets are chosen and adjusted until a good match between measured and computed tides is obtained. This trial and error procedure is carried out for six different 24-hour periods. The tidal range for these periods varies between 2.00 ft. and 3.90 ft., covering both neap and spring tides. Wind speeds for all periods are less than 10 knots while fresh water inflow is negligible. The values of the friction factors leading to a good fit are: North Lake Worth Inlet, F = 0.01; South Lake Worth Inlet, F = 0.08; each of the lagoon sections F = 0.004. The standard deviation of the differences between computed and measured tides at 30-min. time intervals is on the order of 0.1 ft. or less for each of the six different tides; see [4]. The good agreement is also demonstrated in Figure 30 in which the measured and computed tides are plotted for one of the 24-hour periods. The relative high F values for the inlets can be attributed to the flow contraction in the inlets.

With the values of the friction factors described in the previous paragraph, the discharges and water levels in Lake Worth are computed for a sinusoidal ocean tide with an amplitude of 1.4 ft. and a period of 45000 sec. (12.5 hours). The corresponding net discharge is found by time averaging the discharge in a cross section and is found to be equal to 250 cfs to the south. The total volume of water below mean low water between North Lake Worth Inlet and South Lake Worth Inlet is estimated to be on the order of $0.86\ 10^9$ ft^3. It would thus take ($\frac{0.86 * 10^9}{250 * 24 * 3600}$ =) 40 days to renew this volume.

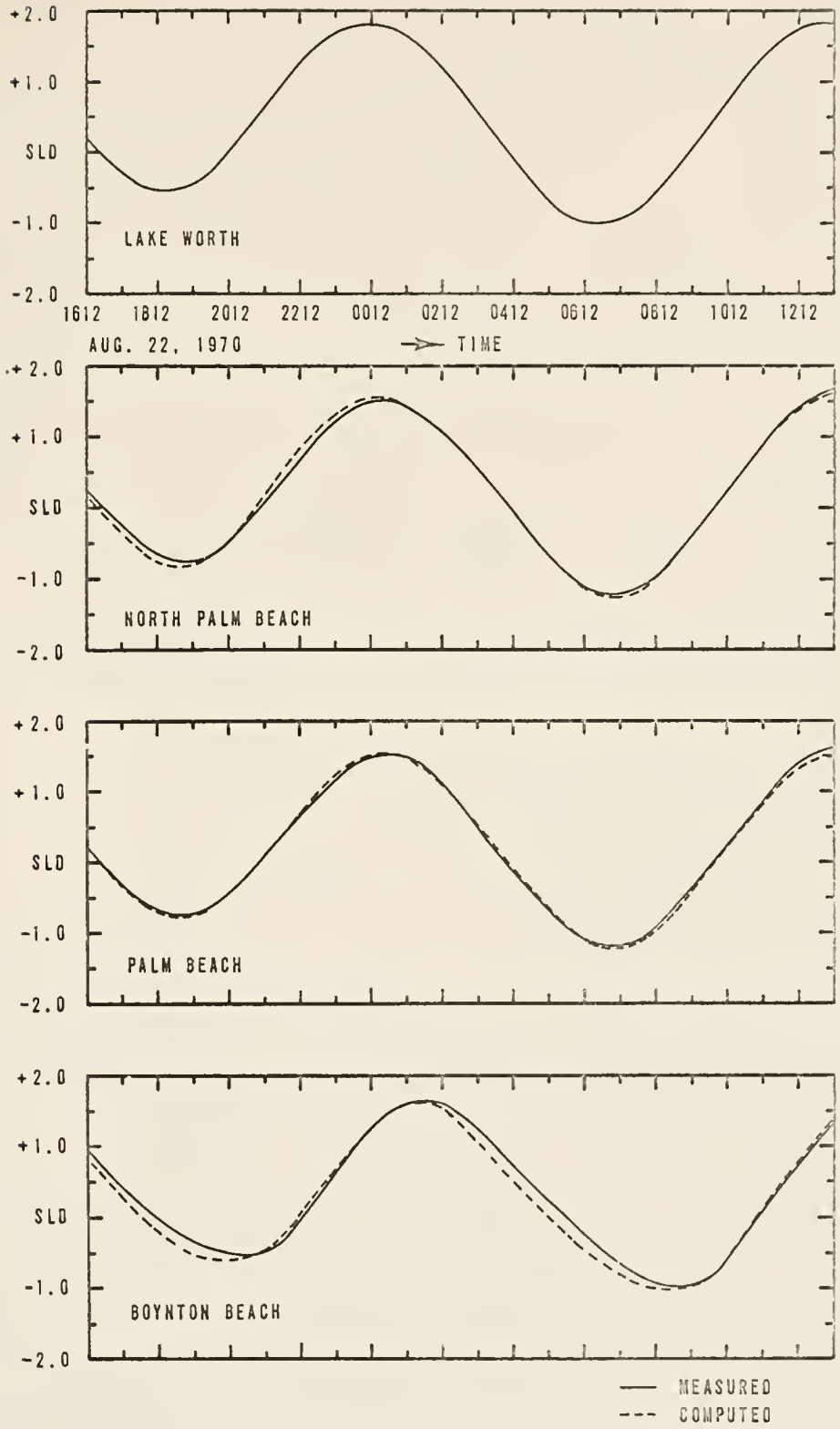

FIGURE 30. MEASURED AND COMPUTED WATER LEVELS IN LAKE WORTH

8. SUMMARY AND CONCLUSIONS

The net displacement of water masses in a lagoon connected to the ocean by narrow, constricted inlets is studied by (1) developing a mathematical description of the phenomenon and (2) carrying out laboratory experiments. Equations describing the flow in the lagoon and in the inlets are derived. Because the mass transport results from the higher order (nonlinear) terms in the equations, only third order terms and higher are neglected. A numerical model is developed to solve for the equations and the boundary conditions. The flow in the lagoon is assumed to be one dimensional, that is the current direction is always along the longitudinal axis of the lagoon. In the model, the algebraic inlet equations are regarded as implicit boundary conditions for the partial differential equations describing the flow in the lagoon. The model is based on an explicit finite difference scheme.

The instantaneous discharges and, therefore, the mass transport are very sensitive to changes in the friction factor F. It is shown that, with the conventional measuring equipment and field procedures, the required accuracy in F can only be obtained by calibrating the numerical model on discharges. That is, determining F by matching computed and measured discharges, rather than matching computed and measured water levels.

An analytic expression is derived for the mass transport due to tidal motion in lagoon systems with a relatively simple geometry. The net transport computed with the analytic model agrees well with the numerically computed transport. The analytic solution is used to

explain the physical concepts of the net transport. It is shown that to satisfy the nonlinear terms in the field equations (the equations describing the flow in the lagoon), the mean surface level in the lagoon must vary with x. The condition imposed by the ocean that at both ends of the lagoon the mean level equals the mean ocean level then introduces a slope in the mean surface level which in turn is responsible for the mass transport. Because the location and dimensions of the inlets play an important role in the net transport, the magnitude of the convective transport can be increased considerably by properly designing these inlets.

Net discharges were measured in an idealized lagoon of uniform width and depth constructed in the laboratory. One end of the lagoon was freely connected to a tidal basin while the other end was connected to the same basin via a submerged weir. Measured and numerically computed net discharges for the different experiments are in good agreement (see Figure 24) which proves the long wave and inlet equations including the second order nonlinear terms to predict well the mass transport.

The results of the study are applied to Lake Worth, Florida. For an average tide (amplitude 1.4 ft., period 12.5 hours), a net discharge southward on the order of 250 cfs was found. Using this figure, it would take approximately 40 days to renew the volume of water below mean low water between North Lake Worth Inlet and South Lake Worth Inlet showing the tide-induced mass transport to be of practical significance.

APPENDIX

APPENDIX A

THE MATHEMATICAL DESCRIPTION OF LONG PERIOD GRAVITY WAVES; EULERIAN DESCRIPTION

The Eulerian method describes the velocities and water surface elevations as a function of time and space. The Cartesian coordinate system shown in Figure 1 will be used.

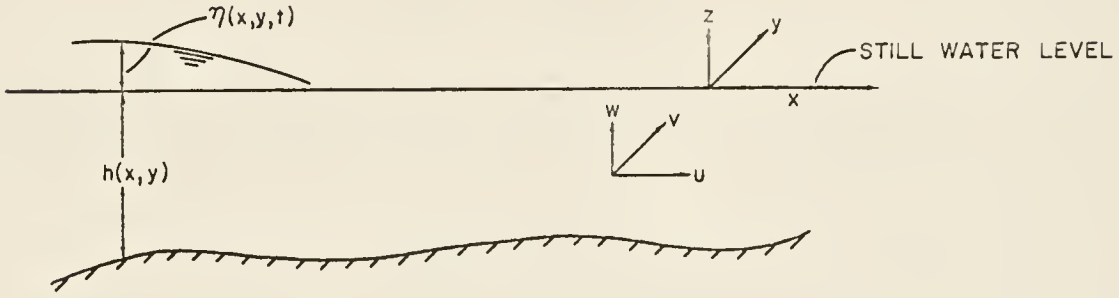

Figure 1. Reference Frame

Assuming incompressible flow, the equation of conservation of mass may be written as

$$\frac{\partial u}{\partial x} + \frac{\partial v}{\partial y} + \frac{\partial w}{\partial z} = 0 \qquad (1)$$

See Prandtl-Tietjens [17], page 100.

Instead of the velocities, the discharges per unit width q_x and q_y defined as

$$q_x = \int_{-h}^{\eta} u \, dz \qquad (2)$$

$$q_y = \int_{-h}^{\eta} v \, dz \tag{2}$$

are introduced.

Integration of Equation (1) with respect to z between the limits -h and η and substituting the foregoing expressions for q_x and q_y yields

$$\frac{\partial q_x}{\partial x} + \frac{\partial q_y}{\partial y} - u(x,y,\eta,t) \frac{\partial \eta}{\partial x} - u(x,y,-h,t) \frac{\partial h}{\partial x} - v(x,y,\eta,t) \frac{\partial \eta}{\partial y} -$$

$$v(x,y,-h,t) \frac{\partial h}{\partial y} + w(x,y,\eta,t) - w(x,y,-h,t) = 0 \tag{3}$$

The kinematic free surface boundary condition (KFSBC), expressing the fact that a water particle cannot leave the surface, may be written as

$$\frac{\partial \eta}{\partial t} + u \frac{\partial \eta}{\partial x} + v \frac{\partial \eta}{\partial y} = w \tag{4}$$

where u, v and w are evaluated at the free surface. The expression for the kinematic bottom boundary condition (KBBC) is

$$u \frac{\partial(-h)}{\partial x} + v \frac{\partial(-h)}{\partial y} = w \tag{5}$$

where u, v and w are evaluated at the bottom. Substituting the expressions for w at the free surface and w at the bottom as given, respectively, by Equations (4) and (5) in Equation (3) yields

$$\frac{\partial \eta}{\partial t} + \frac{\partial q_x}{\partial x} + \frac{\partial q_y}{\partial y} = 0 \tag{6}$$

In this equation, the variables η, q_x and q_y refer to the instantaneous water level fluctuations and discharges. These instantaneous quantities are composed basically of a mean flow component and small turbulent fluctuations and as such can be represented as

$$\begin{aligned} q_x &= \bar{q}_x + q_x' \\ q_y &= \bar{q}_y + q_y' \\ \eta &= \bar{\eta} + \eta' \end{aligned} \tag{7}$$

where the bar refers to the short term mean motion and the prime refers to the fluctuations about this mean. In describing the tidal flow only the mean component is of interest. The equation of conservation of mass with the dependent variables pertaining to the basic motion is obtained by substituting the expressions given by Equations (7) in Equation (6) and then time averaging the result. This yields

$$\frac{\partial \bar{\eta}}{\partial t} + \frac{\partial \bar{q}_x}{\partial x} + \frac{\partial \bar{q}_y}{\partial y} = 0 \tag{8}$$

Time averaging here means averaging over a period large compared to the time scale of the turbulence and short compared to the tidal period. For the derivation of the conservation of mass equation, see also Dronkers [5], page 179 and Henderson [7], page 4.

The starting point for the description of the dynamics of the flow are the Navier-Stokes equations for an incompressible fluid as presented in Daily and Harleman [3], page 113.

$$\frac{\partial u}{\partial t} + u\frac{\partial u}{\partial x} + v\frac{\partial u}{\partial y} + w\frac{\partial u}{\partial z} = -\frac{1}{\rho}\frac{\partial p}{\partial x} + \frac{\mu}{\rho}\left(\frac{\partial^2 u}{\partial x^2} + \frac{\partial^2 u}{\partial y^2} + \frac{\partial^2 u}{\partial z^2}\right) \qquad (9a)$$

$$\frac{\partial v}{\partial t} + u\frac{\partial v}{\partial x} + v\frac{\partial v}{\partial y} + w\frac{\partial v}{\partial z} = -\frac{1}{\rho}\frac{\partial p}{\partial y} + \frac{\mu}{\rho}\left(\frac{\partial^2 v}{\partial x^2} + \frac{\partial^2 v}{\partial y^2} + \frac{\partial^2 v}{\partial z^2}\right) \qquad (9b)$$

$$\frac{\partial w}{\partial t} + u\frac{\partial w}{\partial x} + v\frac{\partial w}{\partial y} + w\frac{\partial w}{\partial z} = -\frac{1}{\rho}\frac{\partial p}{\partial z} - g + \frac{\mu}{\rho}\left(\frac{\partial^2 w}{\partial x^2} + \frac{\partial^2 w}{\partial y^2} + \frac{\partial^2 w}{\partial z^2}\right) \qquad (9c)$$

in which μ = dynamic viscosity

p = pressure = arithmetic mean of the three normal stresses.

The foregoing equations pertain to an inertial frame of reference. When using a coordinate system fixed to the earth, the fluid particles are affected by the Coriolis acceleration, which results from the earth rotation. These accelerations are

in x direction $-\Omega v$

in y direction Ωu

in which $\Omega = 2\omega \sin \phi$

ω = angular velocity of the earth

ϕ = latitude (positive for Northern Hemisphere)

The expression for the Coriolis acceleration presented here assumes $w \ll u$ and $w \ll v$. The vertical component of the Coriolis acceleration is neglected because it is usually small compared to the acceleration g. For a more detailed treatment of the Coriolis force, see Dronkers [5], page 181 and Daily and Harleman [3], page 44.

The last term on the right-hand side of Equations (9a), (9b), and (9c) represents the forces per unit mass of fluid resulting from the deformation of a fluid element. These viscous forces are composed

of normal forces, forces on the vertical planes or lateral forces and forces on the horizontal planes. In tidal flow, the normal viscous forces are small compared to the pressure gradients. When dealing with bodies of water in which the horizontal dimensions are large compared to the vertical dimensions, the lateral viscous forces are generally small and will be neglected here.

Upon introducing the Coriolis acceleration and neglecting the normal and lateral viscous forces, Equations (9a) and (9b) become, respectively

$$\frac{\partial u}{\partial t} + u \frac{\partial u}{\partial x} + v \frac{\partial u}{\partial y} + w \frac{\partial u}{\partial z} - \Omega v = - \frac{1}{\rho} \frac{\partial p}{\partial x} + \frac{1}{\rho} \frac{\partial \tau_{zx}}{\partial z} \tag{10a}$$

$$\frac{\partial v}{\partial t} + u \frac{\partial v}{\partial x} + v \frac{\partial v}{\partial y} + w \frac{\partial v}{\partial z} + \Omega u = - \frac{1}{\rho} \frac{\partial p}{\partial y} + \frac{1}{\rho} \frac{\partial \tau_{zy}}{\partial z} \tag{10b}$$

in which

$$\tau_{zx} = \mu \left(\frac{\partial u}{\partial z} + \frac{\partial w}{\partial x} \right)$$

$$\tau_{zy} = \mu \left(\frac{\partial v}{\partial z} + \frac{\partial w}{\partial y} \right)$$

By virtue of the definition of long waves, the vertical acceleration $\frac{dw}{dt}$ is small compared to the acceleration g and thus Equation (9c) may be written as

$$0 = - \frac{1}{\rho} \frac{\partial p}{\partial z} - g \tag{10c}$$

The conservation of mass equation, Equation (1), times u is added to Equation (10a). This yields

$$\frac{\partial u}{\partial t} + \frac{\partial u^2}{\partial x} + \frac{\partial uv}{\partial y} + \frac{\partial uw}{\partial z} - \Omega v = -\frac{1}{\rho}\frac{\partial p}{\partial x} + \frac{1}{\rho}\frac{\partial \tau_{zx}}{\partial z} \tag{11a}$$

Integration of Equation (10c) with respect to z and requiring that p = 0 at the surface, yields the usual hydrostatic relationship

$$p = -\rho g z + \rho g \eta$$

This expression for p is substituted in Equation (11a) and the resulting equation then is integrated with respect to z between the limits -h and η. After application of Leibnitz rule, the result is

$$\frac{\partial \int_{-h}^{\eta} u\,dz}{\partial t} + \frac{\partial \int_{-h}^{\eta} u^2\,dz}{\partial x} + \frac{\partial \int_{-h}^{\eta} uv\,dz}{\partial y} \overset{o}{} + (uw)\big|_{\eta} \overset{x}{} - (uw)\big|_{-h} \overset{o}{} - u\big|_{\eta}\frac{\partial \eta}{\partial t} \overset{o}{} - u^2\big|_{\eta}\frac{\partial \eta}{\partial x}$$

$$+ u^2\big|_{-h}\frac{\partial(-h)}{\partial x} \overset{x}{} - (uv)\big|_{\eta}\frac{\partial \eta}{\partial y} \overset{o}{} + (uv)\big|_{-h}\frac{\partial(-h)}{\partial y} \overset{x}{} - \Omega\int_{-h}^{\eta} v\,dz = -g(h+\eta)\frac{\partial \eta}{\partial x}$$

$$+ \frac{\tau_{zx}}{\rho}\Big|_{\eta} - \frac{\tau_{zx}}{\rho}\Big|_{-h} \tag{12a}$$

The terms in Equation (12a) marked with "o" constitute the KFSBC given by Equation (4). The terms marked with "x" constitute the KBBC as expressed by Equation (5). Therefore, Equation (12a) may be written as

$$\frac{\partial \int_{-h}^{\eta} u\,dz}{\partial t} + \frac{\partial \int_{-h}^{\eta} u^2 dz}{\partial x} + \frac{\partial \int_{-h}^{\eta} uv\,dz}{\partial y} - \Omega\int_{-h}^{\eta} v\,dz = -g(h+\eta)\frac{\partial \eta}{\partial x}$$

$$+ \tau_{zx}\big|_{\eta} - \tau_{zx}\big|_{-h} \tag{13a}$$

The variables q_x and q_y defined by Equation (2) are now introduced. In doing so, the following approximations are used for the terms resulting from the convective acceleration.

$$\int_{-h}^{\eta} u^2 dz \simeq \frac{1}{h} \left(\int_{-h}^{\eta} u \, dz \right)^2 = \frac{q_x^2}{h}$$

$$\int_{-h}^{\eta} uv \, dz \simeq \frac{1}{h} \int_{-h}^{\eta} u \, dz \int_{-h}^{\eta} v \, dz = \frac{q_x q_y}{h}$$

Based on the foregoing, the equation of conservation of momentum in the x direction becomes

$$\frac{\partial q_x}{\partial t} + g(h + \eta) \frac{\partial \eta}{\partial x} + \frac{1}{h} \frac{\partial q_x^2}{\partial x} + \frac{1}{h} \frac{\partial q_x q_y}{\partial y} - \Omega q_y = \frac{\tau_{zx}}{\rho}\Big|_{\eta} - \frac{\tau_{zx}}{\rho}\Big|_{-h} \qquad (14a)$$

Introducing the expressions for q_x, q_y and η given by Equation (7) and time averaging yields

$$\frac{\partial \bar{q}_x}{\partial t} + \frac{1}{h} \frac{\partial \bar{q}_x^2}{\partial x} + \frac{1}{h} \frac{\partial \bar{q}_x \bar{q}_y}{\partial y} - \Omega \bar{q}_y = -g(h + \bar{\eta}) \frac{\partial \bar{\eta}}{\partial x} - g \overline{\eta' \frac{\partial \eta'}{\partial x}} - \frac{1}{h} \overline{\frac{\partial q_x'^2}{\partial x}}$$

$$- \frac{1}{h} \overline{\frac{\partial q_x' q_y'}{\partial y}} + \overline{\frac{\tau_{zx}}{\rho}}\Big|_{\eta} - \overline{\frac{\tau_{zx}}{\rho}}\Big|_{-h} \qquad (15a)$$

Note that as a result of the application of Leibnitz rule and the kinematic boundary condition, the term, ρuw (one component of the Reynolds stress) has disappeared. Usually, the second, third and fourth terms on the right-hand side are small compared to the first term on that side and will be neglected; therefore

$$\frac{\partial \bar{q}_x}{\partial t} + g(h + \bar{\eta}) \frac{\partial \bar{\eta}}{\partial x} + \frac{1}{h} \frac{\partial \bar{q}_x^2}{\partial x} + \frac{1}{h} \frac{\partial \bar{q}_x \bar{q}_y}{\partial y} - \Omega \bar{q}_y = - \frac{\bar{\tau}_{zx}}{\rho}\Big|_{-h} + \frac{\bar{\tau}_{zx}}{\rho}\Big|_{\eta} \qquad (16a)$$

The corresponding equation for the y direction is

$$\frac{\partial \bar{q}_y}{\partial t} + g(h + \bar{\eta}) \frac{\partial \bar{\eta}}{\partial y} + \frac{1}{h} \frac{\partial \bar{q}_y^2}{\partial y^2} + \frac{1}{h} \frac{\partial \bar{q}_x \bar{q}_y}{\partial x} + \Omega \bar{q}_x = - \frac{\bar{\tau}_{zy}}{\rho}\Big|_{-h} + \frac{\bar{\tau}_{zy}}{\rho}\Big|_{\eta} \qquad (16b)$$

The terms on the right-hand side of Equations (16a) and (16b) result from the external forces. The first term times $-\rho$ represents the bottom stress, the last term times $+\rho$ represents the free surface stress. Assuming quasi-steady flow, the bottom shear stress can be related to the characteristics of the main flow, by one of the well-known resistance laws. Here use is made of the Darcy-Weisbach formula which yields

$$\frac{\tau_{zx}}{\rho}\Big|_{-h} = \frac{f}{8} \bar{q}_x \left| \sqrt{\frac{\bar{q}_x^2 + \bar{q}_y^2}{(h + \bar{\eta})^2}} \right| \qquad (17a)$$

$$\frac{\tau_{zy}}{\rho}\Big|_{-h} = \frac{f}{8} \bar{q}_y \left| \sqrt{\frac{\bar{q}_x^2 + \bar{q}_y^2}{(h + \bar{\eta})^2}} \right| \qquad (17b)$$

f = Darcy-Weisbach resistance coefficient. For a more detailed derivation of Equations (17a) and (17b), see Dronkers [5], page 184. The second term on the right-hand side of Equations (16a) and (16b) results from the stresses exerted by the wind on the water. For expressions relating these stresses and the windspeed and direction, see Dronkers [5], page 184. In view of the foregoing, the dynamic

Equations (16a) and (16b) take the form

$$\frac{\partial \bar{q}_x}{\partial t} + g(h + \bar{\eta}) \frac{\partial \bar{\eta}}{\partial x} + \frac{1}{h} \frac{\partial \bar{q}_x^2}{\partial x} + \frac{1}{h} \frac{\partial \bar{q}_x \bar{q}_y}{\partial y} - \Omega \bar{q}_y = -F \frac{\bar{q}_x \sqrt{\bar{q}_x^2 + \bar{q}_y^2}}{(h + \bar{\eta})^2} + X \tag{18a}$$

$$\frac{\partial \bar{q}_y}{\partial t} + g(h + \bar{\eta}) \frac{\partial \bar{\eta}}{\partial y} + \frac{1}{h} \frac{\partial \bar{q}_y^2}{\partial y} + \frac{1}{h} \frac{\partial \bar{q}_x \bar{q}_y}{\partial x} + \Omega \bar{q}_x = -F \frac{\bar{q}_y \sqrt{\bar{q}_x^2 + \bar{q}_y^2}}{(h + \bar{\eta})^2} + Y \tag{18b}$$

in which $F = f/8$

$$X = \frac{\bar{\tau}_{zx}}{\rho}\Big|_{\eta}$$

$$Y = \frac{\bar{\tau}_{zy}}{\rho}\Big|_{\eta}$$

The two-dimensional equations of conservation of mass and momentum as derived here do not account for rainfall or evaporation. The effect of these phenomena can be introduced into the two-dimensional equations but only in an approximate way; proper formulation of the problem requires a three-dimensional description. In accounting for the effects of rainfall and evaporation, it is assumed that the supplementary discharge may be thought to originate from sources evenly distributed throughout the flow field. In that case, the equation of conservation of mass reads

$$\frac{\partial u}{\partial x} + \frac{\partial v}{\partial y} + \frac{\partial w}{\partial z} = s \tag{19}$$

in which s = strength of source per unit volume.

Integrating with respect to z between the limits -h and η and introducing the variables q_x and q_y yields after time averaging

$$\frac{\partial \overline{q_x}}{\partial x} + \frac{\partial \overline{q_y}}{\partial y} + \frac{\partial \bar{\eta}}{\partial t} = M \qquad (20)$$

in which M = net inflow per unit surface area due to rainfall, lateral inflow, etc.

Determination of the effect of rainfall and evaporation on the dynamics of the flow requires a semi-empirical approach. In case the dynamic effects are important, measurements are needed to determine the empirical constants. The reader is referred to Dronkers [5], page 194 and Stoker [21], page 452.

A similar problem as described in the previous paragraph is encountered when dealing with storage areas in tidal models, frequently found in one-dimensional schematizations of tidal waters. Assuming that the discharge from the storage region may be thought to originate from evenly distributed sources in the flow field, the equation of conservation of mass is the same as Equation (20). M now is defined as the discharge per unit width from the storage region, divided by the width of the conveying channel. For the effect of inflow from the storage area on the dynamics of the flow in the conveying channel, the reader again is referred to Dronkers [5], page 194 and Stoker [21], page 452.

REFERENCES

1. Bagnold, R. A., "Sand Movement by Waves: Some Small Scale Experiments with Sand of Very Low Density," Inst. of Civ. Eng., Vol. 4, February, 1947.

2. Chiu, T. Y., Van de Kreeke, J. and Dean, R. G., "Residence Times of Waters Behind Barrier Islands," Department of Coastal and Oceanographic Engineering, University of Florida, Technical Report No. 7, October, 1970.

3. Daily, J. W. and Harleman, D. R. F., Fluid Dynamics, Addison-Wesley Publishing Company, 1965.

4. Department of Coastal and Oceanographic Engineering, University of Florida, "The Use of Tidal Computations in Establishing Tidal Datums; Results of a Pilot Study," July, 1971.

5. Dronkers, J. J., "Tidal Computations in Rivers and Coastal Waters," North-Holland Publishing Company, 1964.

6. Dronkers, J. J., Discussion of "Water-Level Fluctuations and Flow in Tidal Inlets," by J. Van de Kreeke, Journal of the Waterways and Harbors Division, ASCE, Vol. 94, No. WW3, August, 1968.

7. Henderson, F. M., Open Channel Flow, The Macmillan Company, 1967.

8. Ippen, A. T., Estuary and Coastline Hydrodynamics, McGraw-Hill Book Company, New York, 1966.

9. Keulegan, G. H., "Third Progress Report on Tidal Flow in Entrances, Water Level Fluctuations of Basins in Communication with Seas," Report No. 1146, National Bureau of Standards, U. S. Department of Commerce, September, 1951.

10. King, H. W. and Brater, E. F., Handbook of Hydraulics, McGraw-Hill, Inc., 1963.

11. Lockwood, M. G. and Carothers, H. P., "Preservation of Estuaries by Tidal Inlets," Journal of the Waterways and Harbors Division, ASCE, Vol. 93, No. WW4, November, 1967.

12. Longuet-Higgins, M. S., "Mass Transport in Water Waves," Phil. Trans. Roy. Soc. London, February, 1953.

13. Longuet-Higgins, M. S. and Stewart, R. W., "Radiation Stresses in Water Waves; a Physical Discussion with Applications," Deep Sea Research, Vol. II, pp. 529-562, 1964.

14. Mavis, F. T., "Submerged Thin Plate Weirs," Engineering News Record, July 7, 1949.

15. Mota Oliveira, T. B., "Natural Flushing Ability in Tidal Inlets," Proceedings of XIIth Conference on Coastal Engineering, Washington, D.C., 1970.

16. Platzman, G. W., "The Computational Stability of Meteorological Prediction Equations," Report, Department of Meteorology, University of Chicago, 1958

17. Prandtl, L. and Tietjens, O. G., "Fundamentals of Hydro- and Aeromechanics," Dover Publications, Inc., 1934.

18. Reid, R. O. and Bodine, B. R., "Numerical Model for Storm Surges in Galveston Bay," Journal of the Waterways and Harbors Division, ASCE, Vol. 94, No. WW1, February, 1969.

19. Russell, R. C. H. and Osorio, J. D. C., "An Experimental Investigation of Drift Profiles in a Closed Channel," Proceedings, VIth Conference on Coastal Engineering, Florida, 1958.

20. Shemdin, O. H. and Forney, R. M., "Tidal Motion in Bays," Proceedings of XIIth Conference on Coastal Engineering, Washington, D.C., 1970.

21. Stoker, J. J., Water Waves, Interscience Publishers, Inc., 1966.

22. Stokes, G. G., "On the Theory of Oscillatory Waves," Trans. Cambridge Phil. Soc., Vol. VIII, March, 1847.

23. U. S. Beach Erosion Board, "A Study of Progressive Oscillatory Waves in Water," Tech. Report No. 1, May, 1941.

24. U. S. Department of Commerce, Coast and Geodetic Survey, Tide Tables.

25. Van de Kreeke, J., "Water Level Fluctuations and Flow in Tidal Inlets," Journal of the Waterways and Harbors Division, ASCE, Vol. 93, No. WW4, November, 1967.

26. Van de Kreeke, J., Closure of "Water-Level Fluctuations and Flow in Tidal Inlets," Journal of the Waterways and Harbors Division, ASCE, Vol. 95, No. WW1, February, 1969.

27. Vennard, J. K. and Weston, R. F., "Submergence Effect on Sharp-Crested Weirs," Engineering News Record, June 3, 1943.

28. Verma, A. P. and Dean, R. G., "Numerical Modeling of Hydro-mechanics of Bay Systems," Proceedings, Civil Engineering in the Ocean II, Miami, 1969.

29. Villemonte, J. R., "Submerged Weir Discharge Studies," Engineering News Record, December 25, 1947.

30. Vreugdenhil, C. B., "The Influence of the Friction-term on the Stability of Difference-Methods for Hydraulic Problems," De Ingenieur, jrg. 78, nr 20, May, 1966. (Dutch text)

BIOGRAPHICAL SKETCH

Jacobus van de Kreeke was born in Holland where he received his primary and secondary education. He attended the Technical University in Delft and received the Ingenieurs degree from that institution in 1959.

From 1959 to 1961, he served in the Royal Dutch Navy. Most of this time he spent in New Guinea where he designed and supervised construction of marine structures. When discharged as a Lieutenant, j.g. he joined the Hydraulics Division of Deltaworks, the Hague, Holland. While employed with the Delta service he was involved in coastal engineering research and economic analysis mainly pertaining to the design of the breakwaters of Europoort Harbor (Rotterdam). As part of an exchange program, he worked for six months at the Laboratoire National d'Hydraulique, Chatou, France, carrying out research on wave forces on submerged oil reservoirs.

In 1965, he came to the United States where he was employed with the Department of Coastal and Oceanographic Engineering at the University of Florida. Besides his teaching duties he was involved in breakwater design, sediment transport, beach erosion, tidal computations, and laboratory and field experiments.

In 1967, he joined NESCO and later SEA, where he was involved in studies on sediment pollution.

In 1969, he returned to the University of Florida where he was employed as a Research Associate, while pursuing his doctoral degree

He is the author of several publications in the field of coastal engineering. He is a member of the American Society of Civil Engineers, and a member of the Dutch Institution of Graduate Engineers.

I certify that I have read this study and that in my opinion it conforms to acceptable standards of scholarly presentation and is fully adequate, in scope and quality, as a dissertation for the degree of Doctor of Philosophy.

Bent A. Christensen, Chairman
Professor of Civil Engineering

I certify that I have read this study and that in my opinion it conforms to acceptable standards of scholarly presentation and is fully adequate, in scope and quality, as a dissertation for the degree of Doctor of Philosophy.

Robert G. Dean, Co-Chairman
Professor of Coastal and
Oceanographic Engineering

I certify that I have read this study and that in my opinion it conforms to acceptable standards of scholarly presentation and is fully adequate, in scope and quality, as a dissertation for the degree of Doctor of Philosophy.

Robert G. Blake
Associate Professor of Mathematics

This dissertation was submitted to the Dean of the College of Engineering and to the Graduate Council, and was accepted as partial fulfillment of the requirements for the degree of Doctor of Philosophy.

December, 1971

Dean, College of Engineering

Dean, Graduate School

UNIVERSITY OF FLORIDA
3 1262 08553 7875